Syracuse University

SURFACE

May 2018

Characterization of interplay among DNA repair, histone H3 lysine 9 dimethylation and small interfering RNA pathway in Caenorhabditis elegans

BING YANG
Syracuse University

Abstract

Heterochromatin assembly on repetitive sequences has been proposed to maintain genome integrity in different species. Histone H3 lysine 9 dimethylation (H3K9me2) has been shown to play an important role in mediating the formation of heterochromatin. In our lab, we use *Caenorhabditis elegans* as a model system to study the biological significance of the enrichment of H3K9me2 on repetitive elements and unpaired chromatin. Research of several other labs implicated that distribution of H3K9me2 on repetitive sequences limits transposon transcription and mutation occurrence near repetitive sequences. Additionally, our lab has reported that CSR-1 small RNA pathway (CSR-1, EKL-1, EGO-1 and DRH-3) regulates the deposition of H3K9me2 on unpaired chromatin during meiotic prophase.

In this study, I identified a putative DNA annealing helicase, SMRC-1, that associates with the H3K9me2 methyltransferase MET-2 and a modified form of EKL-1. The majority of this thesis focuses on understanding the interaction between MET-2 and SMRC-1. Characterization of *smrc-1* mutants revealed that SMRC-1 is important for resolving replication stress. Thus the association between SMRC-1 and MET-2 might suggest H3K9me2 functions as an epigenetic regulator of double strand break formations genome wide. Additionally, I found that a modified form of EKL-1 might interact with SMRC-1. Based on these findings, I propose a model whereby SMRC-1 bridges the CSR-1 small RNA pathway with H3K9me2.

Characterization of interplay among DNA repair,

histone H3 lysine 9 dimethylation and small interfering RNA pathway in *Caenorhabditis*

elegans

By

Bing Yang

B.S. Wuhan University, 2011

Dissertation

Submitted in partial fulfillment of the requirements for the degree of

Doctor of Philosophy in Biology

Syracuse University

May 2018

Acknowledgements

I would like to thank my advisor, Dr. Eleanor Maine, for her patience, continuous support and guidance over the course of my study. Her immense knowledge helped me in all the time during my research and writing of this thesis. Her dedication and commitment to science make her an exemplary figure I always look up to. I am grateful to the members of my committee: Dr. John Belote, Dr. Sarah Hall, Dr. Melissa Pepling, Dr. David Pruyne, for their insightful comments and invaluable encouragement.

I thank past and present members of the Maine lab, Xia Xu, Dr. Yiqing Guo, Yini Li, Anniya Gu and Dr. Matthew Sullenberger, for their support and accompany during the last few years. They are not only my labmates but also my close friends. Xia taught me many essential skills in the lab, such as microinjections and immunoprecipitation. Yini, Anniya and I had so much fun during countless late nights in the lab. Also special thanks to all the friends I have made in the biology department and Syracuse community. The board game nights I spent with Alex Nichitean and Pallavi Bharadwaj brought much energy and joy to the stressful graduate life.

Last but not least, I am indebted to my family for their endless love and support. My grandparents and parents are always there for me whenever I need them. Grandpa, you will always be missed. To my brother, for all the encouragements and listening ears.

Table of Contents

Chapter I Introduction

1.1. *C. elegans* germline development

1.1.1 *C. elegans* development

    Caenorhabditis elegans is a free-living nematode species established as a model

organism by Sydney Brenner (Brenner, 1974). Originally isolated from soil, *C. elegans*

are fed *E. coli* cells in the lab. *C. elegans* demonstrates multiple advantages for

studying germline development as an invertebrate model organism. It has two different

sexes: hermaphrodite and male. Hermaphrodites produce gametes of both sexes, and

give rise to hundreds of progeny via self-fertilization. Males account for around 0.1% of

the wild type population. The single X chromosome in males results from X

chromosome nondisjunction during either spermatogenesis or oogenesis in

hermaphrodites (Wood, 1988). Among cross-progeny sired by male sperm, male

animals should be 50% of the population, since there is equal chance of an X sperm or

nullo-X sperm being produced and fertilizing an oocyte. Embryos undergo a series of

embryonic cleavages, some *in utero* and other ex utero. They hatch as L1 larvae and

develop through four different larval stages to become adults over a duration of 55

hours at 22ºC. In a non-stressful environment, L1 larvae reach adulthood in two days.

Under stressful conditions (e.g. starvation), L1 animals will either arrest or transit into

dauer. When conditions become favorable, arrested L1s or dauer larvae will resume

development and reach post-dauer adulthood (Wood, 1988).

    During embryonic cleavage, the zygotic embryo, called P0, divides into two

daughter cells: P1 and AB. P1 further divides into EMS and P2 (Sulston *et al.*, 1983)

(Figure 1.1). A signature feature of the P lineage is the distribution of specialized

ribonucleoprotein particles, called P granules, near the nuclear pore. Later, the P2 cell gives rise to P3 and C, and the division of P3 results in P4 and D (Sulston *et al.*, 1983). P4 is the germline precursor cell, and divides once prior hatching to form Z2 and Z3. Somatic gonad precursors Z1 and Z4 divide and eventually form the somatic gonadal tissues, including distal tip cells (DTCs) and sheath cells in the adults (Sulston *et al.*, 1983) (Figure 1.1). The primordial germ cells, Z2 and Z3, start mitotic divisions starting from L1 stage (Figure 1.1). Beginning in early L4 stage in hermaphrodites, proximal mitotic cells enter meiosis and initiate spermatogenesis. By late L4 stage, mature sperm are produced and stored in the spermatheca. At the adult molt, the hermaphrodite gonad switches to oogenesis and starts generating oocytes (Riddle *et al.*, 1997).

1.1.2 Germ Cell Proliferation

In the mature adult hermaphrodite gonad, germ cells undergoing mitosis and meiosis are arranged in a distal to proximal orientation. Mitotic cells are signaled by distal tip cell to divide and proliferate; this process replenishes the stem cell population. The GLP-1/Notch signaling pathway was identified to mediate the balance between mitosis and meiosis in the germ cell population (Kimble and Simpson, 1997). *glp-1* encodes a transmembrane receptor protein expressed by germ cells adjacent to the DTC. By analogy with its Drosophila counterpart NOTCH, GLP-1 binds a signal ligand on the surface of the distal tip cell: LAG-2 (Austin and Kimble, 1989; Henderson *et al.*, 1994; Yochem and Greenwald, 1989). Binding of LAG-2 triggers the two consecutive rounds of cleavage of GLP-1 protein, releasing the intracellular domain, which is then transported to the nucleus and acts as a transcriptional regulator (Schroeter *et al.*, 1998;

Struhl and Adachi, 1998, 2000). In *glp-1* hermaphrodite mutants, all germline precursor cells enter meiosis prematurely and differentiate into sperm; whereas very few oocytes are produced (Austin and Kimble, 1989). *glp*-1 mRNA has been shown to be evenly distributed throughout the whole gonad. However, starting from the transition zone, the expression level of GLP-1 protein is down-regulated by post-transcriptioanl regulation (Hansen and Schedl, 2013). For example, GLD-1 binds to the 3'UTR of *glp-1* mRNA and leads to its degradation (Marin and Evans, 2003).

In order to find components of the *glp-1* pathway or modulators of *glp-1* activity, our lab carried out a series of genetic screens to search for *ego* (enhancer of *glp-1*) mutants in the *glp-1(bn18)* background (Qiao *et al.*, 1995). The partial loss of *glp-1* function in the *bn18* mutant provides a sensitized background to identify factors that promote the function of *glp-1*. As a result, several *ego* genes were initially identified and characterized by Qiao *et al* (Qiao *et al.*, 1995). Later studies cloned and characterized the molecular function of some of the *ego* genes (Liu and Maine, 2007; She *et al.*, 2009; Smardon *et al.*, 2000). For example, *ego-1* was found to encode an RdRP (RNA-directed RNA polymerase), which is a core component in the siRNA pathway (Smardon *et al.*, 2000) (See section 1.3). Molecular characterization of the *ego-3* gene is described in the Appendix of this thesis.

1.1.3 Chromosome pairing and synapsis during meiosis

The highly dynamic process of chromosome pairing occurs during leptotene and zygotene stages of meiotic prophase I. This process begins when homologous chromosomes initiate elongation and searching for pairing partners. The pairing center

(PC), a region constituting of *cis*-acting repetitive elements at one end of each chromosome, serves as the initiator of pairing events. One of four zinc-finger proteins (HIM-8, ZIM-1, ZIM-2 and ZIM-3) binds to the PC on each chromosome and promotes synapsis (MacQueen *et al.*, 2005; Phillips and Dernburg, 2006). For example, HIM-8 is recruited to the pairing center on chromosome X (Phillips and Dernburg, 2006). The binding of these zinc finger proteins to the PC promotes the formation of axial synapsis filaments along homologous chromosomes. During leptotene/zygotene, the pairing process initiates when the PCs of homologous chromosomes come together and interact (Hillers *et al.*, 2015). There are three different meiosis-specific cohesion complexes, comprised of REC-8, COH-3 and COH-4 in *C. elegans* (Pasierbek *et al.*, 2001; Severson *et al.*, 2009; Severson and Meyer, 2014). They tether sister chromatids together to serve as the basis for axial filament assembly (Hillers *et al.*, 2015). Four different HORMA-domain proteins –HIM-3, HTP-1, HTP-2 and HTP-3-play crucial roles in defining meiotic chromosome structure (Kim *et al.*, 2014) (Figure 1.2). HIM-3 and HTP-3 are shown to be important for initial alignment of homologs during the early stage of axial filament formation (Kim *et al.*, 2014). HTP-1 and HTP-2 are recruited to the axial element by binding to both HIM-3 and HTP-3 (Kim *et al.*, 2014).

During pachytene stage, the axial elements assembled on the paired homologs are connected by another highly conserved meiotic-specific structure known as the synaptonemal complex (SC). In *C. elegans*, four major components of the SC were identified as SYP-1, SYP-2, SYP-3 and SYP-4 (Colaiácovo *et al.*, 2003b; MacQueen *et al.*, 2002; Smolikov *et al.*, 2009) (Figure 1.2). Once assembled properly, the SC tightly

connects and stabilizes the paired homologs and promotes the formation of meiotic crossovers (COs).

1.1.4 Recombination

In most organisms, meiotic recombination between homologous chromosomes is required to ensure successful chromosome segregation during meiosis. In *C.* elegans, one obligate crossover on each set of homologous chromosomes is achieved through balancing crossover recombination and non-crossover repair mediated by meiotic machinery as explained below. To initiate meiotic recombination, double strand breaks (DSBs) need to be generated. In *C. elegans*, multiple factors that promote the formation of DSBs were identified through either homology comparison or genetic screens. *spo-11* was identified to encode a conserved type IV topoisomerase (Dernburg *et al.*, 1998). SPO-11 in yeast catalyzes the formation of meiotic DSBs (Bergerat *et al.*, 1997; de Massy *et al.*, 1995; Keeney *et al.*, 1997; Keeney and Kleckner, 1995). Similarly, SPO-11 introduces meiotic DSBs in *C. elegans* (Dernburg *et al.*, 1998). Genetic screens for mutants exhibiting a high incidence of male progeny (a Him phenotype) identified several factors that are necessary for DSB formation, including *him-17*, *dsb-1* and *dsb-2* (Reddy and Villeneuve, 2004; Rosu *et al.*, 2013; Stamper *et al.*, 2013). In these mutants, the failure to make DSBs and crossovers leads to oocytes displaying 12 univalents, in contrast to 6 bivalents in wild type corresponding to 6 pairs of homologous chromosomes (Reddy and Villeneuve, 2004; Rosu *et al.*, 2013; Stamper *et al.*, 2013). Exposure of these mutants to exogenous DSB-inducing reagents, such as irradiation

could restore bivalent formation by introducing exogenous DSBs (Reddy and Villeneuve, 2004; Rosu *et al.*, 2013; Stamper *et al.*, 2013).

Repair of meiotic DSBs shares many common features with homologous recombination in mitotic cells. Repair of meiotic DSBs starts with strand resection mediated by SPO-11. It is known from the work in *S. cerevisiae* that SPO-11 covalently binds to the DNA strand, and the SPO-11::DNA nucleoprotein complex is then removed to facilitate the short 3'single strand overhang generation (Neale *et al.*, 2005). The conserved MRE-11 5'-3' exonuclease further processes the short 3' ssDNA overhang into a long overhang (Yin and Smolikove, 2013). The RAD-51 recombinase is then loaded onto the ssDNA strand to promote strand invasion during strand exchange (Alpi *et al.*, 2003; Colaiácovo *et al.*, 2003a; Petalcorin *et al.*, 2007). The RAD-51::DNA intermediate complex is then subjected to two different consequent repair pathways: crossover or non-crossover. Crossover repair results from successful strand invasion, whereas non-crossover repair will arise if strand invasion and exchange fail. Non-crossover repair may occur via synthesis-dependent strand annealing (SDSA) or by hon-homologous end joining (NHEJ). SDSA is more accurate, whereas NHEJ often leads to repair errors, such as deletions or insertions (Hillers *et al.*, 2015). When meiotic crossover does occur, the process of choosing the homologous chromosome as the repair template is largely regulated by axial element of the synaptonemal complex. It is hypothesized that the axial element components make the sister chromatid inaccessible for repair and reassure the homolog is utilized as the repair template (Hillers *et al.*, 2015). To process the recombination intermediate, the highly conserved HIM-18 protein serves as a scaffold to recruit nucleases SLX-1 and XPF-1 (Agostinho *et al.*, 2013;

O'Neil *et al.*, 2013; Saito *et al.*, 2009). This protein complex resolves the intermediates and completes the conversion from CO intermediate to mature CO products (Saito *et al.*, 2009).

It has been shown in several other species that once strand exchange successfully takes place, a subset of these intermediates is channeled to two different classes of CO pathway. In *C. elegans*, the class I pathway involves the mismatch repair protein homologs including MSH4 and MSH5 (Kelly *et al.*, 2000a; Winand *et al.*, 1998); in contrast, the class II pathway involves MUS81 and MMS4 (Boddy *et al.*, 2001; Smith *et al.*, 2003). The process of selecting and converting CO intermediates to mature CO sites is poorly understood in various model systems. However, a key player in limiting the number of CO sites on each chromosome in *C. elegans* is COSA-1 (crossover site-associated-1) (Yokoo *et al.*, 2012). COSA-1 is a widely conserved cyclin-related protein, and it localizes specifically at the single CO site on each homologous chromosome pair (Yokoo *et al.*, 2012). It is believed that COSA-1 reinforces the formation of meiotic CO by restricting the CO promoting factors to designated sites. *cosa-1* mutants display normal homolog pairing and DSB formation, however, CO events do not occur in the *cosa-1* mutant (Yokoo *et al.*, 2012). The mature CO products are ultimately formed during meiosis II.

1.2. Epigenetic regulation

The building block of chromatin, the nucleosome, is composed of DNA wrapped twice around the histone octomer core. DNA and protruding N-terminal tails of the histone proteins are subject to a variety of covalent modifications, *e.g.*, methylation, acetylation, *etc*. The detailed genome-wide distribution of DNA modification can be mapped via

bisulfite sequencing followed with high throughput sequencing; and histone

modifications across the whole genome can be mapped though chromatin

immunoprecipitation (ChIP) coupled with high throughput sequencing. In parallel, the

transcriptional status of each gene in the genome could be determined by RNA

sequencing. Through comparing the distribution of DNA or histone modifications near a

specific gene and the corresponding RNA transcript level, researchers have defined

active or repressive histone modifications (also called 'marks"). For example, active

marks often recruit transcription factors to target genes, and this promotes gene

expression. Conversely, repressive marks cause the formation of closed chromatin

structure and therefore repress gene expression (Van Wynsberghe and Maine, 2013).

1.2.1 DNA modification

DNA methylation has been implicated in repressing transcription. Neither traditional 5-

methyl cytosine (5mC, cytosine nucleotide in DNA that is modified by the addition of a

methyl residue to its 5th carbon) nor cytosine DNA methyltransferase have been

reported in *C. elegans*. However, 6-methyl Adenine (6mA, methyl group added on the

6th carbon of Adenine in DNA) and a potential DNA methyltransferase, DAMT1, have

been described recently in *C. elegans* (Greer *et al.*, 2015). DAMT1 has been shown to

catalyze the addition of 6mA both *in vivo* and *in vitro* (Greer *et al.*, 2015). Importantly,

the level of 6mA increases transgenerationally in *spr-5* mutants. *spr-5* encodes the only

known H3K4 demethylase in *C. elegans*, and *spr*-5 mutants exhibit increased H3K4me2

(Greer *et al.*, 2015; Katz *et al.*, 2009). Conversely, deletion of *dnmt1* in a *spr-5* mutant

background partially rescues the elevation of H3K4me2 (Greer *et al.*, 2015). Hence,

there is a positive correlation between H3K4me2 and 6mA. The crosstalk between 6mA and H3K4me2 suggests that this specific type of DNA methylation might promote gene expression by elevating the H3K4me2.

1.2.2 Chromatin regulation

In *C. elegans*, functional genome-wide profiling of different histone modifications through chromatin IP (ChIP) coupled with next-generation sequencing has partially revealed the landscape of chromatin in embryos, larvae and adults (see modENCODE). Consistent with data from studies of other organisms, marks such as H3K4me2/3, H3K9 acetylation(ac), H3K27ac and H3K36me2/3, are positively associated with transcribed genes (Liu *et al.*, 2011). In contrast, marks such as H3K9me2/3 and H3K27me2/3, correlate with reduced gene transcription (Liu *et al.*, 2011). These correlations are widely observed in many species. In this dissertation, most of my research focuses on H3K9me2, a mark associated with heterochromatin formation and transcriptional repression.

1.2.2.1 H3K9me2 distribution pattern

In many organisms, it is known that unsynapsed chromatin during meiosis is subject to histone modifications, which leads to transcriptional silencing (Turner, 2007). H3K9me2 has been reported as a transcriptional repression mark on unpaired chromatin (Khalil *et al.*, 2004; Turner *et al.*, 2005). In *C. elegans*, H3K9me2 is highly enriched on unpaired chromatin, such as the single X chromosome in wild type males, during meiosis and is thought to silence gene expression (Kelly *et al.*, 2002). Immunolabeling results using

antibody against H3K9me2 showed a strong focus in pachytene nuclei in the male

gonad; FISH (fluorescence in situ hybridization) using a label to identify the X

chromosome confirmed the strong focus as the X chromosome (Kelly *et al.*, 2002).

Elevated H3K9me2 is also widely detected on unpaired chromosomes in animals

lacking paring center (PC) proteins, such as *him-8* and *zim-2* mutants. Consistently, the

active transcription marker H3K4me2 appeared to be absent from the unpaired X

chromosome. In addition, XO hermaphrodites have reduced X chromosome gene

transcriptional levels compared to XX hermaphrodites, suggesting a transcriptionally

repressive state on unpaired X chromosome (Kelly *et al.*, 2002). In contrast to the X

chromosome, the autosomes in males exhibit a low level of H3K9me2 (Kelly *et al.*,

2002). In wild type hermaphrodites, H3K9me2 shows an even distribution on all

chromosomes with a slight enrichment on chromosome ends (Kelly *et al.*, 2002;

Mlynarczyk-Evans *et al.*, 2013). On a global scale, high resolution ChIP-seq data

revealed the distribution pattern of H3K9me2 (Guo *et al.*, 2015; McMurchy *et al.*, 2017;

Zeller *et al.*, 2016). A strong enrichment of H3K9me2 on repetitive elements (RE) is

consistently found in both embryos and adults (Guo *et al.*, 2015; McMurchy *et al.*, 2017;

Zeller *et al.*, 2016). The involvement of H3K9me2 in regulating repetitive element

transcription is an area of active research in *C. elegans*.

1.2.2.2 Histone H3K9me2/3 modification

Histone methyltransferases carry out the addition of methyl-groups to histone tails. One

common protein domain shared by histone methyltransferases is the SET domain; there

are 38 SET domain containing proteins present in *C. elegans.* MET-2 is identified as the

methyltransferase responsible for H3K9me1/2, and SET-25 is identified as the

methyltransferase responsible for H3K9me3 (Andersen and Horvitz, 2007; Bessler *et*

al., 2010; Towbin *et al.*, 2012). In *met-2* mutants, H3K9me1 and H3K9me2 are

abolished, while H3K9me3 is reduced compared to wild type in both embryos and germ

line (Towbin *et al.*, 2012). The *met-2 set-2*5 double mutant lacks detectable H3K9me in

both embryos and adults, suggesting that SET-25 primarily utilizes H3K9me2 as a

substrate for addition of a third methyl group (Towbin *et al.*, 2012).

To understand the biological significance of H3K9me in *C. elegans*, a series of

transcriptome studies have been performed by different research groups including our

lab. Guo *et al* (2015) carried out RNA-seq on RNA isolated from gonads with or without

MET-2 in order to identify genes whose transcription is regulated by lack of H3K9me1/2

and partial loss of H3K9me3. Interestingly, only a few germline-specific genes (less than

5% of total germline-specific genes) are differentially expressed between these two

genotypes. To further understand the effect of complete loss of H3K9me on the

transcriptome, Zeller *et al* compared transcript data between wild type and the *met-2*

set-25 double mutant and observed very few genes with altered transcript abundance.

Taken together, it can be concluded that loss of H3K9me has little impact on gene

transcription, arguing that this heterochromatic mark might have an independent role

other than silencing genes. However, loss of H3K9me does result in de-repression of

RE, which mainly consists of transposons. Therefore, these results suggesting that

H3K9me is important for silencing the REs (McMurchy *et al.*, 2017; Zeller *et al.*, 2016).

Additionally, in the absence of H3K9me, mutations and R loops tend to accumulate in

repetitive elements. R-loops are DNA::RNA hybrids, and most likely result from

simultaneous transcription and replication from the opposite direction at the same DNA locus. The authors suggest that H3K9me maintains the genome integrity of repetitive elements by limiting the collision between DNA replication machinery and transcription machinery (Zeller *et al.*, 2016).

1.2.2.3 Links between recombination and histone modification

A correlation between H3K9me2 and initiation of meiotic recombination in *C. elegans* has been described by Reddy and Villeneuve (Reddy and Villeneuve, 2004). *him-17* encodes a protein containing six copies of a conserved C2CH motif, that is also found in P-element transposase (Liu and Maine, 2007; Reddy and Villeneuve, 2004). Mutations of *him-17* cause defects in recombination, including failure to form DSBs, chiasmata, or crossovers (Reddy and Villeneuve, 2004). In addition, *him-17* null mutants show reduced and delayed H3K9me2 accumulation in both hermaphrodites and males. These observations suggest a connection between DSB formation and H3K9me2 (Reddy and Villeneuve, 2004).

To gain more insights into potential linkage between H3K9me2 and DSB formation, the Dernberg group mapped the distribution of DSBs by performing RAD-51 ChIP-seq. They found an enrichment of DSBs on chromosome arms (Kotwaliwale *et al.*, 2013). H3K9me2 has also been shown to accumulate on chromosome arms genome-wide (Guo *et al.*, 2015; McMurchy *et al.*, 2017; Zeller *et al.*, 2016), similar to the distribution pattern of DSBs. However, a detailed comparison of the distribution pattern of DSBs and H3K9me2 at subtelomeric regions revealed an inverse correlation between these two features (Yu *et al.*, 2016). This finding indicates that the presence of H3K9me2

might inhibit the formation of DSBs. One more line of evidence supporting this possibility is the significant increase in meiotic recombination on chromosome arms in *met-2(0)* mutants, which lack H3K9me1/2 (Kotwaliwale *et al.*, 2013). Taking these findings together, it is highly possible that H3K9me2 might play an important role in restricting the genome wide distribution of DSBs.

γ-H2AX is another histone modification that has been linked to DSBs in several organisms, including *C. elegans*. The conserved chromatin mark γ-H2AX (a phosphorylated form of H2AX) has been proposed to play a key role in mediating the DNA repair process in both mitosis and meiosis. In response to DSBs induced by an exogenous source, such as IR (Irridiation), the phosphorylated form of H2AX is recruited to and incorporated at the corresponding site, which further leads to the recruitment of downstream DNA repair machinery (Burma *et al.*, 2001; Kobayashi, 2004; Paull *et al.*, 2000; Rogakou *et al.*, 1998). Once the DNA repair process is completed, γ-H2AX is dephosphorylated (Chowdhury *et al.*, 2005).

1.3. Small RNA pathways in *C. elegans*

1.3.1 Exogenous and endogenous siRNA pathways

RNA interference (RNAi) is a mechanism to regulate gene expression through both transcriptional and post-transcriptional regulation. In early studies, dsRNA was found to be more effective compared to sense or anti-sense RNA in silencing corresponding genes in *C. elegans* (Fire *et al.*, 1998). The strong potency and transgenerational effect of dsRNA treatment implied the existence of a catalytic or amplification process downstream. Studies in other organisms designed to understand the biochemical

components of the small RNA effector identified the RISC (RNA-induced silencing complex), which comprises a 22nt -26nt long guide RNA and an Argonaute protein (Hammond *et al.*, 2001). In *C. elegans*, forward genetic screens aiming to dissect the molecular pathway of RNA interference identified a set of Rde (<u>R</u>NAi <u>de</u>ficient) and Mut (<u>Mut</u>ator) genes (Ketting *et al.*, 1999; Tabara *et al.*, 1999). These factors were first shown to be involved in exogenous RNAi, where dsRNA is provided by an external source. Later, some of these genes were shown to be involved in endogenous RNAi, where the trigger dsRNA is generated from endogenous template. In the exogenous RNAi pathway, double-strand RNA introduced by feeding, soaking or injection is processed by DCR-1 (Dicer endonuclease), DRH-1/3 (dicer-related helicase-1/3) and RDE-1 (RNAi deficient) Argonaute protein complex into primary siRNAs (small interfering RNA), which then bind to their corresponding Argonaute and silence mRNA targets based on a base-pairing principle (Sijen *et al.*, 2001; Tabara *et al.*, 1999; Tabara *et al.*, 2002). RRF-1, an RNA-dependent RNA polymerase, synthesizes secondary siRNAs to amplify the silencing signal from the primary triggering siRNA in somatic tissue (Sijen *et al.*, 2001). In the endogenous RNAi pathway, templates derived from aberrant transcripts, transposons, and repetitive sequences are processed into 26G siRNAs, which are then loaded onto various Argonaute proteins to form RISC complexes (Duchaine *et al.*, 2006; Yigit *et al.*, 2006). Similar to the exogenous RNAi pathway, secondary siRNAs are synthesized by RNA-dependent RNA polymerases using the target mRNA as the template (Billi *et al.*, 2014). For example, EGO-1, a germline-specific RdRP, functions in collaboration with EKL-1 and DRH-3 to generate

secondary siRNAs that load onto CSR-1 Argonaute (Gu *et al.*, 2009; Smardon *et al.*, 2000).

1.3.2 Post-transcriptional gene silencing (PTGS) and transcriptional gene silencing (TGS)

In many organisms, small RNA-mediated mechanisms have been described as regulating gene expression at the post-transcriptional and transcriptional levels. Post-transcriptional silencing of gene expression occurs at the RNA level and involves microRNA, siRNA and piRNA. Briefly, in *C. elegans*, miRNA binds to the 3'UTR of its target mRNA and leads to translational repression by directing the silencing complex to its target, whereas siRNA binds to its target mRNA and mediate the decay of mRNA in most cases (Billi *et al.*, 2014). In contrast, TGS is executed via the establishment of heterochromatin status in the vicinity of the targeted gene or inhibition of transcription elongation (Billi *et al.*, 2014). TGS was first discovered in *Schizosaccharomyces pombe,* where it was shown to be involved in heterochromatin formation near the centromere (Creamer and Partridge, 2011). It is postulated that the RITS (RNA-induced transcription silencing) complex bridges RNAi and heterochromatin assembly (Creamer and Partridge, 2011). Nascent transcripts derived from centromeric repeats form dsRNA, which is then cleaved into siRNA. The RITS complex contains the siRNA, an Argonaute, and other proteins recognizing histone methylation, and it recruits histone modification activities (Creamer and Partridge, 2011).

TGS mediated by RNAi has also been described in *C. elegans*. Two distinct argonaute For example, a subset of 22G siRNAs are transported into the nucleus by the

Argonaute NRDE-3 (Nuclear RNAi deficient), where they associate with ERGO-1

Argonaute to form a complex that prevents transcription through driving the addition of

the repressive marker, H3K9me3, at target genomic loci (Gu *et al.*, 2012; Guang *et al.*,

2010). Also, our lab has reported that knocking out members of the CSR-1 22G siRNA

pathway (EGO-1, CSR-1, EKL-1, DRH-3) resulted in alteration of H3K9me2 distribution

in *C. elegans* germline (Maine *et al.*, 2005; She *et al.*, 2009). Gu *et al* (2009) reported

that DRH-3, EKL-1 and EGO-1 form a core RDRP complex that is required for 22G-

siRNA production. The 22G-siRNA generated by the complex is then loaded on to the

Argonaute CSR-1 to silence its target genes. (Claycomb *et al.*, 2009; Gu *et al.*, 2009). In

ego-1 null mutants, H3K9me2 did not appear to be enriched on unpaired chromatin

(Maine *et al.*, 2005). In *csr-1*, *drh-3* and *ekl-1* mutants, H3K9me2 marks were broadly

distributed on both paired and unpaired chromatin, in contrast to strong enrichment on

unpaired chromatin in wild type (She *et al.*, 2009). These observations suggest that the

heterochromatic states may be partly triggered by small RNAs.

Although it has been proposed that small RNA machinery regulates

heterochromatin assembly, there is no evidence suggesting a direct interaction between

components of the small RNA pathway and H3K9me2 methyltransferase. We speculate

that there might be a factor that bridges these two pathways. We sought to identify

MET-2 interactor that might connect these two pathways and allow us to further

understand the mechanism of how CSR-1 pathway impacts H3K9me2 distribution.

Note: Chapter II is a collaborative project between Maine lab in Syracuse

University and Yanowitz lab in University of Pittsburgh. The following people contributed

to this project: Xia Xu (Syracuse University) generated the anti-MET-2 antibody and

performed the MET-2 immunoprecipitation coupled with tandem MS sequencing Logan Russell (University of Pittsburgh) conducted the RAD-51 labelling, *dog-1* deletion assay, *unc-58* reversion assay, *smrc-1* trangenerational broods assay and part of the *smrc-1;spo-11* DAPI-staining body quantification; Eleanor Maine (Syracuse University) aided in construction of certain double mutants and in phenotypic analysis of *smrc-1* mutants; and Judith Yanowitz (University of Pittsburgh) designed and supervised the experiments carried out by Logan Russell.

■	HIM-3	▬	SYP-1
■	HTP-3	■	SYP-2
■	HTP-1		
■	HTP-2		
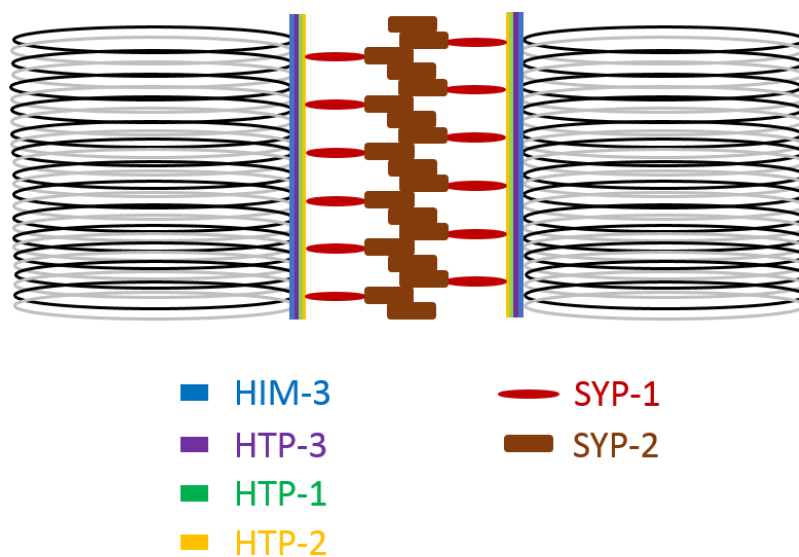
Figure 1.2. Model of synaptonemal complex (SC) assembly. The two homologous chromosomes (black and grey) were connected by the SC complex, which comprising the axial elements and the transverse elements. The axial elements are attached along the chromosomes, whereas the transverse elements containing SYP-1 and SYP-2 tie the axial elements together.

Chapter II. C. *elegans* SMRC-1 links DNA repair and chromatin regulation

2.1 Introduction

Histone methyltransferases carry out the addition of methyl-groups to histone tails. One common protein domain shared by most histone lysine methyltransferases is the evolutionarily conserved SET domain, which drives the catalytic activity. SETDB1 was identified as a histone H3 lysine 9 (H3K9) methyltransferase in human cells, where it is predominantly nuclear (Schultz *et al.*, 2002). Characterization of SETDB1 in chromatin regulation has revealed its major role in heterochromatin establishment and maintenance (Matsui *et al.*, 2010; Schultz *et al.*, 2002). For example, mammalian SETDB1 is recruited by methyl-CpG binding protein, MDB1, during DNA replication to deposit H3K9me2 on newly synthesized histone H3 to reinforce heterochromatin assembly (Sarraf and Stancheva, 2004). MET-2, the sole *C. elegans* member of the SETDB1 family, has been shown to be responsible for germline and embryonic H3K9me2 (Andersen and Horvitz, 2007). In *C. elegans*, SET-25 is the histone methyltransferase primarily responsible for H3K9me3 (Andersen and Horvitz, 2007; Bessler *et al.*, 2010; Towbin *et al.*, 2012). H3K9me3 is substantially reduced in *met-2* mutants, and evidence suggests that H3K9me2 is a necessary precursor to H3K9me3 at many sites (Towbin *et al.*, 2012).

Mapping studies have demonstrated preferential H3K9me2 accumulation at certain classes of repetitive sequence across the genome (Guo *et al.*, 2015; Zeller *et al.*, 2016). H3K9me3 has a similar, although distinct distribution (Liu *et al.*, 2011; McMurchy *et al.*, 2017; Towbin *et al.*, 2012; Zeller *et al.*, 2016). Immunolabeling studies reveal an intriguing pattern of H3K9me2 accumulation during meiosis. In particular, H3K9me2

accumulates preferentially on chromatin regions that do not synapse, including the male

X chromosome, other chromosomes or large chromosomal regions that fail to synapse

due to mutation or genomic rearrangement, and extrachromosomal arrays (Bean *et al.*,

2004; Kelly *et al.*, 2002; Maine *et al.*, 2005). The abundance and distribution of

H3K9me2 is altered in certain small RNA pathway mutants (Maine *et al.*, 2005; She *et al.*, 2009).

Transcriptomic studies suggest that H3K9me2 has little impact on the transcript

profile of protein-coding genes (Guo *et al.*, 2015; McMurchy *et al.*, 2017; Zeller *et al.*,

2016), but correlates with elevated expression of certain repetitive sequences

(McMurchy *et al.*, 2017; Zeller *et al.*, 2016). Moreover, H3K9 methylation may play an

indirect role in limiting R-loop formation and, subsequently, DNA replication stress at

repetitive sequences (Zeller *et al.*, 2016).

In order to understand how MET-2 activity is targeted, we sought to identify factors

associated with MET-2 *in vivo*. Here we describe one such factor, SMRC-1. SMRC-1

is the sole *C. elegans* ortholog of vertebrate SMARCAL1 (SWI/SNF-related, matrix

associated, actin-dependent regulator of chromatin, subfamily A-like 1). SMARCAL1

and its *Drosophila* ortholog, MARCAL1/HARP, are helicases with rewinding (annealing)

activity (Bansbach *et al.*, 2009; Kassavetis and Kadonaga, 2014; Yusufzai and

Kadonaga, 2008). SMARCAL1-related proteins comprise a distinct subfamily of

SWI/SNF ATPases and are thought to protect genome integrity by promoting the repair

and restart of stalled DNA replication forks (Betous *et al.*, 2012; Lugli *et al.*, 2017; Poole

and Cortez, 2016). *In vitro*, SMARCAL1 proteins bind single strand (ss) DNA and have

rewinding helicase activity on RNA:DNA substrates and DNA:DNA substrates, e.g.,

replication forks and D-loops at Holliday junctions (Betous *et al.*, 2012; Kassavetis and

Kadonaga, 2014). Although SMARCAL1 has no reported role in meiosis, it presumably

functions in pre-meiotic S phase, and it has been shown to interact with proteins that

function in homologous recombination, e.g. RPA (Ciccia *et al.*, 2009). We detect both

SMRC-1 and MET-2 in nuclei throughout the germ line. Loss of SMRC-1 function

disrupts germline development and embryogenesis and elevates sensitivity to DNA

damage and replication stress. Meiotic recombination is altered in *smrc-1* mutants, and

meiotic H3K9me2 levels drop in *smrc-1* mutants over successive generations. Sterility

is nearly 100% in *smrc-1 met-2* double mutants and replication stress is enhanced.

Taken together, our data suggest an essential link between chromatin state and

annealing helicase activity in the germ line.

2.2 RESULTS

2.2.1 MET-2 is present in germ cell nuclei

To investigate MET-2 regulation, we generated a series of reagents to evaluate the distribution of MET-2 in the germ line. These include polyclonal antibody generated against MET-2 peptide, GFP- and 3xFLAG-tagged *met-2* transgenes inserted by *mosI*-mediated single copy insertion (mosSCI) (Frokjaer-Jensen *et al.*, 2008), and 3xFLAG-tagged endogenous *met-2* generated by CRISPR-Cas9 (see Experimental Procedures) (Arribere *et al.*, 2014; Paix *et al.*, 2014b). Immunolabeling with each of these reagents detects germline MET-2 primarily in nuclei, both for the male and hermaphrodite (Figure 1A, B) (Experimental Procedures). In addition, anti-MET-2 antibody also detects some nuclear and cytoplasmic puncta. Anti-MET-2 labeling does not detect nuclear signal or cytoplasmic puncta in *met-2(n4256)* gonads, indicating these signals are specific for MET-2 (Figure 2.1A). Similarly, epitope-tagged MET-2 is detected most strongly in the nucleus and in weak cytoplasmic foci (Figure 2.1B). We conclude that most germline MET-2 localizes to nuclei, although a cytoplasmic pool is present as well. We note that a previous study of MET-2 activity in the embryo reported the presence of mCherry-tagged MET-2 exclusively in the cytoplasm (Towbin *et al.*, 2012). As our reagents detect embryonic MET-2 in both nuclei and cytoplasm (B. Mutlu and S. Mango, personal communication), we hypothesize that the mCherry epitope may be removed prior to nuclear import.

Nuclear MET-2 appears to be relatively punctate during mitosis and leptotene-zygotene stages of first meiotic prophase and become more diffuse throughout the nucleoplasm as nuclei move through pachytene (Figure 2.1). To better visualize MET-2

relative to chromatin, we performed confocal microscopy of tissue spreads

(Experimental Procedures). In both hermaphrodites and males, the MET-2 signal

appears almost exclusively in the nucleoplasm and not associated with chromatin

(Figure 2.1B; Figure 2.2C). This nucleoplasmic distribution resembles that observed for

several other histone-modifying enzymes in *C. elegans*, e.g., the MES-2/3/6 complex

that methylates H3K27 (Holdeman *et al.*, 1998; Korf *et al.*, 1998; Xu *et al.*, 2001). We

conclude that any association of MET-2 with chromatin is transient.

2.2.2 MET-2 associates with SMRC-1

We took a co-immunoprecipitation (co-IP) approach to identify factors that associate

with MET-2 in the germ line (see Experimental Procedures). We first verified the

specificity of our anti-MET-2 antibody on protein blots containing wild type and *met-2(n4256)* whole worm extracts (Figure 2.1C). Anti-MET-2 antibody detected a protein at

~150 kD in wild type extract that was absent from *met-2(n4256)* extract (Figure 2.1C).

Consistent with indirect immunofluorescence detection of a non-specific signal in *met-2(n4256)* tissue, we detected a protein of ~100 kD in *met-2(n4256)* extract.

   Our co-IP strategy was to use protein extracts prepared from adult *him-8* (high

incidence of males) mutants in an attempt to enrich for factors that might be important

for targeting MET-2 activity to unsynapsed chromosomes. As a negative control, we

performed the IP with protein extract generated from adult *met-2(n4256)* mutants. In

him-8 mutant hermaphrodites, the X chromosomes typically fail to pair and synapse

during meiosis, leading to production of a high proportion of nullo-X gametes and,

therefore, male progeny (Phillips *et al.*, 2005). H3K9me2 is enriched on these

unsynapsed X chromosomes in both male and hermaphrodite *him-8* mutants (Bean *et al.*, 2004; Kelly *et al.*, 2002). We performed an anti-MET-2 protein blot to verify the recovery of MET-2 in our co-IP experiments (Figure 2.1C) and then identified proteins in the co-immunoprecipitate via tandem mass spectrometry (see Experimental Procedures). One candidate of interest was SMRC-1, the *C. elegans* SMARCAL1 ortholog. To verify an association between MET-2 and SMRC-1, we used CRISPR-Cas9 to add a triple *flag* sequence to the endogenous *smrc-1* gene (see Experimental Procedures). We prepared extracts from adults, performed anti-FLAG IP, and subjected the recovered proteins to anti-MET-2 immunoblot. We consistently detected MET-2 in the 3xFLAG::SMRC-1 co-IP (Figure 2.2A).

2.2.3 SMRC-1 is expressed throughout the germ line

We evaluated germline expression of 3xFLAG::SMRC-1 by performing anti-FLAG immunolabeling. We note that these animals appear to develop normally and have brood sizes similar to controls (see Table 2.1), suggesting the epitope tag does not noticably impact SMRC-1 function. We detect 3xFLAG::SMRC-1 in proliferative and meiotic germ cells in XX and XO animals, primarily in nuclei (Figure 2.2C). Labeling intensity drops in nuclei that are actively undergoing mitotic division or are leptotene-zygotene stage (transition zone). The signal is relatively strong in late-stage oocyte nuclei, suggesting that embryos may inherit substantial amount of SMRC-1.

In mitotic and early meiotic nuclei, we detect 3xFLAG::SMRC-1 primarily in nuclei although not preferentially on chromatin (Figure 2.2B,C). The signal increases in pachytene nuclei where it does not appear to be enriched on chromatin (Figure 2.2B,

C). In condensation phase spermatogenesis, SMRC-1 primarily locates at the nuclear

periphery, dissociated from chromatin (Figure 2.2B). In oocytes, the signal appears

evenly distributed within the nucleus (Figure 2.2C). To better visualize SMRC-1 relative

to MET-2, we generated a *3xmyc::smrc-1 3xflag::met-2* strain (Experimental

Procedures). Consistent with single labeling experiments, co-labeling for

3xMYC::SMRC-1 and 3xFLAG::MET-2 suggested some overlap between the two

proteins in the nucleoplasm (Figure 2.2D). We also note that SMRC-1 puncta are not

observed, in contrast with MET-2 puncta present in some nuclei.

2.2.4 SMRC-1 limits sensitivity to DNA replication stress

To evaluate the biological function of *smrc-1*, we generated *smrc-1* mutations using the

CRISPR-Cas9 system (see Experimental Procedures, Figure 2.S1) (Arribere *et al.*,

2014; Paix *et al.*, 2014b). We generated: a nonsense allele, *om136*; two frameshift

alleles, *om138* and *ea8*; and a deletion allele, *ea46* (Figure 2.S2). Given the predicted

significant truncation of SMRC-1 protein by all three point mutations, and the predicted

deletion of SMRC-1 by *ea46*, we expect all four to be null alleles. We outcrossed and

balanced the mutations prior to characterizing the phenotype.

In mammals, SMARCAL-1 plays a crucial role in resolving replication fork stress

induced by DNA damage (Bansbach *et al.*, 2009; Boerkoel *et al.*, 2002; Ciccia *et al.*,

2009; Elizondo *et al.*, 2009; Postow *et al.*, 2009). Therefore, we asked whether *smrc-1*

mutants would manifest defects in DNA damage repair. To examine the role of *smrc-1*

in resolving replication stress, we exposed wild type *smrc-1* mutants to a replication fork

stalling -inducing agent, hydroxyurea (HU). The survival rate of L1 animals post HU

exposure reflects their ability to resolve the DNA lesions and resume development. At

25 mM HU, the survival rate of *smrc-1* mutants decreased significantly compared to wild

type (Figure 2.3A). Among adult *smrc-1* survivors of the 2.5 mM treatment, 46% were

sterile, and this effect increased with increasing HU concentration to 100% at 25 mM

(Figure 2.S3). In contrast, sterile wild type escapers were not observed at HU

concentrations lower than 25 mM (Figure 2.3A). Hence, in *smrc-1* mutants, both

somatic tissues and germline appear more susceptible to replication stress than

wildtype. This hypersensitivity suggests a prominent role for SMRC-1 in limiting DNA

replication stress.

In human cells, SMARCAL1 was found to localize to stalled replication forks and

form foci in response to HU treatment (Bansbach *et al*., 2009). To test whether SMRC-

1 shares a similar distribution pattern, we compared the localization pattern of

3xFLAG::SMRC-1 after a 24 hour 25mM HU treatment of L4 animals to a no treatment

control.

2.2.5 *smrc-1* mutants have elevated germline apoptosis

DNA damage has been shown to induce germ cell apoptosis in *C. elegans* (Gartner *et

al*., 2000). We observed elevated germ cell apoptosis in *smrc-1*, as measured by CED-

1::GFP expression, which marks cells during early apoptosis (Zhou *et al*., 2001) (Figure

3C), and by staining with the vital dye, acridine orange (Figure S4). Elevated *ced-1::gfp*

expression was particularly evident throughout the germ lines of *smrc-1* sterile adults

raised at 25°C (Figure 2.3C). We hypothesized that germ cells die as a consequence of

DNA damage accumulating in the absence of SMRC-1 activity. To test this idea, we

examined whether germ cell apoptosis was suppressed by the absence of CEP-1, an essential component of the DNA damage checkpoint machinery active in late pachytene stage (Schumacher *et al.*, 2001). The increase in germ cell apoptosis is completely suppressed in *cep-1; smrc-1* double mutants (Figure 2.3C). In contrast, apoptosis is not significantly suppressed by the inactivation of PCH-2 (Figure 2.S4), a component of the machinery that monitors unpaired pairing centers (Bhalla and Dernburg, 2005). We conclude that unrepaired DNA damage occurring in *smrc-1* mutants causes elevated germline apoptosis by triggering the DNA damage checkpoint.

2.2.6 *smrc-1* mutants have germline development defects

Analysis of *smrc-1* mutants revealed temperature- sensitive defects in the germ line, including reduced fecundity, an increased frequency of males, and embryonic lethality (Tables 2.1-2). In general, these defects are more severe in the absence of maternal *smrc-1(+)* product. *smrc-1(-/-)* offspring (F1 generation) of *smrc-1(+/-)* mothers are viable and fertile (Table 2.1, Table 2.S1). We refer to these animals as *smrc-1(M+Z-)* to indicate that they received wild type maternal gene product. Although fertile, they produce fewer embryos than wild type controls (Table 2.1). Their *smrc-1(M-Z-)* progeny, who do not inherit wild type maternal product, include some that die as embryos (~29% for *om136* at 25°C, Table 2.1), others that develop as sterile adults (~8% for *om136* at 25°C, Table 2.2), and a high incidence of males (a Him phenotypes; ~4.5% male offspring for *om136* at 25°C, Table 2.1). Those that develop as fertile hermaphrodites produced fewer embryos than M+Z- animals, and a significantly lower percentage of those embryos are viable (Table 2.1).

To investigate the developmental cause(s) of *smrc-1(M-Z-)* sterility, we DAPI-

stained a set of sterile adult hermaphrodites and evaluated their germline phenotypes.

Some gonad arms have very few germ cells and do not contain gametes (39%, n=41);

in some cases, these germlines are disorganized and contain nuclei with abnormal

morphology and/or that appear to be degenerating. Presumably these germlines are

undergoing extensive apoptosis. In contrast, some gonad arms have relatively normal

germline organization, but lack sperm, oocytes, or both gamete types (61%, n=41). In

cases where oocytes and sperm are present, typically some of the oocytes are

endomitotic (Emo). This phenotype reflects a defect in ovulation, sperm-egg interaction,

or egg activation (Geldziler *et al.*, 2011) and can be the direct or indirect result of

gamete defects.

The *C. elegans* Him phenotype results from impaired meiotic chromosome

segregation leading to production of nullo-X gametes. Consistent with this possibility,

we observe a mixture of bivalent and univalent chromosomes at diakinesis in *smrc-1*

mutants, as described below. A common cause of this phenotype is crossover failure,

leading to premature dissociation of bivalents at diakinesis (Broverman and Meneely,

1994). To investigate if the *smrc-1* Him phenotype might also reflect impaired

recombination, we assayed recombination frequency in control and *smrc-1* animals in

two intervals on chromosome I (Figure 2.3D). Our data indicate a ~3 to 4-fold increase

in recombination in at least some regions within the gene cluster in *smrc-1* mutants

compared with controls (Figure 2.3D). This altered recombination rate may reflect an

increased abundance of DSBs, a shift in the balance of crossover (CO) vs non-

crossover (NCO) repair, and/or a change in the placement of DSBs/COs in the *smrc-1*

27

mutant. We investigated recombination further by evaluating COSA-1 foci in the *smrc-1*

background. COSA-1 protein promotes CO events and typically associates with

homologous chromosomes at the single site of crossover (Yokoo *et al.*, 2012). We

evaluated GFP::COSA-1 foci in *gfp::cosa-1;smrc-1(om136)* animals and did not observe

an increased number (data not shown).

2.2.7 SMRC-1 activity limits formation of SPO-11-independent DSBs

We considered whether the loss of SMRC-1 function during DNA replication might lead

to DSB formation that, in germline stem cells, could carry over into meiosis and impact

the recombination rate. In early *C. elegans* meiosis, SPO-11 initiates DSB formation at

multiple sites along the chromosome; most DSBs are repaired via non-crossover, but

one DSB per chromosome is repaired via crossover (Dernburg *et al.*, 1998; Hillers *et al.*,

2015). In the absence of SPO-11 activity, chiasmata do not form, and bivalents

prematurely dissociate at diakinesis (Dernburg *et al.*, 1998; Hillers *et al.*, 2015).

Introduction of DSBs from exogenous sources, such as ionizing radiation treatment, can

partially rescue the chiasmata formation defect in *spo-11* mutants (Dernburg *et al.*,

1998; Hillers *et al.*, 2015).

    We took advantage of the *spo-11* phenotype to test whether mitotic DNA damage

in *smrc-1* mutants might include DSBs that carry through to impact meiosis. We

generated *smrc-1; spo-11* double mutants and evaluated their diakinesis chromosomes

(see Experimental Procedures). For consistency, we assayed the most proximal oocyte

(at the -1 position) in each gonad arm. In *smrc-1(ea8)* and *smrc-1(om138)* single

mutants, we observed 4-7 DAPI-bright bodies (Figure 4A). Faint links were sometimes

visible between what appear to be distinct chromosomes, suggesting aberrant joining of DNA between non-homologous chromosomes, perhaps as a result of damage-related DSBs. The presence of 7 DAPI-bright bodies is consistent with production of occasional male offspring. In *smrc-1(om138);spo-11(ok79)* double mutants at 25°C, we observed a 5-12 DAPI-bright bodies, again with faint links between some chromosomes, consistent with production of damage-related DSBs (Figure 2.4A). Hence, SMRC-1 activity appears to limit production of DSBs that would allow inappropriate connections between chromosomes.

RAD-51, the ssDNA binding protein that facilitates homology search during homologous recombination, associates with ssDNA adjacent to DSBs and promotes their repair (Rinaldo *et al.*, 2002). We performed anti-RAD-51 labeling to evaluate the distribution of DSBs in the *smrc-1(om138)* germ line. We observed RAD-51 foci primarily in meiotic nuclei and more rarely in mitotic nuclei, similar to wild type controls (Figure 2.4B). However, foci persist longer than in wild type controls, suggesting that DSB repair is delayed. Moreover, the number of foci was elevated in *smrc-1(om138)* compared with wildtype, particularly in the M-Z- (F2) generation. These results are consistent with *smrc-1* mutants containing both SPO-11-mediated and DNA damage-associated DSBs.

We used RAD-51 labeling to evaluate DSB distribution in *smrc-1;spo-11* germ lines. As expected, we detected very few RAD-51 foci in association with meiotic chromosomes in the *spo-11(ok79)* germ line ((Alpi *et al.*, 2003); Figure 2.4B). In contrast, we observed RAD-51 foci within the mitotic and meiosis I prophase regions in *smrc-1(om138);spo-11(ok79)* and *smrc-1(om136);spo-11(me44)* germ lines; these foci

presumably represent DSBs that formed as a consequence of DNA damage during mitotic or pre-meiotic S phase and subsequently undergo repair during meiosis (Figure 2.4B). Overall, the presence of elevated RAD-51 foci in *smrc-1;spo-11* relative to *spo-11* is consistent with the diakinesis chromosome counts described above.

Analysis of the proliferative germ line is consistent with *smrc-1(0)* lesions being processed differently from SPO-11-induced DSBs. The number of RAD-51 foci within the proliferative germ line was greater in wild type and *spo-11(ok79)* than in *smrc-1;spo-11* double mutants. This result might indicate a delay in RAD-51 binding to DNA breaks formed as a consequence of the *smrc-1* mutation. In addition, the number of RAD-51 foci in the proliferative zone was greater in *smrc-1;spo-11* than in the *smrc-1* M-Z- single mutant, perhaps indicating an increased sensitivity to DNA damage in the absence of SPO-11.

2.2.8 SMRC-1 limits accumulation of poly G/C tract deletions

DOG-1 (deletions of G-rich DNA), a helicase related to human FANCJ, is essential for proper replication of poly G/C tracts in *C. elegans* (Cheung *et al.*, 2002). Proteins that function in the recombination checkpoint or homologous recombination, e.g., CEP-1 and XPF-1, are implicated in maintaining poly G/C tract integrity in *dog-1* mutants (Youds *et al.*, 2008; Youds *et al.*, 2006). We evaluated poly G/C tract integrity in a *smrc-1; dog-1* background by assessing the deletion rate within the G/C-rich exon 5 of the *vab-1* gene (see Experimental Procedures). We observed a significantly increased frequency of animals with *vab-1* deletions in *smrc-1; dog-1* double mutants compared to *dog-1* single mutants at both 20°C (~1.8-fold) and 25°C (~2.0-fold) (Figure 2.4C). As a control, we did not observe accumulation of *vab-1* deletions or insertions in either *smrc-1(ea8)* or

smrc-1(ea46) single mutants. We conclude that SMRC-1 activity limits the

accumulation of deletions with poly G/C regions and has a particularly important

function in the absence of DOG-1 activity.

In *C. elegans*, mutations that result in accumulation of DNA damage, due to either

an increased number of DNA lesions or impaired DNA damage repair machinery, are

classified as "mutators" (Ketting *et al.*, 1999; Yanowitz, 2008). Since our data suggest

that SMRC-1 activity limits accumulation of DNA damage, we asked whether SMRC-1

limits accumulation of mutations broadly. We assayed for reversion of the dominant

unc-58(e665) phenotype in a *smrc-1* mutant background (see Experimental

Procedures). *unc-58* reversion assay allows detection of intragenic and extragenic

suppressors and is commonly used to quantify mutator activity (Harris *et al.*, 2006b).

Indeed, at both 20°C and 25°C, we observed an increase in the *unc-58* reversion

frequency of ~3.3-fold and ~4.9-fold, respectively, in a *smrc-1* mutant background

compared to wild type (Figure 2.4D).

2.2.9 Fertility decreases over successive *smrc-1* generations

Because *smrc-1* mutants have an elevated mutation rate, we were interested in

determining the long-term viability and fertility of *smrc-1* strains. We serially passaged

16 *smrc-1* lines at 25°C, recording brood size in each generation (see Experimental

Procedures). To eliminate bias, we passaged the first L4 larva at each generation; if

that animal developed as a sterile adult, we rescued the line by passaging a fertile

sibling. Among the 16 serial lines, we observed a broad range in fecundity at each

generation, ranging from 0 to >100 offspring (Figure 2.5A). Although many lines had to

be rescued once or twice over the course of 30 generations, only five of the 16 lines were successfully passaged without rescue (Figure 2.5A). The *smrc-1* mutant populations also trend toward reduced fecundity in progressive generations. The occasional "rescue" events seen across generations are attributed to our protocol of eliminating sterile animals. These populations also appear to get sicker with passaging. We hypothesize that *smrc-1* mutant strains accumulate mutations over time that reduce health and fertility.

2.2.10 The impact of *smrc-1* loss on germline H3K9me2

We assessed the extent to which loss of SMRC-1 activity impacts H3K9me2 distribution in the germ line by performing indirect immunofluorescence experiments (see Experimental Procedures). We examined *smrc-1(om136)* XX and XO germlines in the F2 M-Z- generation as well as the serially passaged lines described above. We also generated *smrc-1(om136)/qC1; him-8* strains in order to examine H3K9me2 on the non-synapsed X chromosomes in hermaphrodites. In early generations, the H3K9me2 labeling pattern appears comparable to wild type in both *smrc-1* XX and XO germ cells (Figure 2.5B). However, in animals passaged for 30 serial generations, we observed a marked decline in H3K9me2 labeling in many individuals (Figure 2.5C). In *smrc-1(ea8)* XO males at F30, 43% of the germlines examined from five independently passaged lines exhibited a much reduced H3K9me2 signal compared to wildtype, whereas 57% exhibited an intensity similar to wild type (n=21) (Figure 5C). Similarly, in *smrc-1(ea8)* hermaphrodites at F30, 30% of germlines examined from these lines exhibited a much

reduced H3K9me2 signal compared to wildtype, whereas 70% exhibited an intensity similar to wild type (n=20) (Figure 2.5C).

2.2.11 *met-2* loss of function enhances *smrc-1* sterility

We investigated the genetic relationship between *smrc-1* and *met-2* by using a CRISPR/Cas9 approach to generate a *smrc-1 met-2* double knockout (Experimental Procedures) and assaying the phenotype in parallel with *met-2* and *smrc-1* single mutants. Typically, the *smrc-1 met-2* M+Z- progeny of *smrc-1 met-2/qC1* heterozygotes were fertile even under conditions of temperature stress (Table 2.2). However, ~90% of their *smrc-1 met-2* M-Z- progeny were sterile at 25°C (Table 2.2), and the brood size of rare fertile M-Z- animals was very small (Table 2.1). In addition, ~43% of *smrc-1 met-2* M-Z- animals had a protruding vulva (Pvl phenotype; Table 2.2). Interestingly, DNA damage is also known to cause abnormal vulva precursor cell death (Weidhaas *et al.*, 2006). Therefore, the Pvl phenotype may reflect death of vulval precursor cells due to elevated DNA damage in the *smrc-1 met-2* background. In contrast to the double mutant, *met-2* and *smrc-1* strains very gradually produce fewer progeny over numerous generations (Andersen and Horvitz, 2007); this study). The *smrc-1 met-2* phenotype is consistent with SMRC-1 and MET-2 acting redundantly to promote one or more essential germline process(es), e.g., to limit DNA damage and/or limit recombination at repetitive regions.

To investigate the germline defects in *smrc-1 met-2* double mutants, we DAPI-stained sterile hermaphrodites and examined their germline development. Germ cells were present in 100% of the 70 gonad arms examined. 24% (17/70) of gonad arms

exhibited a somatic defect wherein the distal tip cell did not appear to have migrated properly and germ cells were clustered in the vicinity of the vulva; no gametes were present. Somatic gonad development appeared normal in the remaining gonad arms (53/70), and most (48/70) contained gametes. Specifically, 23 arms contained sperm but no oocytes, 23 arms contained sperm and Emo oocytes, and 2 arms contained sperm and non-Emo oocytes. Thus, numerous developmental defects underlie the *smrc-1 met-2* sterility.

We considered that the *smrc-1 met-2* double mutants might have elevated sensitivity to DNA replication stress. We assayed their sensitivity to HU treatment in parallel with *met-2(n4256)* single mutant and wild type controls. With respect to survival, *met-2(n4256)* mutants showed mildly elevated sensitivity compared with wild type at doses of 2.5-10 mM HU; at 25 mM HU, *met-2* sensitivity is similar to wild type (Figure 2.3A). In contrast, the *smrc-1 met-2* double mutant exhibited higher HU sensitivity than *smrc-1* single mutants, especially at the 5-10 mM HU treatment range (Figure 3A; see legend). This result is all the more notable in that we had to test *smrc-1(M+Z-) met-2* animals (because most *smrc-1(M-Z-) met-2* animals are sterile), where maternal SMRC-1 product may have afforded some protection from the HU exposure. In contrast to viability, the impact of HU treatment on fertility of survivors was similar in *smrc-1 met-2* doubles and *smrc-1* controls (Fig. 2.3A). This result suggests that the developmental sterility we observe in *smrc-1 met-2* mutants is not linked to an increase in sensitivity to replication stress.

2.2.12 The relationship between SMRC-1 and SET-25 activity

SET-25 is the *C. elegans* histone methyltransferase responsible for H3K9 trimethylation (Towbin *et al.*, 2016). To test whether loss of H3K9me3 has a synergistic effect on *smrc-1* phenotypes, we constructed a *smrc-1 set-25* double mutant. 8.5% of *smrc-1 set-25* hermaphrodites were sterile at 25°C (n=433), a figure not significantly different from *smrc-1* single mutants (Table 2.2). Moreover, the sterile phenotype resembles that observed in *smrc-1* single mutants, and we did not observe obvious somatic defects. One interpretation of these results is that SMRC-1 and SET-25 act in a common pathway with respect to some functions. If so, we reasoned that *set-25* mutants might be sensitive to HU treatment, and this sensitivity would not increase in *smrc-1 set-25* mutants. We evaluated HU sensitivity of these strains using the L1 treatment strategy described above. The *set-25* single mutant strain behaved similarly to wild type with respect to viability and fertility (Figure 2.3A). With respect to viability, the *smrc-1 set-25* double mutant strain had a sensitivity intermediate between *smrc-1* and *smrc-1 met-2* over the 5-10 mM HU range, but was similar to *smrc-1* single mutants at 25 mM HU (Figure 2.3A). With respect to fertility, *smrc-1* and *smrc-1 met-2* animals had similar sensitivity to HU treatment (Fig. 2.3A). Overall, our results suggest MET-2 and SET-25 activities both help to ameliorate the impact of DNA replication stress caused by loss of SMRC-1 activity during larval development under milder (2.5-10 mM HU) conditions. In contrast, MET-2 and SET-25 activities do not have protective effects in the soma under more stressful conditions (25 mM HU treatment) or in the germ line under any condition we tested.

The *met-2(n4256) set-25(tm5021)* double mutant has previously been described

as having slow growth and embryonic lethality at 25°C, as well as elevated HU

sensitivity and elevated CEP-1-dependent germline apoptosis (Zeller *et al.*, 2016).

Although these defects are similar to those we observed for *smrc-1* and *smrc-1 met-2*,

sterility was not reported for *met-2 set-25.* We generated the *met-2(n4256) set-

25(tm5021)* double mutant and grew it in parallel with *smrc-1 met-2* and *smrc-1 set-25*

to compare germline development in these three strains. At 25°C, embryonic lethality

was very high in *met-2 set-25* double mutants, as reported, and adult escapers were

fertile (Table 2.2). Similarly, *met-2 set-25* individuals were fertile when raised at 20°C.

Similarities in the *smrc-1 met-2* and *met-2 set-25* may reflect shared function of SMRC-

1 and SET-25; differences in phenotype might reflect from the participation of these

proteins in additional, independent processes. We hypothesize that the very serious

germline developmental defects in *smrc-1 met-2* mutants may result, at least in part,

from a reduced ability to repair DNA damage.

2.3 DISCUSSION

2.3.1 SMRC-1 limits DNA replication stress

Here we report that *C. elegans* SMRC-1 physically associates with the histone methyltransferase, MET-2, and that mutations in the two genes have a highly penetrant synthetic sterile phenotype. We also report that SMRC-1 activity limits DNA replication stress, consistent with the proposed role of SMARCAL1 family proteins in other species (reviewed by Poole and Cortez, 2016). Mutations in *smrc-1* cause elevated sensitivity to the replication fork stressor, hydroxyurea, and nuclear SMRC-1 abundance increases in mitotic germ cell nuclei in response to DNA replication stress. Related to these observations, *smrc-1* mutations enhance the occurrence of poly G/C tract deletions in the *dog-1* mutant background. It has been suggested that secondary structure at poly G/C tracts promotes replication fork stalling (Arthanari and Bolton, 2001), and DOG-1 functions to prevent the formation of such G-rich secondary structures (Youds *et al*., 2006). We suggest that *smrc-1* is essential for maintaining the integrity of the G-rich genome, most likely by resolving stalled replication forks. Recent studies in human cultured cells showed that an endogenous source of replication stress, telomeres, require SMARCAL1 activity (Cox *et al*., 2016).

2.3.2 What are the possible functions of SMRC-1 in meiosis?

SMRC-1's presence in meiotic nuclei is consistent with it having an additional function distinct from DNA replication. Most studies of SMARCAL1 function have been performed in mitotic cells, and mammalian SMARCAL1 was shown to associate with the ssDNA binding protein, RPA, during DNA replication and catalyze replication fork

regression, ultimately promoting branch migration (Betous *et al.*, 2013; Betous *et al.*, 2012; Bhat *et al.*, 2015; Yusufzai and Kadonaga, 2008). However, Holliday junctions are also present during meiotic recombination, and the *C. elegans* RPA protein, RPA-1, is detected in pachytene nuclei and promotes meiotic DSB repair (Martin *et al.*, 2005). The elevated meiotic recombination that we observed in *smrc-1* mutants (Figure 2.3D) may result from unresolved DSBs carried through from mitotic cells and/or enhanced crossover (CO) in meiotic cells. Our RAD-51 labeling data (Figure 2.4B) and analysis of *smrc-1;spo-11* diakinesis nuclei (Figure 2.4A) indicate that mitotic DSBs occurring in the absence of SMRC-1 activity can result in COs. Interestingly, we noticed a late-pachytene persistence of RAD-51 foci in *smrc-1* mutants, which implies that aberrant DSB repair is delayed in the absence of SMRC-1 activity. In *C. elegans*, the process of CO homeostasis ensures that most DSBs are repaired via a non-crossover (NCO) mechanism and only one DSB per chromosome is resolved via CO (Hillers *et al.*, 2015). Human SMARCAL1 promotes DSB repair via non-homologous end joining (NHEJ) in cultured cells (Keka *et al.*, 2015), and *Drosophila* Marcal1 mediates the synthesis-dependent strand annealing (SDSA) step in DNA (Holsclaw and Sekelsky, 2017). Perhaps SMRC-1 functions to limit meiotic recombination by promoting NCO repair.

2.3.3 SMRC-1 – MET-2 associations in mitosis versus meiosis

Several lines of evidence indicate that H3K9 methylation limits transcription and recombination at repetitive sequences. H3K9me2 strongly associates with certain classes of repetitive sequence (Guo *et al.*, 2015; McMurchy *et al.*, 2017; Zeller *et al.*, 2016). In *met-2 set-25* double mutants, which lack H3K9 methylation, transcripts from

those repetitive elements are detected at increased abundance and indels accumulate within the same repetitive regions (Zeller *et al.*, 2016). In this current study, the physical association between MET-2 and SMRC-1 directly links DNA repair and heterochromatin regulation. During DNA replication, we propose that SMRC-1 bound to the leading strand at stalled replication forks recruits and/or stabilizes MET-2 activity ahead of the replication fork, and this interaction may be especially prevalent at repetitive regions (see Figure 5D). MET-2-mediated H3K9me2 may reduce the rate of DNA replication progression to assure the complete and accurate replication of the error-prone repetitive sequences. MET-2 recruitment/ stabilization may function as a positive feed-back loop to attract more SMRC-1, thus reinforcing replication fidelity. Additionally, reestablishing the heterochomatic status on the duplicated chromatin has been shown to be important for maintaining genome stability (Gonzalez and Li, 2012; Li and Zhang, 2012; Margueron and Reinberg, 2010). Histone methylation, such as H3K9me2/3, is one of defining modifications associated with heterochromatin. SETDB1, the homolog of MET-2 in mammalian systems, has been shown to be recruited to the nascent chromatin to methylate histones (Alabert and Groth, 2012). Thus, we propose that at the stalled replication fork, SMRC-1 might be targeting MET-2 to the newly assembled nucleosomes to deposit H3K9me2. Therefore, the MET-2 and SMRC-1 association might maintain the genome integrity both ahead and behind the replication fork.

In the meiotic germ line, the SMRC-1 - MET-2 association might prevent or limit unequal crossing over at repetitive regions (see Figure 5D). Through ChIP-seq analysis of RAD-51 distribution, Yu *et al.* (2016) mapped the distribution pattern of meiotic DSBs. RAD-51 is enriched on chromosomal arms, but inversely correlated with repetitive

sequences that are also enriched on chromosome arms (Yu *et al.*, 2016). This disparity

is consistent with the idea that H3K9me2 may prevent formation of DSBs, and hence

recombination, at repetitive sequences. Consistent with this idea, meiotic

recombination is increased at chromosome arm regions in *met-2* mutants (Yu *et al.*,

2016). We suggest that SMRC-1 may participate in this mechanism to prevent

recombination at repetitive regions. The association between MET-2 and SMRC-1

could serve as a surveillance system to prevent DSB formation at repetitive regions,

thus limiting the occurrence of CO at these sequences.

2.4 Methods

Nematode culture and genetic

Standard culture conditions were used (Epstein and Shakes 1995).   The following

mutations, balancer chromosomes, and transgenes were used in this study (see

www.wormbase.org). LGI: *cep-1(gk138), dog-1(gk10), ego-1(om84).* LGIII: *met-*

2(n4256), 3xflag::met-2 (this study), *set-25(tm5021)*, *smrc-1* mutations *om136, om138,*

ea8, *ea46* and transgenes *3xflag::smrc-1*, *3xmyc::smrc-1* (this study), *qC1 [dpy-*

19(e1259) glp-1(q339) nIs189[myo-2::gfp]], qC1 [dpy-19(e1259) glp-1(q339) qIs26[lag-

2::gfp rol-6(su1006)]]. LGIV: *csr-1(tm892), him-8(e1489)*; *spo-11(me44), spo-11(ok79),*

nT1. LGV: *bcIs39 [plim-7::ced-1::GFP+lin15(+)].* LGX: *unc-58(e665).* To generate a

smrc-1 met-2 double mutant, *smrc-1(om138)* was generated in the *met-2(n4256)/qC1*

background. Homozygous *smrc-1(om138) met-2(n4256)* was outcrossed twice and

rebalanced. *smrc-1(om136) set-25(tm5021)* and *met-2(n4256) set-25(tm5021)* doubles

were generated by conventional recombination and confirmed by DNA amplification.

The *smrc-1(om138) 3xflag::met-2* chromosome was made by using CRISPR editing to generate the *om138* frameshift mutation on the *3xflag::met-2* chromosome.

CRISPR/Cas9

The *dpy-10* co-CRISPR strategy (Arribere *et al.*, 2014; Paix *et al.*, 2014a) was adapted to facilitate selection of transformants. Unique CRISPR/Cas9 guides near the start codons of *smrc-1* and *met-2* were selected under the guidance of the CRISPR design website http://crispr.mit.edu. To generate the *om136* nonsense and *om138* frameshift mutations, primers matching the guide sequences were incorporated into the pDD162 vector through overlapping PCR. Repair templates to introduce mutations through homologous recombination were purchased from Invitrogen. To generate epitope-tagged transgenes, repair templates containing 33bp flanking sequences and the appropriate tag sequence (*flag* or *myc*) were amplified by high fidelity PCR and purified. Injection mixes contained the following DNAs: 50 ng/ul Cas9 nuclease plasmid; 25 ng/μl *dpy-10(cn64)* repair template (100 nucleotide oligo); 25 ng/μl each guide RNA (gRNA) plasmid (*dpy-10* and the gene of interest); 50ng/ul repair template for gene of interest (PCR product). Roller progeny of injected adults were picked to single plates and allowed to lay eggs before being assayed by single worm PCR. The *smrc-1(ea8)* frameshift allele was generated through non-homologous end joining (no repair template was introduced); an sgRNA downstream of the *smrc-1* start codon was cloned into pRB1017. A DNA mixture containing sgRNA vectors for *smrc-1* and *dpy-10*, a DNA repair oligonucleotide to create *dpy-10(cn64),* and pDD162 Peft-3::Cas9 was injected into the gonads of N2 day 1 adult hermaphrodites. The *smrc-1(ea46)* deletion allele

was generated by using synthetic crRNA (2 nmol IDT) targeting sites near the 5' start codon and 3' stop codon. A mixture of crRNA, tracrRNA, purified Cas9 enzyme, and a single-stranded oligonucleotide repair template was injected.

mosSCI

The *mex-5* promoter was amplified from genomic DNA using the following primers: 5'-cctaggtcacaacggcaaaatatcag-3' and 5'-cattctctgtctgaaacattcaattg-3' (Merritt *et al.*, 2008); an AvrII restriction enzyme site was introduced for cloning into pCFJ151 (Frokjaer-Jensen *et al.*, 2008). The *met-2* coding sequences were amplified from genomic DNA. Coding sequences for GFP and 3×FLAG were amplified from plasmid provided by Dr. David Greenstein. The epitope tag module was inserted at last codon before the stop codon using overlapping PCR. The *mex-5p::met-2::gfp::3xflag::met-2 3'UTR* was inserted into pCFJ151 vector. The final construct was injected at 50ng/µl along with pCFJ90 (2.5ng/µl), pGH8 (10ng/µl), pCFJ104 (5ng/µl), pCFJ601 (30ng/µl) and pMA122 (10ng/µl) into EG6699 bearing the ttTi5605 Mos1 transposon (Frokjaer-Jensen *et al.*, 2008).

DAPI staining and clutch/brood size assays

DAPI-staining was performed as described (Qiao *et al*. 1995). The numbers of embryos (clutch size), viable progeny (brood size), and fertile/infertile adults produced were determine according to standard methods, as follows. L4 hermaphrodites were singled onto freshly seeded plates; as egg-laying adults, they were transferred to new plates every 24 hours. The number of embryos on each plate was recorded immediately after

the hermaphrodite was removed. After 2 days (at 25°C) or 3 days (at 20°C) the numbers of fertile adult hermaphrodites, sterile adult hermaphrodites, and adult males were recorded for each plate.

MET-2 antibody

RT-PCR was performed to confirm the predicted N-terminal sequence of the *met-2* coding region, as cDNA sequence for this region was not available in www.wormbase.org. A peptide corresponding to the N-terminal 17 amino acids (MDQQEPSNNVDTSSILS) was used to immunize rabbits (Yenzym Antibodies LLC). Pre-immune serum from several rabbits was tested via IF to identify individuals that did not already produce significant anti-nematode antibodies. Antibodies were affinity purified against the peptide antigen prior to use. Control IF and protein blots indicated that the antiserum detected an antigen absent in *met-2(n4256)* null mutants (see Figure 2.1A).

Protein blot

Nematodes were grown to appropriate stage on nematode growth medium (NGM) plates and then harvested by rinsing the plates with M9 buffer. Worm pellets were collected by centrifuging at 13,200 rpm for 1 min; the supernatant was aspirated, a volume of sample buffer equal to the pellet volume was added to the tube, and material was resuspended. Material was boiled at 95°C for 10 mins with periodic vortexing. Extracts were resolved on SDS-PAGE (7.5% -15% gradient) and transferred to nitrocellulose membrane. Membranes were incubated with primary antibody (anti-

FLAG, Sigma, 1:500; anti-MET-2, this study, 1:500) overnight at 4°C, washed, and incubated with horseradish peroxide-conjugated secondary antibody (1:5000). Signal was visualized with ECL substrate (Pierce).

Immunohistochemistry

Indirect immunolabeling of dissected gonads was carried out as previously described (Guo *et al.*, 2015; Maine *et al.*, 2005; She *et al.*, 2009). Adults (24 hour post-L4) were dissected in PBS + 0.2mM levamisole in deep-well slides. Tissue was fixed with 3% PFA for 5 mins followed by a 100% cold methanol for 1 min and incubated with 30% GS/PBST as the blocking reagent for 1 hour at room temperature. Primary antibody diluted in 30% GS/PBST (mouse anti-FLAG, sigma, 1:200; mouse anti-H3K9me2, Abcam 1220, 1:200; rabbit anti-MYC, Invitrogen, 1:200) was added and tissues were incubated at 15°C overnight. Secondary antibody was Alexa-fluor-488 conjugated goat anti-mouse (1:200) and Alexafluor 568-conjugated donkey anti-rabbit (1:200).

We note that H3K9me2 abundance appears normal in strains with endogenous *met-2* tagged at the N-terminus via CRISPR (Figure S1C). Therefore, the N-terminal tag does not appear to decrease MET-2 expression. In contrast, H3K9me2 signal is moderately reduced in mosSCI lines carrying a C-terminal tag on the *met-2* transgene; this is the case even when the endogenous *met-2* gene is deleted and despite the fact that the *met-2(n4256)* reduced brood size phenotype was fully rescued in these lines (Figure S1B).

HU assay

Assays were carried out as previously described (Craig *et al*., 2012). In brief,

hydroxyurea (HU) was dissolved in M9 to a stock concentration of 2M. HU stock

solution was further diluted with M9 (final volume of 250ul) and spread on to 10cm

plates containing 10ml of NGM media, final concentrations of 2.5mM, 5mM, 10mM and

25mM HU were prepared. HU solution was left to soak into NGM media overnight, and

plates were used within 24 hours. HU plates were seeded with OP50 and dried for 2

hours under a fume hood. L1 worms of various genotypes were picked from NGM

plates and transferred to HU-soaked NGM plates. Worms were incubated at 25 °C for

16 hours, and then transferred to freshly seeded NGM plates. After 48 hours, adults

were scored and survival rates were calculated.

Immunoprecipitation and mass spectrometry

MET-2 IP was performed with nuclear extract prepared from *him-8(e1489)* adults as

follows. 500-750 ul of pelleted worms were resuspended in 1 ml HB buffer (150 mM

Hepes pH 7.6, 10 mM KCl, 5 mM $MgCl_2$, 12% sucrose, 0.1 mM EDTA), the volume was

split into two tubes, and 100 ul glass beads (710-1180 microns) were added to each

tube. Tissue was disrupted using a FastPrep 120 for two 15 sec pulses on setting 5.5s,

with 10 min on ice in between pulses. Beads were pelleted by spinning 2 min at 800

rpm in a microfuge. Supernatants were pooled into a clean microfuge tube, NP40

added to a final concentration of 0.2%, and tube placed on ice for 30 min. The tube was

spun at 8000 rpm for 2 min; pellet was washed by pipetting up and down to disperse in

1 ml of HB solution and then spun again at 8000 rpm for 2 min. The pellet was

resuspended in HS solution (300 mM NaCl, 20 mM Tris pH 7.6, 25% glycerol, 1.5 mM

MgCl$_2$, 0.2 mM EDTA), and sufficient vol of 900 mM NaCl was added to adjust final

concentration to 300 mM NaCl. Protease inhibitor cocktail (Roche) was added and tube

placed on ice for 30 min. The extract was spun at 10000 rpm for 30 min at 4°C to pellet

debris. Protein concentration was determined by Bradford assay. To IP MET-2, 3-5 ug

of anti-MET-2 antibody was incubated with ~300-500 ng of protein overnight at 4°C with

rotation. After removing an in aliquot to use as input, an appropriate vol of precleared

Protein A/G beads was added and incubated for $\geq$ 2 hr at 4°C with rotation. Beads

were pelleted, washed at RT with FA buffer twice(1 mM EDTA, 50 mM HEPES-KOH,

140 mM NaCl, 0.1% sodium deoxycholate, 1% Triton X-100), FA-500 (FA with 500 mM

NaCl) once, and protein was eluted at RT for 10 min with 2X SDS loading buffer. Beads

were pelleted at 2000 rpm for 1-2 min. The supernatant was removed to a new tube,

beta-mercaptoethanol was added, tube was place at 95°C for 10 min, vortexed, and

spun to pellet debris. The supernatant was loaded onto a protein gel. Using size

standards (Bio-rad, Precision Plus protein standards) as a guide, the gel lane was cut

into 4 pieces for tandem mass spec analysis of proteins (Keck Facility, Yale).

3xFLAG::SMRC-1 IP and immunoblot analysis were performed as follows. Anti-

FLAG antibodies were coupled with protein G Dynabeads (Invitrogen) to reach a final

concentration of 5ug antibody/mg beads following the Thermo Fisher protocol.

Synchronized worms were harvested from ten 60mm NGM and collected by centrifuging

at 13,200 rpm for 1min. Supernatants were aspirated, worm pellets were snap frozen in

liquid nitrogen and stored in -80°C freezer until use. Worm pellets were thawed on ice

and an equal volume of H-100 buffer containing NP40 (50 mM Hepes, pH 7.5, 100 mM

KCl, 1mM MgCl2, 1 mM EDTA, 10% glycerol); proteinase inhibitor cocktail (Roche) was

added to the tube. Extracts were prepared by using a FastPrep as described above. 3-5 mg of protein extract was incubated with 1 mg of antibody-coupled Dynabeads overnight at 4°C with rotation. Beads were washed twice with 1ml of H-100 buffer for 5 min each. Proteins were eluted with 20ul of sample buffer at 55°C for 10 min.

Recombination assays

Recombination between visible markers was measured by standard methods (Kelly *et al.*, 2000b). We generated *dpy unc /++; smrc-1(+)* and *dpy unc/++; smrc-1(om136)/qC1* strains carrying either *unc-11 dpy-5* or *dpy-5 unc-13.* We scored full broods from a set of *dpy unc /++; smrc-1(+)* and *dpy unc/++; smrc-1(om136)* hermaphrodites for Dpy Unc, Dpy non-Unc, and Unc non-Dpy, and non-Dpy non-Unc phenotypes. The measureable recombination rate is Dpy non-Unc + Unc non-Dpy/total. This value represents approximately half of the total recombinants. The *smrc-1* mutation was maintained over the *qC1* balancer chromosome until the generation to be assayed.

***unc-58* suppression and *dog-1* enhancement**

We assayed for suppression/reversion of the *unc-58(e665)* phenotype as described (Harris *et al.*, 2006a) in *unc-58* control and *smrc-1(ea8);unc-58* mutants raised at 20ºC. To determine whether *smrc-1* enhanced the *dog-1* phenotype, we assayed for accumulation of insertions and deletions within the GC-rich exon 5 of *vab-1* as described (Youds *et al.*, 2006) in *dog-1(gk10)* controls and *smrc-1(ea8); dog-1(ea8)* grown at 20ºC and 25ºC. Before performing the assay, strains were outcrossed and

assayed to eliminate any *vab-1* deletions that might have accumulated. Controls also were performed with the *smrc-1(ea46)* deletion allele at 25°C to ensure that *smrc-1* itself does not accumulate *vab-1* deletions. Nested DNA amplification was performed with oligonucleotides flanking *vab-1* exon 5.

Transgenerational broods and sterility

Six lines of balanced *smrc-1(ea8)/qC1* were maintained at 25ºC for three generations. They were expanded to 16 unbalanced founders on 12-well NGM plates seeded with OP50. To avoid bias towards healthy animals, the first L4 progeny was passaged to start the next generation. Two days after passaging, I estimated the total number of progeny in the previous generation and scored them using the categories: 0, <20, 20-40, 40-80, 80-100, and >100. If a worm was sterile, became eviscerated, or otherwise died before any offspring were produced, the line would be rescued by a healthy worm from the previous generation. Sterile worms were scored as zero progeny and eviscerated/dead worms were not scored.

Figures
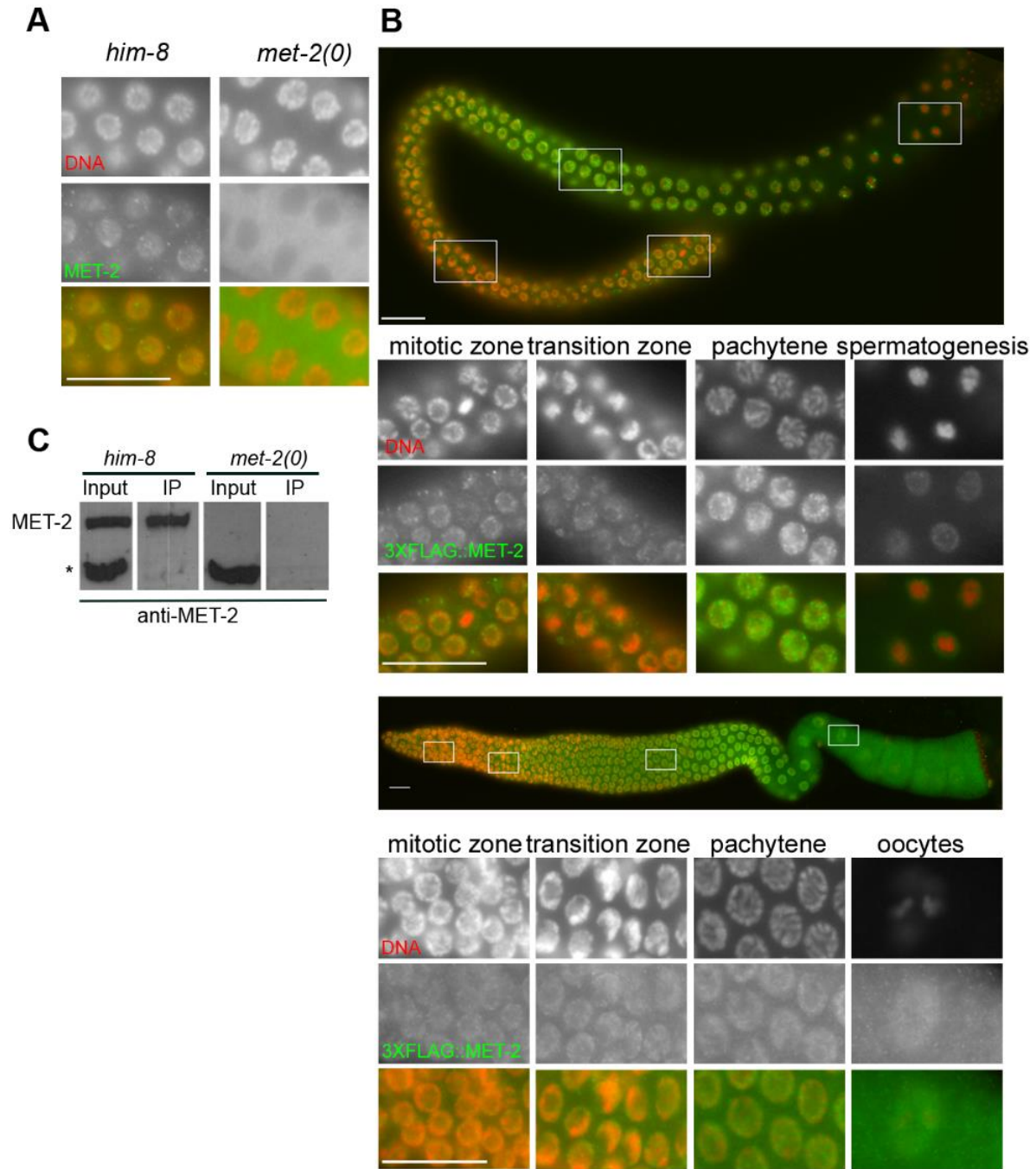
Figure 2.1. Germline MET-2 is detected predominantly in nuclei.

(A) Dissected *him-8* and *met-2* adult male gonads were immunolabeled with anti-MET-2 antibody and counterstained with DAPI to visualize DNA. Pachytene nuclei are shown. Nuclear signal is not detected in *met-2(0)* tissue. Scale bar: 16 μm.

(B) Nuclear 3xFLAG::MET-2 is detected throughout the XO and XX germ line. Images show dissected adult gonads labeled with anti-FLAG antibody (green) and counterstained with DAPI (red). Scale bar: 16 μm.   immunolabeling with anti-FLAG antibody. Upper panel includes a complete male gonad. Lower panels correspond to the boxed regions. Scale bar: 16 μm.

(C) Protein blots containing total lysate (left two lanes) and immunoprecipitated material (right two lanes) were probed with anti-MET-2 antibody. Protein extracts were prepared from *him-8(e1489)* and *met-2(n4256)* mutants, and IP was performed with anti-MET-2 antibody. *, Cross-reacting polypeptide routinely observed on protein blots but not recovered in IP under our conditions.
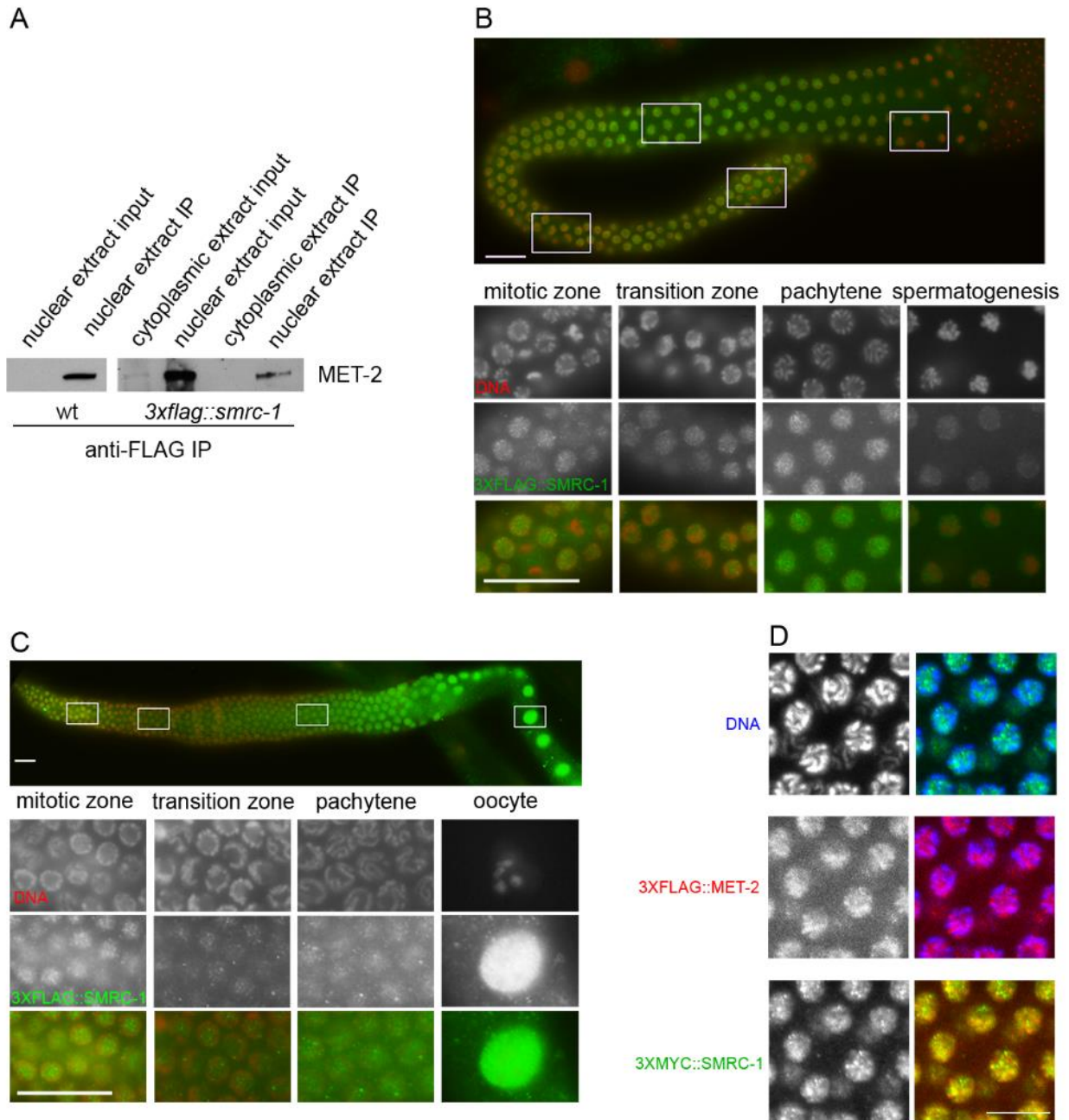
Figure 2.2. SMRC-1 associates with MET-2 and localizes to germline nuclei.

(A) Protein blot containing total lysate and material immunoprecipitated with anti-FLAG
were probed with anti-MET-2. Extracts were prepared from the indicated wild type and
3xflag::smrc-1 strains.

(B and C) Nuclear 3xFLAG::SMRC-1 is detected throughout the (B) XO and (C) XX

germ line. Images show dissected adult gonads labeled with anti-FLAG antibody

(green) and counterstained with DAPI (red). Scale bar: 16 µm.

(D) 3xFLAG::MET-2 and 3xMYC::SMRC-1 show a similar pattern of nuclear localization.

Images show a portion of a dissected adult gonad germ line (pachytene)

immunolabeled with anti-FLAG (red) and anti-MYC (green) antibodies and

counterstained with DAPI (blue). Scale bar: 5 µm.
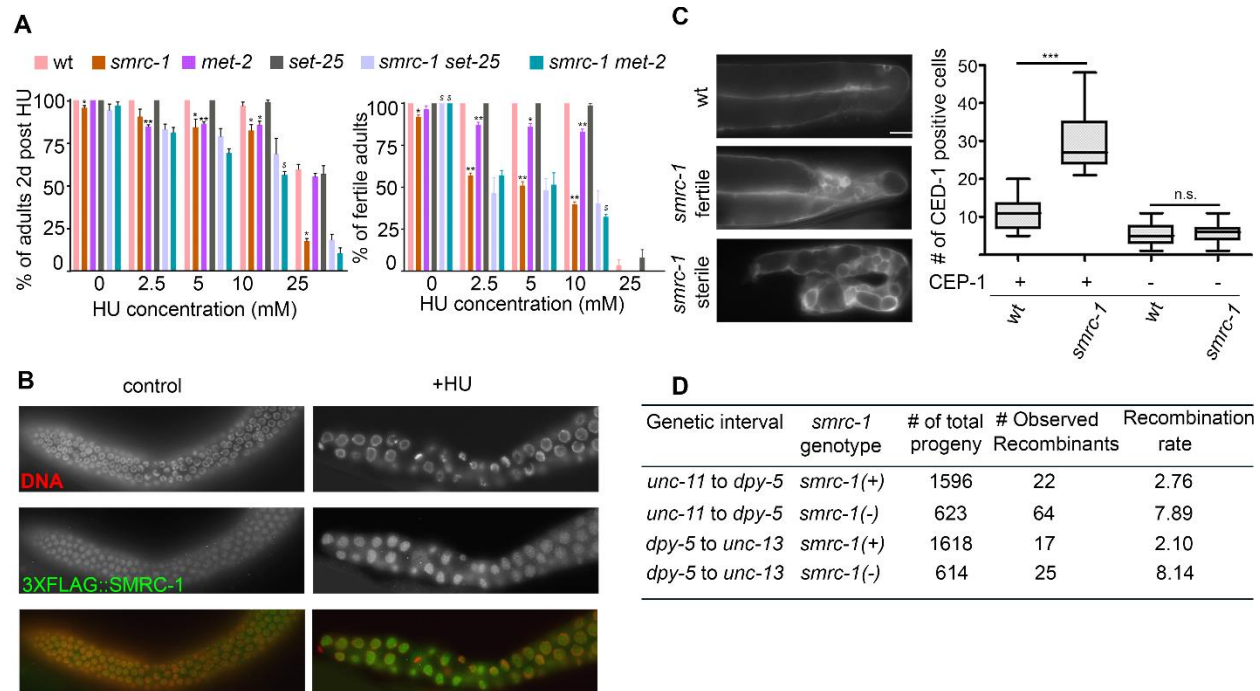
Figure 2.3. Genome integrity is compromised in *smrc-1* mutants.

(A) Graph shows survival of L1 larvae exposed to HU for 16 hr at 25°C and then transferred to regular NGM plates and maintained for at 25°C for 48 hr. Fertility of adult survivors is shown separately. * $p < 0.05$ and ** $p < 0.005$ compared to wild-type; $ $p < 0.05$ compared to *smrc*-1. T-test with arcsine transformation. N = 3 trials.

(B) 3xFLAG::SMRC-1 abundance in mitotic germline nuclei is elevated upon HU treatment. Images show gonads dissected from control and HU-treated adults and immunolabeled with anti-FLAG antibody. L4 larvae were exposed to 25mM HU for 24 hours at room temperature to reach adulthood. After treatment, adults were immediately dissected and fixed following with anti-FLAG immunolabeling.

(C) Apoptosis is elevated in *smrc-1* mutants. Images show CED-1::GFP expression in control and representative fertile and sterile *smrc-1; ced-1::gfp* adult gonads. CED-1::GFP expression visualizes sheath cell engulfment of apoptotic germ cells. The

apoptosis rate was quantified by counting the number of CED-1::GFP positive cells per

gonad in control and fertile *smrc-1* mutants; *smrc-1* sterile animals were excluded from

the quantification because the extensive apoptosis and irregular cell morphology made

quantification difficult. The increase in germ cell apoptosis depends on CEP-1

expression. ***P<0.001, Student's t test. Scale bar: 16 μm.

(D) Recombination frequency were mapped in two genetic intervals. Wild type animals

were used as a control. *smrc-1(om136)* was used to perform this assay.

A N2 smrc-1

spo-11 smrc-1;spo-11

% of cells

4
5
6
7
8
9
10
11
12

N2 smrc-1 spo-11 smrc-1;spo-11

B

TZ Zone 1 Zone 2 Zone 3 Zone 4 Zone 5 Zone 6

RAD-51 foci per nucleus
0
1-2
3-4
5-6
7-8
>8

N2
% of total nuclei
TZ Zone 1 Zone 2 Zone 3 Zone 4 Zone 5 Zone 6

smrc-1
% of total nuclei
TZ Zone 1 Zone 2 Zone 3 Zone 4 Zone 5 Zone 6

spo-11
% of total nuclei
TZ Zone 1 Zone 2 Zone 3 Zone 4 Zone 5 Zone 6

smrc-1;spo-11
% of total nuclei
TZ Zone 1 Zone 2 Zone 3 Zone 4 Zone 5 Zone 6

C

Temperature	Genotype	Total	Deletion	Frequency
20°C	dog-1	173	18	10.4
	smrc-1;dog-1	349	64	18.3
25°C	dog-1	189	14	7.4
	smrc-1;dog-1	188	18	14.5
	smrc-1	43	0	0

D

Temperature	Genotype	Total	Revernant	Frequency
20°C	unc-58	1,798,760	2	1.11×10^{-6}
	smrc-1; unc-58	1,090,440	6	5.50×10^{-6}
25°C	unc-58	782,880	1	1.28×10^{-6}
	smrc-1; unc-58	792,200	5	6.31×10^{-6}

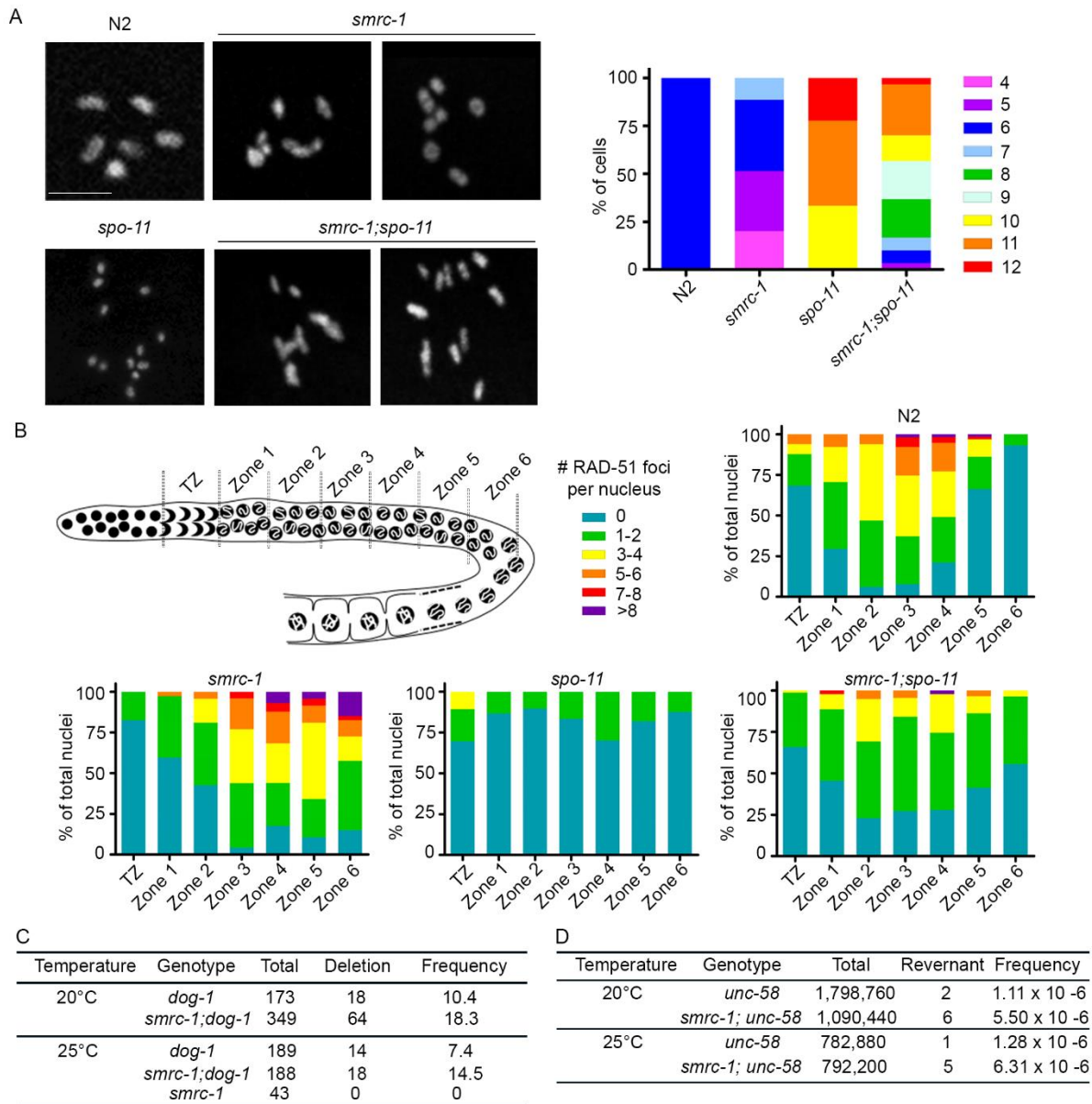**Figure 2.4. *smrc-1* mutations might cause SPO-11 independent DSBs in the germline**

(A) The loss of SMRC-1 activity causes DSBs and partially restores recombination in the absence of SPO-11 activity. Images show representative diakinesis nuclei at the -1 or -2 oocyte position. Wild type image contains 6 DAPI-bright bodies, representing 6 bivalents, and *spo-11(ok79)* image contains 12 DAPI-bright bodies, representing 12

univalents. At 25°C, *smrc-1(om138)* and *smrc-1(ea8)* oocytes contain 4-7 distinct

DAPI-bright bodies of variable size; larger bodies often appear to be distinct

chromosomes held together by DNA bridging. At 25°C, *smrc-1(om138);spo-11(ok79)*

oocytes contain 5-12 DAPI-bright bodies of variable size. Scale bar: 5 μm.

(B) RAD-51 labeling during meiotic prophase in wildtype, *smrc-1, spo-11* and *smrc-*

1;spo-11 were quantified. Diagram indicates the organization of a hermaphrodite

germline from transition zone to prior to diplotene been evenly divided into six zones

based on cell row counts. The heat map represents the percentage of total nuclei

containing indicated number of RAD-51 foci.

(C) The *dog-1* phenotype is enhanced by *smrc-1.* Data represent the frequency of

deletions within the *vab-1* exon 5 poly G/C tract. See Experimental Procedures.

(D) Reversion of the *unc-58(e665)* visible phenotype is enhanced by the loss of *smrc-1*

activity at both 20ºC and 25ºC.

A

B

| | wt male | smrc-1(om136) male | wt hermaphrodite | smrc-1(om136) hermaphrodite |

DNA

H3K9me2

C

| | wt male | smrc-1(ea8) male | smrc-1(ea8) male | wt hermaphrodite | smrc-1(ea8) hermaphrodite | smrc-1(ea8) hermaphrodite |

DNA

H3K9me2

57.14% n=21   42.86% n=21   70% n=20   30% n=20

D
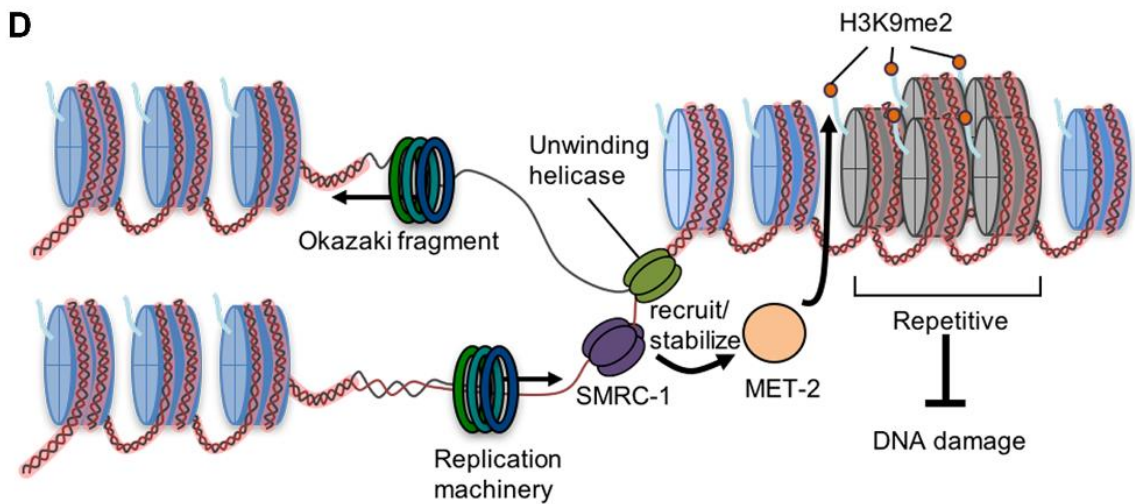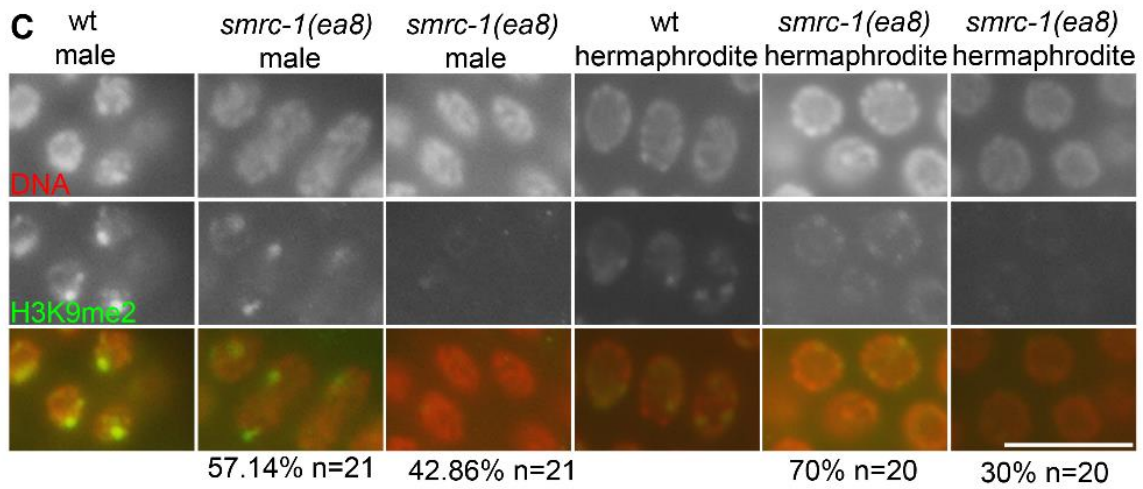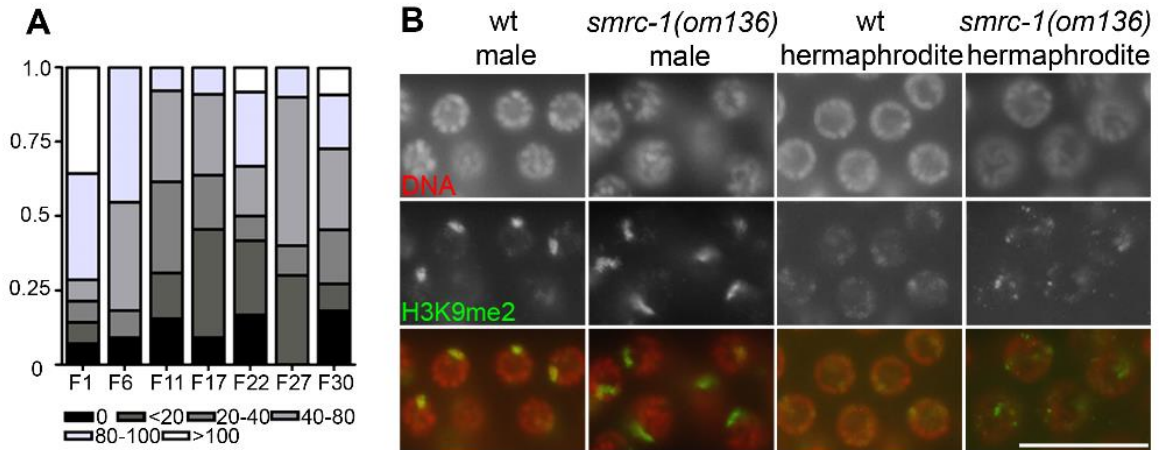
Figure 2.5. H3K9me2 labeling is reduced in serially passed *smrc-1* mutants.

(A) *smrc-1* brood remain highly variable in *smrc-1* lines serially passaged for 30
generations.

(B) H3K9me2 distribution as detected by immunolabeling appears fairly normal in *smrc-1(om136)* F2 worms at 25ºC. Gonads were dissected at 18 hr post-L4 stage and
labeled with anti-H3K9me2 antibody and counterstained with DAPI to visualize DNA.
Each panel shows a set of pachytene nuclei.   Scale bar: 16 μm.

(C) H3K9me2 distribution is variably reduced in *smrc-1(ea8)* F30 animals at 25°C.
Gonads were dissected at 18 hr post-L4 stage and labeled with anti-H3K9me2 antibody
and counterstained with DAPI to visualize DNA. Each panel shows a set of pachytene
nuclei. Scale bar: 10 μm.

(D) Model for SMRC-1 activity.

Table 2.1. *smrc-1* developmental defects

Genotype	Temp °C	n	Avg clutch ± SEM	% Dead embryos	% Male
N2 wildtype	20	7	220.6 ± 6.7	0.6	0.1
3xflag::smrc-1	20	10	238.3 ± 8.5	1.0	0.1
smrc-1(om136) M+Z-	20	8	222.6 ± 8.2	9.2	0.8
smrc-1(om136) M-Z-	20	10	155.5 ± 20.6	25.0	3.8
smrc-1(om138) M+Z-	20	6	173 ± 6.8	19.6	1.4
smrc-1(om138) M-Z-	20	11	139.8 ± 9.5	26.5	2.0
smrc-1(om138) met-2(n4256) M+Z-	20	11	159.4 ± 3.52	21.2	2.2
smrc-1(om138) met-2(n4256) M-Z-	20	12	11.2 ± 7.8	20.2	2.6
N2 wildtype	25	7	168.7 ± 4.8	3.1	0.1
3xflag::smrc-1	25	5	157.4 ± 1.6	3.8	0.1
smrc-1(om136) M+Z-	25	15	130 ± 3.9	29.2	4.5
smrc-1(om136) M-Z-	25	13	53.5 ± 9.0	72.2	5.5
smrc-1(om138) M+Z-	25	7	120.3 ± 6.7	39.6	3.5
smrc-1(om138) M-Z-	25	8	58.6 ± 13.8	47.5	3.7
smrc-1(om138) met-2(n4256) M+Z-	25	12	124.2 ± 7.6	54.1	1.4
smrc-1(om138) met-2(n4256) M-Z-	25	12*	1.6 ± 1.6	94.8	NA

n, Number of broods assayed.   * We note that only 1/12 hermaphrodites produced embryos. Clutch size, embryonic lethality and male frequency were collected as described in methods (n= number of broods assayed).

Table 2.2. *smrc-1* is synthetic sterile and lethal with *met-2*.

genotype	% sterile XX (n)	% dead embryos (n)	% protruding vulva (n)
smrc-1(om136)	7.5 (402)	30 (590)	0 (402)
smrc-1(om138)	8.3 (460)	26.8 (656)	0 (460)
met-2(n4256)	0 (217)	7.3 (234)	0 (217)
set-25(tm5021)	0 (335)	5.6 (355)	0 (335)
smrc-1 met-2	92 (301)	52.2 (624)	36.5 (301)
smrc-1 set-25	7.9 (189)	30.2 (278)	0 (189)
met-2 set-25	0 (108)	64.8 (307)	0 (108)

Table lists data for the M-Z- F2 generation raised at 25°C.

Table 2.3. *smrc-1* mutants display elevated meiotic recombination frequencies

Genetic interval	*smrc-1* Genotype	Total # progeny	# Observed Recombinants	Recombination rate*
unc-11 to *dpy-5*	*smrc-1(+)*	1596	22	2.76
unc-11 to *dpy-5*	*smrc-1(om136)*	1623	64	7.89
dpy-5 to *unc-13*	*smrc-1(+)*	1618	17	2.1
dpy-5 to *unc-13*	*smrc-1(om136)*	614	25	8.14

Meiotic recombination rate within two different genetic intervals defined by *unc-11* to *dpy-5* and *dpy-5* to *unc-13* were scored in wild type and *smrc-1* backgrounds. *As described in Materials and methods, ~50% of recombinants were observable; the recombination rate listed here was calculated using # observed recombinants x 2.
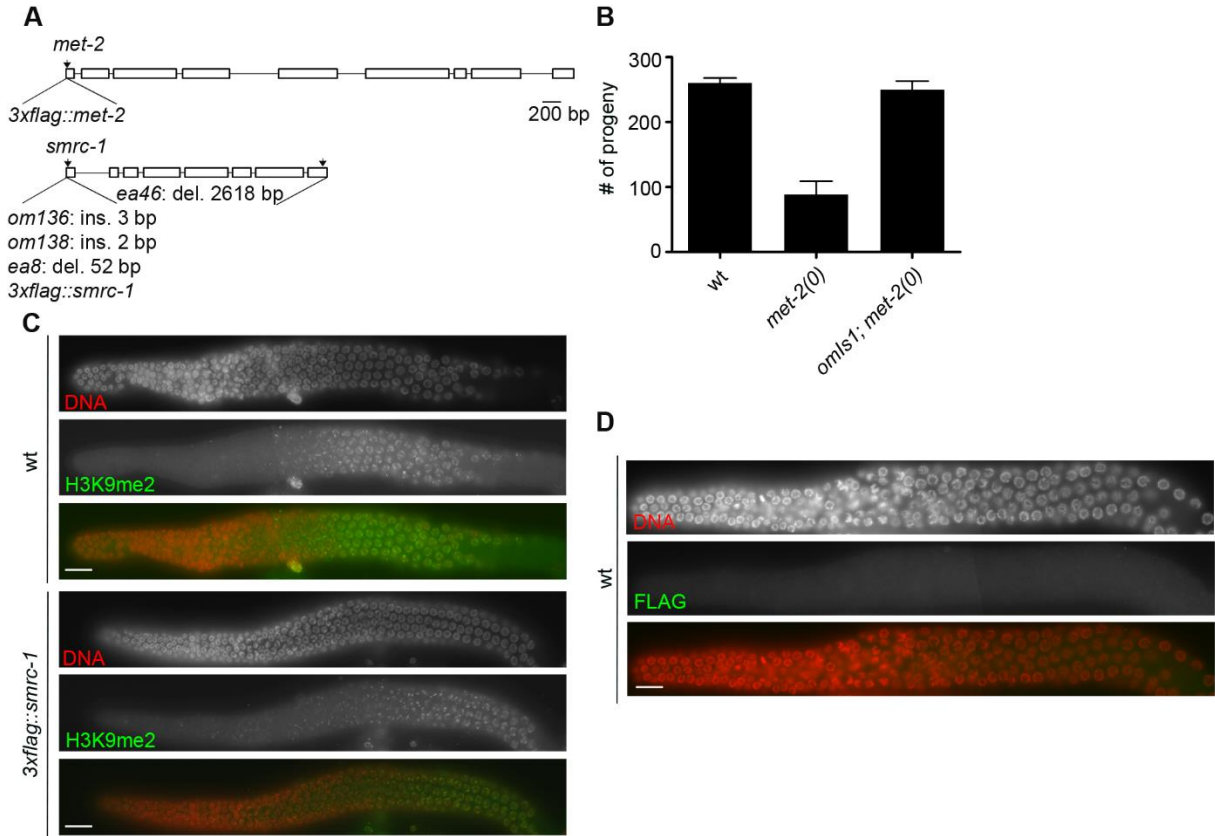
Figure 2.S1. Generation of transgenic lines used in this study

(A) Locations of epitope tags and mutant lesions generated via CRISPR. Boxes and lines represent exons and introns, respectively. Black arrows indicate predicted Cas9 cutting site for each injected sgRNA. *smrc-1(om136)* contains a stop codon inserted in-frame at the 5th codon in exon 1. *smrc-1(om138)* is a frameshift allele generated by inserting two nucleotides at codon 7 of exon 1. *3xflag::smrc-1* and *3xflag::met-2* were generated by in-frame insertion of *3xflag* coding sequences immediately after the start codon. See Experimental Procedures.

(B) Broods of wildtype, *met-2(n4256)*, and mosSCI-tagged *met-2::gfp* lines at 20°C.

(C) Immunolabeling of H3K9me2 in wild type and endogenously tagged *3xflag::met-2* germline. Gonads are oriented with distal end to the left.

(D) Negative control for anti-FLAG labeling.
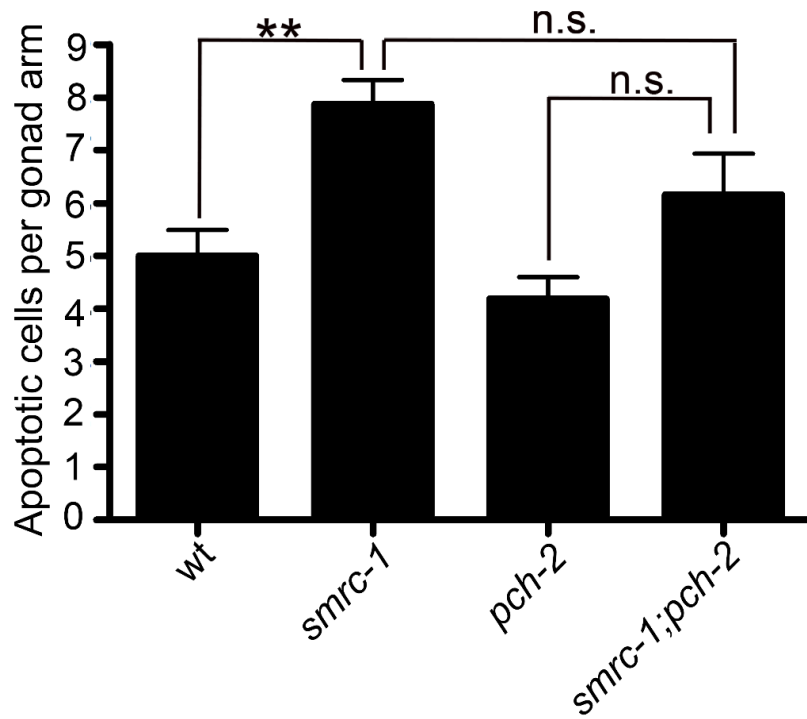
Figure 2. S2. pch-2 does not suppress the increased germ cell apoptosis in smrc-1 mutant. Quantification of germ cell apoptosis measured by acridine orange staining.

Table 2.S1. *smrc-1* F1 animals derived from balanced *smrc-1/qc1gfp*

hermaphrodites are fertile and viable at 25°C.

Genotype	Temp °C	n	Avg clutch ± SEM	% Dead embryos	Non-green fertile (F1)	Non-green sterile (F1)
om136/qc1gfp	25	5	148 ± 7	3.9	34 ± 2	0
om138/qc1gfp	25	4	136 ± 1	3.8	32 ± 0.3	0

Chapter III Multiple candidate proteins associates with MET-2

3.1 Introduction

The interesting distribution pattern of H3K9me2 in *C. elegans* (see Introduction 2.2.1) triggered us to ask how H3K9me2 gets targeted to specific chromatin regions. To answer this question, our lab is interested in identifying H3K9me2 methyltransferase (MET-2) co-factors. An interaction between MET-2 and SMRC-1 has been described in Chapter II. In this chapter, I will address the other candidate interactors of MET-2 that I identified through immunoprecipitation coupled with mass spectrometry.

3.2 Results

3.2.1 Recovery of candidate MET-2 interactors

We generated epitope (GFP and 3×FLAG) tagged MET-2 under control of a germline-enriched promoter, *mex-5p*, using the *Mos1*-single copy insertion method (Frokjaer-Jensen *et al.*, 2008) (see Methods). Since we aimed to identify interactors that are important for the MET-2 function in germline, we chose a germline-specific promoter to enrich the expression of the transgene in germ cells. Immuno-labeling using anti-FLAG antibody showed that the MET-2::GFP::3XFLAG fusion protein is localized in germline nuclei, which is consistent with our α-MET-2 antibody labeling results (Figure 3.1A, also see chapter II). To validate that the *omIs4* transgene is useful for immunoprecipitation (IP), I did immunoprecipitation with anti-FLAG antibody and successfully detected the presence of MET-2::GFP::3XFLAG in the IP eluate (Figure 3.1B). I then subjected the material from transgenic line to immunoprecipitation using anti-FLAG antibody coupled with MS/MS sequencing to recover factors that associate with MET-2::GFP::3XFLAG. In parallel, extract from wild type strain N2 was utilized as a negative control. The resulting

MS data was processed to detect proteins uniquely detected in the IP eluate from MET-2 transgenic animals, but not in the negative control strain (Table 3.S1). For subsequent analysis, we primarily focused on several proteins that localize to the nucleus (Table 3.1). Analysis of two other proteins is described in the Appendix.

To test whether there is an interaction between the candidate protein and MET-2, we took two different approaches. Firstly, when a mutation in the candidate gene was available, we obtained that mutant strain and assessed the H3K9me2 distribution pattern in the male germline. When a mutation was not available, we subjected *him-8* animals to RNAi to knock down the candidate gene product and then examined the H3K9me2 distribution pattern in the male germline. Secondly, I performed reverse co-immunoprecipitation by using antibody against the candidate interactor or epitope-tagged transgene product. (Note: only part of the list was tested this way.)

3.2.2 Candidate interactors

This section describes further analysis of four factors. Three of them appear to influence the H3K9me2 distribution pattern: HEL-1, CDC-48.2 and HTZ-1 (Table 3.1). In animals lacking the function of these proteins, we observed a reduction of the H3K9me2 mark on unsynapsed X chromosomes compared to wildtype. We followed up on these H3K9me2 results as described below.

HEL-1

HEL-1 (helicase-1) has been shown to be important for pre-mRNA splicing and nuclear export in various species (Fleckner *et al.*, 1997; MacMorris *et al.*, 2003). Interestingly, a

mutation in the homolog of HEL-1 in *Drosophila* was identified as an enhancer of position-effect variegation (PEV) mutations (Eberl *et al.*, 1997). PEV is the effect of a chromosomal rearrangement that places a euchromatic gene in a heterochromatin region. Many enhancers and suppressors of position-effect variegation are mutations in important chromatin modifiers, including H3K9 and H3K4 methyltransferase (Elgin and Reuter, 2013). Therefore, we hypothesize that HEL-1 may also play a role in heterochromatin regulation.

To address whether HEL-1 is an interactor of MET-2, we obtained two different antibodies (MacMorris *et al.*, 2003) to try reciprocal immunoprecipitation. Unfortunately, I was not able to immunoprecipate HEL-1 with either antibody (data not shown). I utilized the CRISPR method to tag the endogenous *hel-1* gene with *3xflag*, and I successfully constructed *hel-1::3xflag* transgenic lines. By immunolabeling, we observed the expression pattern of HEL-1::3XFLAG in the germline (Figure 3.2). It is enriched in nuclei, which is consistent with previously observations. Then I did reverse-immunoprecipitation using anti-FLAG antibody. I recovered HEL-1::3XFLAG, but not MET-2 (Figure 3.2) in the immunoprecipitated fraction. Although I could not confirm the interaction between HEL-1 and MET-2, the impact of *hel-1* knockdown on H3K9me2 intensity is worth further investigation.

HTZ-1

HTZ-1 (histone H2A variant) has been studied in many other organisms, and its incorporation into nucleosomes is suggested to promote heterochromatin assembly (Baldi and Becker, 2013). In *C. elegans*, HTZ-1 is highly linked with dosage

compensation. Immuno-labeling (Petty *et al.*, 2009; Whittle *et al.*, 2008) and chromatin immunoprecipitation (Whittle *et al.*, 2008) experiments showed that HTZ-1 is highly enriched on autosomes and excluded from X chromosomes in somatic cells. However, the role of HTZ-1 in the germline had not been explored since dosage compensation has not been reported in the germline. To test the interaction between HTZ-1 and MET-2, we requested HTZ-1 antibody from Dr. Gyorgyi Csankovszki and performed reverse co-immunoprecipitation. However, I did not recover HTZ-1 using this antibody in immunoprecipitation (Figure 3.3). Due to time limitations, I did not further pursue the possibility of an interaction between HTZ-1 and MET-2.

CDC-48.2

CDC-48.2 belongs to the AAA ATPase family. Mutation in *cdc-48.2* has been shown to cause an increase in histone H3 serine 10 phosphorylation (H3S10ph) in the *C. elegans* germline (Sasagawa *et al.*, 2010). Interestingly, H3S10ph has been reported to block H3K9me2 detection by immuno-labeling but not protein blotting (Duan *et al.*, 2008). We are concerned that the reduced H3K9me2 levels we observed in *cdc-48.2* (RNAi) animals may result from elevated H3S10ph levels, masking the H3K9me2 marks (Figure 3.3). To test this idea, it would be interesting to examine the level of H3S10ph along with H3K9me2 in *cdc-48.2* (RNAi). These experiments are beyond the scope of this thesis.

DLC-1

Another protein subjected to the above survey is the highly conserved dynein protein,

DLC-1. In *C. elegans,* DLC-1 has been implicated to function not only in dynein-dependent cellular processes, but also dynein-independent events, such as regulating meiotic chromosome movement   and inhibiting the germ cell proliferation in *C. elegans* germline (Dorsett and Schedl, 2009). Upon *dlc-1* RNAi, I did not observe alternation of H3K9me2 distribution in male germline (Figure 3.4). In addition, reciprocal immunoprecipitation using the *dlc-1::gfp* transgenic line did not confirm the interaction between DLC-1 and MET-2 (Figure 3.4).

3.3 Discussion

Identification of MET-2 interactors specifically in the germline

To identify MET-2 binding partners that directs its activity to specific genomic loci in germ line, a strain expressing FLAG and GFP tagged MET-2 protein primarily expressed in the germ cells was established. This transgenic line serves as a good substrate to enrich MET-2 binding partners in germ cells due to the germline-specific promoter *mex-5* (Merritt *et al*., 2008). We could easily detect the expression of the MET-2::GFP::3XFLAG protein in germ cells through either immunolabeling or protein blot in germ cells. However, the strength of the *mex*-5 promoter versus the endogenous *met-2* promoter needs to be considered, since the binding partners could vary if the expression level of the MET-2 transgenic protein is different from its endogenous level. Therefore, we subjected the identified MET-2 binding proteins to further protein-protein interaction studies to confirm the interactions. After the immunoprecipitation purification of the tagged MET-2 protein complex, LC-MS/MS analysis detected a set of proteins that may interact with MET-2. We prioritized the proteins that are known to be expressed in the nuclei (see Table 2.1) and immunoprecipitated two of them, HEL-1 and

DLC-1. However, I was not able to validate the interaction between MET-2 and each of them. This may be due to the low binding affinity with MET-2. In addition, the different transgenic lines, such as *dlc-1::gfp* and *hel-1::3xflag,* contain different genetic backgrounds from the *mex-5p::met-2::gfp::3xflag* transgenic line. These differences might cause the binding affinity to between MET-2 and the candidate protein interactor to be distinct in the immunoprecipitation experiment and the reciprocal anti-DLC-1::GFP and anti-HEL-1::3XFLAG immunoprecipitation experiment.

MET-2 might be involved in various biological processes

The function of the MET-2 homolog, SETDB1, in mammals has been intensively explored. SETDB1 was originally identified through an interaction with the ETS transcription factor, ERG, and shown to specifically add methyl groups to H3K9 (Yang *et al.*, 2002). Later, various transcriptional regulators were identified to recruit SETDB1 to target regions and place repressive heterochromatin marks. For example, the binding of SETDB1 to KAP1 leads to the establishment of the heterochromatic status of the KAP1 targeting genes (Schultz *et al.*, 2002). More recently, Thompson *et al.* reported that hnRNP K also mediates the SETDB1 recruitment in a KAP1-dependent way (Thompson *et al.*, 2015). Interestingly, a SWI/SNF superfamily component, SMRCC1, was also shown to interact with SETDB1 in the immunoprecipitation experiment carried out by Thompson *et al* (Thompson *et al.*, 2015). This result suggests that SETDB1 might also be involved in mediating chromatin remodeling, which alters chromatin status of specific genomic regions. Furthermore, interactions between SETDB1 and other histone modifiers, including histone deacetylases HDAC1/2, result in a protein complex that participates in multiple transcriptional repression pathways (Yang *et al.*, 2003).

SETDB1 also plays a role in maintaining the heterochromatin structure during DNA replication by forming a protein complex with methylated DNA binding proteins, MBD1 and MCAF1 (Sarraf and Stancheva, 2004). These observations implicate SETDB1 in diverse cellular processes. Similarly, MET-2 appears to be involved in various biological pathways in *C. elegans* based on the functions of the candidate proteins that co-purify with MET-2 in the immunoprecipitation experiment (see Table 2.S1).

Although the biochemical and molecular function of SETDB1 has been well characterized, analyzing the phenotypes of the SETDB1 knockout animals is necessary to better understand the function of SETDB1. However, studies to learn the outcome of SETDB1 abolishment in mouse mutant individuals revealed that mouse embryos lacking functional *Setdb1* gene product die pre-implantation (Dodge *et al.*, 2004), making it impossible to assess the impact of H3K9me2 loss on adults. Later studies using *SETDB1* conditional knockout mouse ES cell lines showed slow cell growth phenotype after depletion of SETDB1 expression (Matsui *et al.*, 2010). Thus, *C. elegans* *met-2* mutants serve as a good model to study the impact of MET-2 loss individually and also across generations.

3.4 Methods

RNA interference

RNAi was carried out as described (Timmons *et al.*, 2001). Briefly, L1 *him-8* animals were subjected to dsRNA feeding for 48 hours at 25°C for *dlc-1*, *cep-1, htz-1* and *dcaf-1*. L3 *him-8* animals were fed with *hel-1* dsRNA for 24 hours at 25°C.

Immunofluorescence labeling

Indirect immunolabeling procedures were carried out as previously described (Guo *et al.*, 2015; Maine *et al.*, 2005; She *et al.*, 2009). Adults were dissected in PBS + 0.2mM levamisole in deep-well slides. Worms were fixed with 3% PFA for 5 mins followed by 100% cold methanol for 1 min and incubated with 30% GS/PBST as the blocking reagent for 1 hour at room temperature. Primary antibody diluted in 30% GS/PBST (mouse anti-H3K9me2, Abcam 1220, 1:200) was added and tissues were incubated at 15°C overnight. Secondary antibody was Alexa-fluor-488 conjugated goat anti-mouse (1:200).

Immunoprecipitation

IP and immunoblot analysis were performed as follows. Anti-FLAG/GFP antibodies were coupled with protein G Dynabeads (Invitrogen) to reach a final concentration of 5ug antibody/mg beads following the Thermo Fisher protocol. Synchronized adults were harvested from ten 60mm NGM and collected by centrifuging at 13,200 rpm for 1min. Supernatants were aspirated and worm pellets were snap frozen in liquid nitrogen and stored in -80ºC freezer until use. Worm pellets were thawed on ice and an equal volume of H-100 buffer containing NP40 (50 mM Hepes, pH 7.5, 100 mM KCl, 1mM MgCl2, 1 mMEDTA, 10% glycerol) and proteinase inhibitor cocktail (Roche) was added to the tube. Extracts were prepared by using a FastPrep as described in Chapter II. 3-5 mg of protein extract was incubated with 1 mg of antibody-coupled Dynabeads overnight at 4ºC with rotation. Beads were washed twice with 1ml of H-100 buffer for 5

min each. Proteins were eluted with 20ul of sample buffer at 55ºC for 10 min. The

eluate was subjected to SDS-PAGE separation following by either MS/MS sequencing

(Yale Keck Facility) or protein blot.

mosSCI

The *mex-5* promoter was amplified from genomic DNA using the following primers: 5'-

cctaggtcacaacggcaaaatatcag-3' and 5'-cattctctgtctgaaacattcaattg-3' (Merritt *et al.*,

2008); an AvrII restriction enzyme site was introduced for cloning into pCFJ151

(Frokjaer-Jensen *et al.*, 2008). The met-2 coding sequences were amplified from

genomic DNA. Coding sequences for GFP and 3XFLAG were amplified from plasmid

provided by Dr. David Greenstein. The epitope tag module was inserted at last codon

before the stop codon using overlapping PCR. The *mex-5p::met-2::gfp::3xflag::met-2*

3'UTR construct was inserted into pCFJ151 vector. The final construct was injected at

50ng/μl along with pCFJ90 (2.5ng/μl), pGH8 (10ng/μl), pCFJ104 (5ng/μl), pCFJ601

(30ng/μl) and pMA122 (10ng/μl) into EG6699 bearing the ttTi5605 Mos1 transposon

(Frokjaer-Jensen *et al.*, 2008).

Figures and tables

Table 3.1. Summary of proteins of interest identified in this study

Protein		Altered H3K9me2 after RNAi knockdown or mutation	Reverse co-IP
CEP-1	Transcription factor, human p53 homolog	- (RNAi)	Not tested
DLC-1	Dynein light chain 1, homolog pairing was significantly delayed in *dlc-1 (RNAi)* animals (Sato *et al.*, 2009)	- (RNAi; see Figure 3.4)	- *dlc-1::gfp* (Morthorst and Olsen, 2013) (Figure 3.4)
HEL-1	RNA helicase, important for pre-mRNA transportation out of nucleus (MacMorris *et al.*, 2003)	+ (RNAi; see Figure 3.3)	- *hel-1::3xflag* (Figure 3.2)
CDC-48.2	ATPase, simultaneous depletion of CDC-48.1 and CDC-48.2 resulted in chromosome separation during meiosis (Sasagawa *et al.*, 2007)	+ (Mutant; see Figure 3.3)	Not tested
DCAF-1	Ubiquitin ligase associated factor	-	Not tested
HTZ-1	Histone H2A variant	+ (RNAi; see Figure 3.3)	? HTZ-1 antibody

"-": Negative, not significantly different from control

"+": Positive, different from control

Table 3.S1. List of proteins recovered only in the *met-2::3xflag::gfp*

immunoprecipitated material

>200 kDa	
MET-2	
H2A.V	Histone H2A.V
DYL-1	Dynein light chain 1, cytoplasmic
UNC-52	Basement membrane proteoglycan
UNC-22	Twitchin
CEP-1	Transcription factor, human tumor suppressor p53 homolog, promote DNA-damage induced apoptosis and is required for meiotic segregation
DPF-2	Dipeptidyl peptidase family member 2

100-200 kDa	
MET-2	
PYC-1	Pyruvate carboxylase 1
GYS-1	Probable glycogen [starch] synthase
CLP-1	Calpain
DCAF-1	DDB1- and CUL4-associated factor (DACF1/VprBP) homolog
RAB-3	Ras-related protein Rab-3
CDC-48.2	Transitional endoplasmic reticulum ATPase homolog 2
TAX-4	Cyclic nucleotide-gated cation channel
DPF-2	Dipeptidyl peptidase family member 2

37-100 kD	
MET-2	
SUCB1	Probable succinyl-CoA ligase [ADP-forming] subunit beta, mitochondrial
CCT-8	putative theta subunit of the eukaryotic cytosolic ('T complex') chaperonin
IF4A	Eukaryotic initiation factor 4A
MMSA	Probable methylmalonate-semialdehyde dehydrogenase [acylating]
HEL-1	ATP-dependent RNA helicase DDX39B homolog
DARS-1	aspartyl(D) amino-acyl tRNA synthesase
C53C9.2	
CCT-4	a putative delta subunit of the eukaryotic cytosolic ('T complex') chaperonin
GLH-1	ATP-dependent RNA helicase
B0303.3	orthologous to the human gene 3-KETOACYL-COA THIOLASE BETA-SUBUNIT OF TRIFUNCTIONAL PROTEIN
SRB-6	Serpentine receptor class beta-6
ATAT-2	Alpha-tubulin N-acetyltransferase 2
C37H5.5	Nucleolar complex protein 3 homolog
PFN-1	Profilin
Msp-10	Major sperm protein 10
C15H7.4	nematode specific, phenotype: protruding vulva (via RNAi)

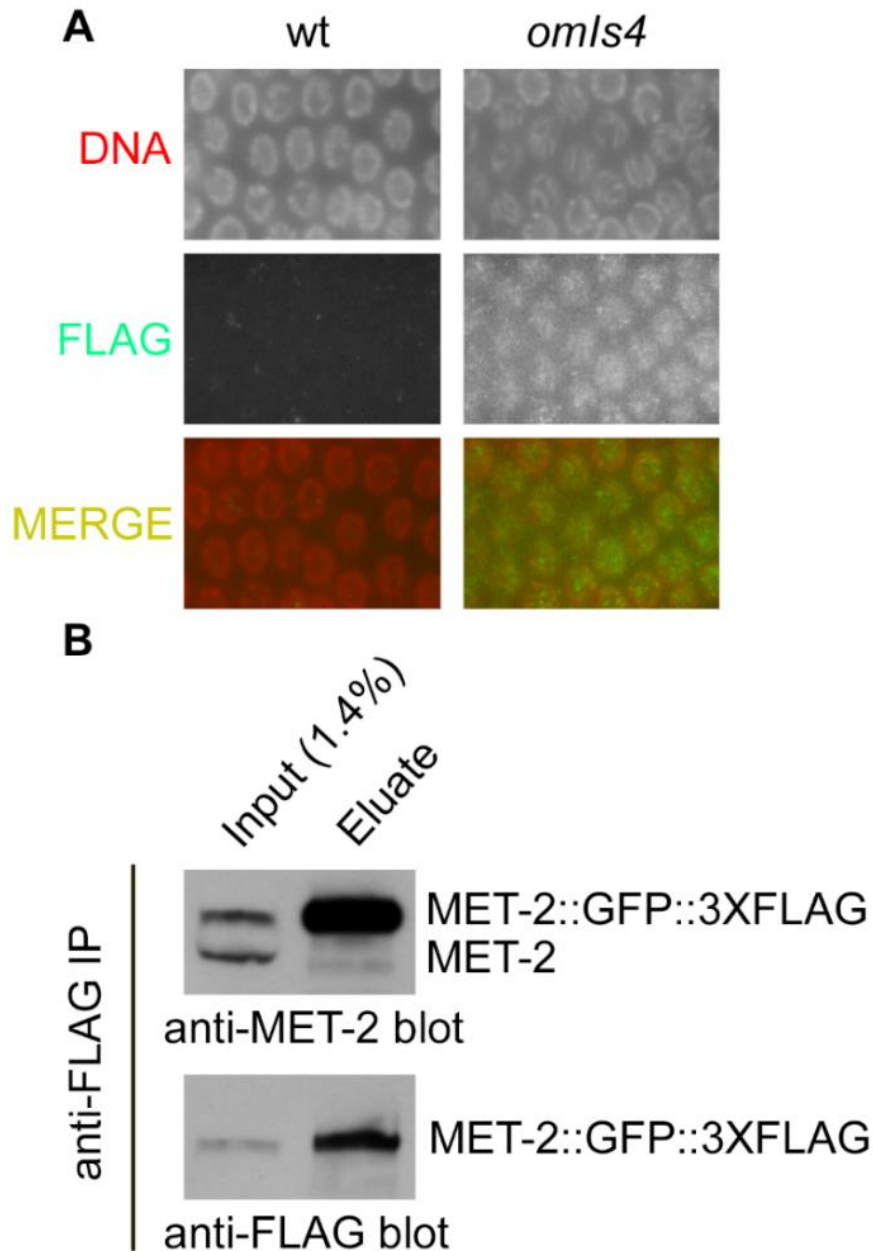| <37 kD	
MET-2	
DYL-1	see above
SHOC-2	Leucine-rich repeat protein soc-2
H2A.V	see above

Figure 3.1. Immunoprecipitation to recover MET-2-associated factors

A.   Immunolabeling using anti-FLAG antibody in *omIs4* and wild type (negative

control) hermaphrodite germline; pachytene stage nuclei are shown. *omIs4* transgene:

mex-5p::met-2::gfp::3xflag.

B.   Immunoprecipitation using anti-FLAG antibody with *omIs4* transgenic worm

lysate. Both input (left column) and eluate (right column) were subjected to anti-MET-2 and anti-FLAG immuno-blot. MET-2 antibody recognized both the endogenous MET-2 and the transgenic fusion protein in the input material, MET-2::GFP::3XFLAG was enriched in the eluate as shown by both blots. (MET-2: ~150 kDa)
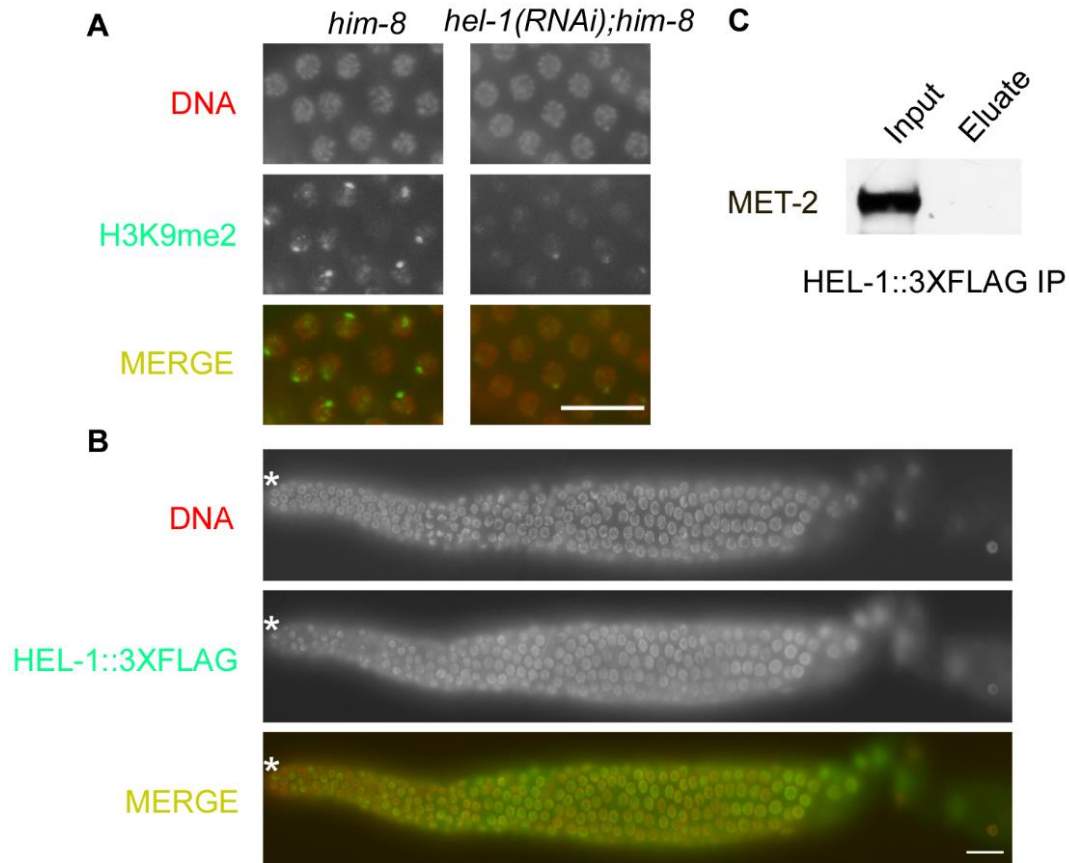
Figure 3.2. *hel-1* activity impacts H3K9me2 distribution

A.   Knockdown of *hel-1* expression reduces the H3K9me2 enrichment on the X chromosome in the male meiotic germ cell nuclei.

B.   HEL-1 localizes to the nuclei of germ cells. *hel-1::3xflag* hermaphrodites were dissected and stained with DAPI (to visualize DNA) and anti-FLAG antibody.

C.   Extracts from *hel-1::3xflag* adults was subjected to immunoprecipitation using anti-FLAG antibody. MET-2 did not co-IP with HEL-1::3XFLAG.

*, Distal end of gonad arm
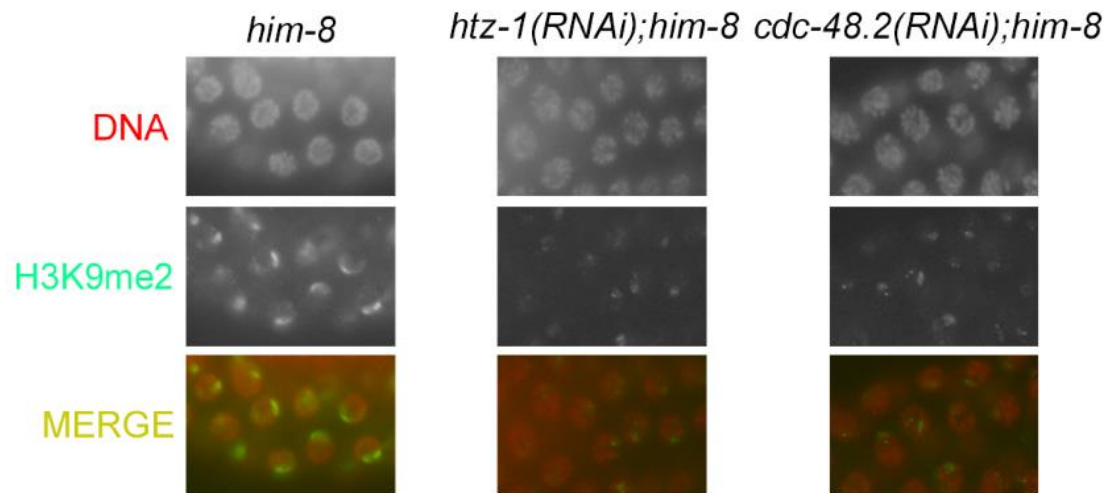
Figure 3.3. *htz-1* **and** *cdc-48.2* **might regulate H3K9me2 allocation.** Each panel

shows pachytene nuclei in an adult male germline co-labeled with DAPI to visualize

DNA and anti-H3K9me2 antibody.

Figure 3.4. MET-2 was not recovered in DLC-1 immunoprecipitation

A.   The H3K9me2 distribution in *dlc-1(RNAi);him-8* animals is comparable to *him-8* animals.

B.   Immunoprecipitation using anti-GFP antibody on protein extract from *dlc-1::gfp* animals fails to detect MET-2 in the IP eluent. (DLC-1::GFP: ~40 kDa; MET-2: ~150 kDa)

Chapter IV SMRC-1 might interact with a modified form of EKL-1

4.1 Introduction

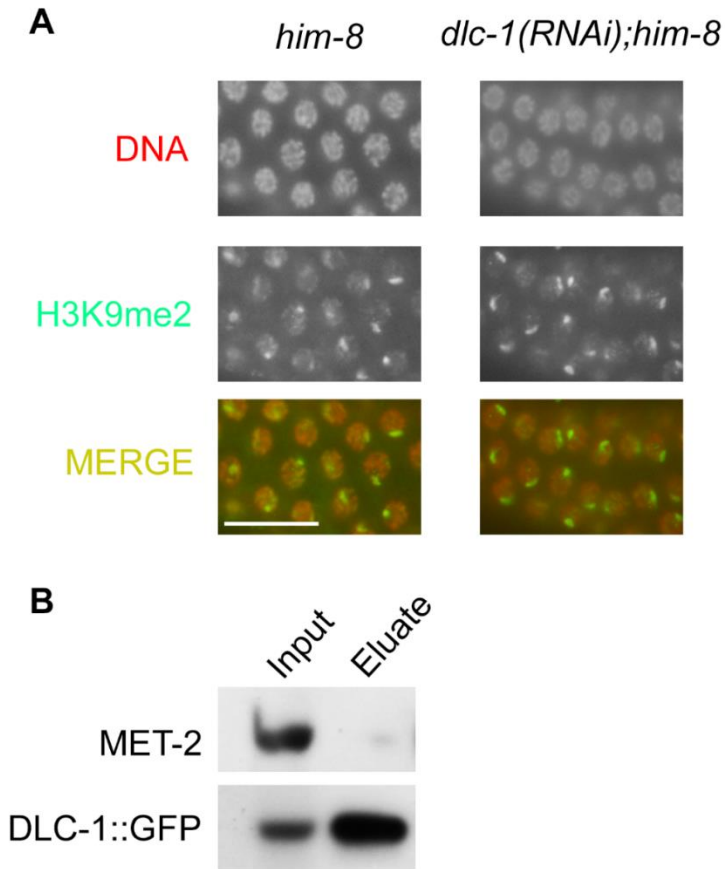EKL-1, a Tudor-domain protein, is required for the biogenesis of 22G-siRNA in *C. elegans* (Gu *et al.*, 2009). It associates with DRH-3 and EGO-1 to form a complex, which is critical for processing 26G-siRNAs into 22G-siRNAs (Gu *et al.*, 2009). In *C. elegans,* P granules are known to contain proteins important for RNA metabolism, such as siRNA pathway components (Updike and Strome, 2010). Consistent with its role in small RNA pathway, EKL-1 is primarily detected in the P granules of germ cells (Xu and Maine, unpublished). Importantly, *ekl-1* mutants display an altered H3K9me2 distribution pattern in *C. elegans* germ cells (She *et al.*, 2009). The enrichment of H3K9me2 on unpaired chromatin is absent in the *ekl-1* mutant animals, whereas the paired chromosomes seem to accumulate more H3K9me2 marks compared to wild type (She *et al.*, 2009). The connection between the CSR-1 small RNA pathway and H3K9me2 in *C. elegans* prompted us to address the mechanism by which the CSR-1 small RNA pathway interacts with this heterochromatic histone modification. Other members of the Maine lab generated anti-EKL-1 antibody and performed co-immunoprecipitation to recover candidate interactors of EKL-1 (X. Xu and E. Maine, unpublished). EKL-1 had previously been reported as interacting with DRH-3. And our lab recovered DRH-3 in the anti-EKL-1 co-IP experiments. In this chapter, I will describe an interaction between SMRC-1 and EKL-1. Together with the finding that SMRC-1 associates with MET-2 (chapter II), this result may establish a link between the CSR-1 small RNA pathway and MET-2.

4.2 Results

SMRC-1 is identified as a candidate interactor of EKL-1

Antibody was generated against an EKL-1 peptide and assayed for specificity and

efficiency in *C. elegans* by both protein blot and indirect immunofluorescence labeling of

dissected tissue (X. Xu and E. Maine, unpublished data). *ekl-1* is predicted to encode a

protein that is ~70 kDa in size (wormbase.org). The antibody recognizes an ~71 kDa

protein by protein blot. EKL-1 protein by protein blot is absent from the *ekl-1(om83)* null

mutant (data not shown). Immuno-labeling detected EKL-1 expression mainly on the P

granules (E. Maine, unpublished data). To recover EKL-1 interactors, this α-EKL-1

antibody was used to conduct co-IP experiments coupled with tandem MS/MS

sequencing. We also recovered anther DRH-3 interactor, EGO-1, in the co-IP

experiment (Table 4.1). Detection of EGO-1 and DRH-3 validated our approach to

identify other EKL-1 interactors.

SMRC-1 was recovered as a candidate EKL-1 interactor. Since SMRC-1

associates with MET-2 (see chapter II), we were particularly interested in testing

whether SMRC-1 might connect an siRNA pathway and MET-2. To confirm the

association between EKL-1 and MET-2, we performed anti-FLAG immunoprecipitation

using the CRISPR-generated *3xflag::smrc-1* transgenic strain described in Chapter II

and probed for the presence of EKL-1 in the co-IP material. This experiment

consistently detected a product of ~75 kDa in the eluate (Figure 4.1A, 4.1B). We

assume the 75 kDa protein is EKL-1 since this anti-EKL-1 detects no non-specific

proteins in whole extracts. Intriguingly, the size of EKL-1 appears to have shifted from

~71 kDa in the input lane to ~75 kDa in the eluate lane. This increase in size of EKL-1

on protein blots suggested the presence of a post-translational modification, such as phosphorylation or ubiquitination. Here, I refer the modified protein as EKL-1^M. Since SMRC-1 is majorly detected in the nucleus, whereas EKL-1 is largely detected in the P-granules, we propose that the underrepresented EKL-1^M might be a very low abundance form that is localized in the nucleus and interacts with SMRC-1. To elucidate the specific form of modification in EKL-1^M, enrichment of the modified EKL-1^M through large scale of ant-FLAG immunoprecipitation using the *3xflag::smrc*-1 strain would be the first step in the future. To understand the specific modification of EKL-1^M, we plan to subject the enriched EKL-1^M to LC-MS/MS.

4.3 Discussion

Modified form of EKL-1 might locate to the nucleus in germ cells

We have shown that EKL-1 majorly localizes to the P granules in germ cells and SMRC-1 is mainly expressed in the nucleus. For the association between EKL-1^M and SMRC-1 to take place, we speculate that the EKL-1^M might be distributed to the nucleus and interact with SMRC-1. Since we were not able to visualize the modified form of EKL-1 when we subjected the whole worm lysate to anti-EKL-1 protein blot, we hypothesize that the EKL-1^M might be underrepresented from whole extract. To test this hypothesis, we need to visualize and locate the expression of EKL-1^M. To achieve this goal, a series of experiments needs to be carried out. In order to enrich the modified form of EKL-1, we first need to identify the specific form of modification associated with it. The first step would be using antibody against FLAG to immunoprecipitate 3XFLAG::SMRC-1 and the EKL-1^M that associates with it. The immunoprecipitated material would be subjected to

mass spec sequencing that is able to identify the specific post-translational modification associated with EKL-1^M. Once the specific post-translational modification is identified, then we need to generate antibody that recognizes EKL-1^M specifically. When a functional antibody against EKL-1^M is made, we would be able to perform immuno-labelling and detect the protein expression profile of EKL-1^M in germ cells.

4.4 Methods

EKL-1 immunoprecipitation and MS/MS sequencing

EKL-1 IP was prepared from *him-8(e1489)* adults as follows. 500-750 ul of pelleted worms were resuspended in 1 ml FA buffer (50 mM Hepes pH 7.6, 140 mM NaCl, 0.1% Sodium deoxycholate, 1% Triton X-100, 1 mM EDTA), the volume was split into two tubes, and 100 ul glass beads (710-1180 microns) were added to each tube. Tissue was disrupted using a FastPrep 120 for two 15 sec pulses on setting 5.5s, with 10 min on ice in between pulses. Beads were pelleted by spinning 2 min at 800 rpm in a microfuge. Supernatants were pooled into a clean tube, which was then was spun at 8000 rpm for 30 min. Supernatent was kept for the following experiment. Protein concentration was determined by Bradford assay. To IP EKL-1, 3-5 ug of anti-EKL-1 antibody was incubated with ~300-500 ng of protein overnight at 4°C with rotation. After removing an in aliquot to use as input, an appropriate vol of precleared Protein A/G beads was added and incubated for $\geq$ 2 hr at 4°C with rotation. Beads were pelleted, washed at RT with FA buffer (1 mM EDTA, 50 mM HEPES-KOH, 140 mM NaCl, 0.1% sodium deoxycholate, 1% Triton X-100) 2X, and protein was eluted at RT for 10 min with 2X SDS loading buffer. Beads were pelleted at 2000 rpm for 1-2 min. Supernatant was removed to a new tube, beta-mercaptoethanol was added, tube was place at 95°C

for 10 min, vortexed, and spun to pellet debris. Supernatant was loaded onto a protein gel. Using size standards (Bio-rad, Precision Plus protein standards) as a guide, the gel lane was cut into 4 pieces for tandem mass spec analysis of proteins (Keck Facility, Yale).

FLAG IP

3xFLAG::SMRC-1 IP and immunoblot analysis were performed as follows. Anti-FLAG antibodies were coupled with protein G Dynabeads (Invitrogen) to reach a final concentration of 5ug antibody/mg beads following the Thermo Fisher protocol. Synchronized worms were harvested from ten 60mm NGM and collected by centrifuging at 13,200 rpm for 1min. Supernatants were aspirated, worm pellets were snap frozen in liquid nitrogen and stored in -80°C freezer until use. Worm pellets were thawed on ice and an equal volume of H-100 buffer containing NP40 (50 mM Hepes, pH 7.5, 100 mM KCl, 1mM MgCl2, 1 mMEDTA, 10% glycerol); proteinase inhibitor cocktail (Roche) was added to the tube. Extracts were prepared by using a FastPrep as described above. 3-5 mg of protein extract was incubated with 1 mg of antibody-coupled Dynabeads overnight at 4ºC with rotation. Beads were washed twice with 1ml of H-100 buffer for 5 min each. Proteins were eluted with 20ul of sample buffer at 55ºC for 10 min.

Figures and tables

Table 4.1. % peptide coverage for proteins of interest

Protein	Peptide Coverage
EKL-1	22.4%
EGO-1	8.3%
DRH-3	8.3%
SMRC-1	2.6%

Mass spectrometric analysis of the EKL-1 immunoprecipitated eluent fraction, only % of peptide coverage for proteins of interest are shown.
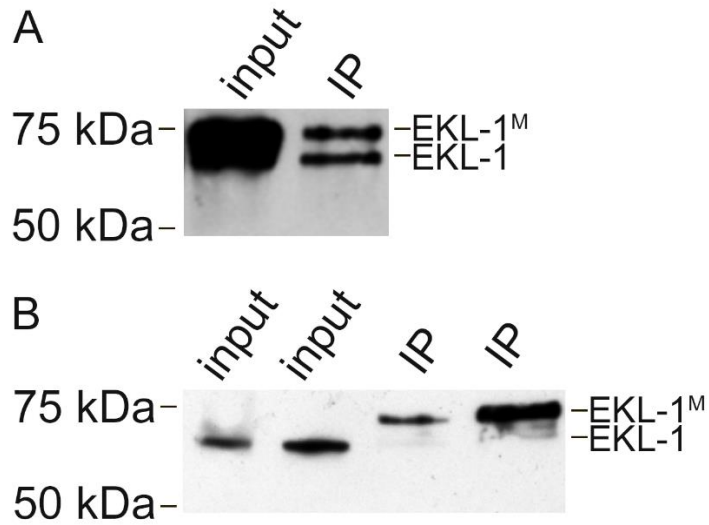
Figure 4.1. SMRC-1 might associate with a modified form of EKL-1

A.   Antibody against EKL-1 of total lysates (left lane) and proteins

immunoprecipitating with an antibody against FLAG (right lane) in extract from

3xflag::smrc-1 transgenic strains.

B.   Antibody against EKL-1 of total lysates (left two lanes) and proteins

immunoprecipitating with an antibody against FLAG (right two lanes) in extract from

3xflag::smrc-1;him-8 transgenic strains. Blots were lightly exposed.

Chapter V Discussion

We reported a series of studies attempting to identify interacting partners of MET-2. In Chapter II, we described such a factor, SMRC-1, as a novel interactor that functions together with MET-2 to maintain genome integrity. The expression profile of both MET-2 and SMRC-1 were examined, and the function of SMRC-1 was dissected through both genetic and biochemical methods as well in this Chapter. The other interesting potential interactors of MET-2 were described in Chapter III. We also reported an association between SMRC-1 and EKL-1[M] in Chapter IV. Here, I will discuss some possible models relating to the functions of MET-2 and SMRC-1 in the *C. elegans* germline.

MET-2 and SMRC-1 interacts in germline, might also in somatic tissue

Multiple lines of evidences suggested that distribution of H3K9me2 in somatic and germline tissues might be regulated differently. First, we found that H3K9me2 is detected at a much lower level in germline compared to the somatic tissues by protein blotting (Guo *et al.*, 2015). Therefore, the ChIP-seq data from whole animals might majorly represent the situations in somatic tissues. Utilizing germ cells that are purified from animals expressing GFP driven by a germline-specific *pie-1* promoter, Ho *et al* did ChIP-seq using anti-H3K9me2 antibody. The ChIP-seq data collected in this germline-specific manner revealed an even distribution of H3K9me2 along each of the chromosomes, in contrast to a repeat-enriched distribution pattern of H3K9me2 in somatic tissues (Ho *et al.*, 2014). Second, our lab assayed small RNA pathway members to look for factors that play important roles in regulating deposition of H3K9me2 in pachytene nuclei (She *et al.*, 2009). The results showed that members in

the csr-1 siRNA pathway are involved in regulating meiotic H3K9me2 (She *et al.*, 2009). It has been previously reported that the CSR-1-bound siRNAs target germline-expressed genes, and members in this CSR-1 siRNA pathway, including EKL-1, CSR-1 and EGO-1 are majorly expressed in the germline (Claycomb *et al.*, 2009). Thus, it is very likely that the CSR-1 siRNA pathway regulates the distribution of H3K9me2 in germ cells during meiosis but not in somatic tissue.

The interaction between MET-2 and SMRC-1 we reported in Chapter II suggested a potential link between histone modification and DNA damage. The immunoprecipitation experiments we performed to test the interaction between these two proteins were conducted using whole worm extracts. This result informed us that these two proteins associate in a complex, but do not show that these two proteins actually associate in the germline due to the complexity of whole worm extracts. Our immuno-labeling studies revealed that both SMRC-1 and MET-2 are expressed in but not limited to the germline tissue. Thus, colocalization analysis between MET-2 and SMRC-1 was mandatory in order to test that whether these two proteins are in close proximity in the germline. Results in Figure 2.2 showed that MET-2 and SMRC-1 partially colocalize in both mitotic and meiotic nuclei. However, at the scale of immunofluorescence, we are not able to assess if MET-2 and SMRC-1 colocalize on chromatin.

The genomic distribution of MET-2 in young adult animals was analyzed by McMurchy *et al*, and they reported that MET-2 is distributed along the distal ends of the autosomes and is strongly associated with repeat-enriched sequences (McMurchy *et al.*, 2017). This set of data represents the net distribution of MET-2 on chromatin in the

various tissues extracted from whole animals, and recapitulate the distribution of H3K9me2 along chromosomes based on previous reports. Intriguingly, our immuno-labeling result showed that MET-2 is evenly distributed in the nucleus with no obvious enrichment along chromosome arms, thus it would be interesting to probe the distribution of MET-2 on chromatin in a germline-specific manner. Also, there is no report regarding the SMARCAL1 distribution genomewide, although local enrichment of SMARCAL1 over telomeric sequences in human culture cells has been confirmed via chromatin immunoprecipitation assays (Cox *et al.*, 2016). In order to better understand the function of the interaction between SMRC-1 and MET-2, an in-depth mapping of the distribution of these two proteins on chromatin in the germline would be needed.

In addition, it is highly possible that MET-2 and SMRC-1 also interact in somatic tissues, as we detected the expression of both MET-2 and SMRC-1 in the nuclei of intestinal cells (data not shown). Thus, I hypothesize that the interaction between SMRC-1 and MET-2 might not be restricted to the germline. To test this idea, immunoprecipitation with epitope-tagged SMRC-1 transgenes driven by a tissue-specific promoter could provide some information about the specific location where the interaction between SMRC-1 and MET-2 takes place.

Direct or indirect impact of SMRC-1 loss on H3K9me2 in the germline

We observed that transgenerational loss of *smrc-1* led to a disruption of H3K9me2 distribution in animals that had been passaged for 30 generations. Given the interaction between SMRC-1 and MET-2 and the known functions of SMRC-1 and MET-2, the loss of SMRC-1 could result in several downstream effects. First, in the absence of SMRC-1,

we observed a reduction of MET-2 average expression when the animals were challenged with replication stress compared to animals with functional SMRC-1. Based on this result, we hypothesize that the cumulative effects of *smrc-1* loss over many generations might cause replication stress and lead to a decreased level of MET-2, which subsequently results in an overall reduction of H3K9me2. Second, since we observed that SMRC-1 also plays an important role in regulating DNA repair, we hypothesize that the loss of SMRC-1 might cause random mutations in other genes that are important for H3K9me2 regulation. Consistent with random mutations, we observed that at the 30th generation, the fertility of animals varies significantly. There were completely sterile individuals as well as animals with a moderate clutch size. Third, reduction in MET-2 level in the germline due to the loss of SMRC-1 might cause misregulation of genes that promote H3K9me2 deposition. In conclusion, the effects we observed in the variability of H3K9me2 loss could result from a combination of above effects.

Location of the interaction between SMRC-1 and EKL-1^M

It is known that the 70kDa form of EKL-1 is expressed in embryos, and both germline and somatic tissue in adult animals (Claycomb *et al.*, 2009). It will be interesting to identify the tissues where the larger EKL-1^M is expressed if we are able to obtain an antibody that is specific for EKL-1^M. If it is present in the nuclei of germ cells, then a co-localization assay needs to be carried out in order to determine whether SMRC-1 and EKL-1^M are located in close proximity in the nucleus of germ cells. In the *ekl-1(om83)* mutant, H3K9me2 distribution was disrupted, with a reduction of labeling on unpaired

92

chromatin as well as an ectopic labeling of paired chromatin, such as the autosomes in wildtype males (She *et al.*, 2009). Presumably, the deletion in the *om83* allele causes abolishment of full length EKL-1 and also EKL-1^M. Thus it is hard to evaluate the contribution of EKL-1^M in regulating the proper deposition of H3K9me2. Generation of a mutant allele that specifically lacks the EKL-1^M would be useful to address the role of EKL-1^M in regulating the H3K9me2 distribution. It would be interesting to examine the co-localization of MET-2, SMRC-1 and EKL-1^M. If these three proteins were acting at the same location in the nucleus, I hypothesize the following model that depicts the interaction among these three proteins. Initially, formation of a DSB at a replication fork triggers the SMRC-1 binding near the damaged site, SMRC-1 then recruits the histone methyltransferase, MET-2, to compact the heterochromatin structure. In parallel, SMRC-1 recruits EKL-1^M, which might be associated with other small RNA machinery members to generate DNA damage siRNAs to silence corresponding aberrant transcripts.

Involvement of small RNA in DNA repair processes has been widely described as a general phenomenon in multiple species, including fungi, yeast, plants, Drosophila and mammalian cells (Hall *et al.*, 2003; Keskin *et al.*, 2014; Lee *et al.*, 2009; Michalik *et al.*, 2012; Storici *et al.*, 2007). An interplay between the small RNAs derived from aberrant transcripts near DNA damage sites and the DNA damage response (DDR) was initially reported in the fungus, *Neurospora crassa* (Lee *et al.*, 2009). It is largely agreed that the RNA-dependent RNA polymerase, QDE-1, amplifies the aberrant RNA transcripts at repetitive genomic loci and processes them into small RNA termed qiRNA (quelling-induced RNA). QiRNA then loads onto Argonaute QDE-2 to target possible

abnormal transcripts from damaged DNA sites (Lee *et al.*, 2010). Interestingly,

replication protein A has been shown to interact with QDE-1 directly in N. *crassa* (Lee *et al.*, 2010). In multiple organisms, replication protein A (RPA) has been shown to respond to DNA damage by directly binding to SMARCAL1 (Ciccia *et al.*, 2009).

However, there is no ortholog of SMARCAL1 found in N. *crassa*. Lee *et al* also found that QDE-1 could directly synthesize dsRNA using the ssDNA bound by RPA at replication as template, and they further proposed that QDE-1 functions not only as an RNA-dependent RNA polymerase but also as a DNA-dependent RNA polymerase (Lee *et al.*, 2010). Similarly, next-generation sequencing revealed the presence of DNA damage-induced small RNAs in the proximity of the DSB sites in plants (Wei *et al.*, 2012). Interestingly, the orthologue of Dicer protein in Arabidopsis, DCL, was shown to be required for proper repair of DSBs induced by irradiation (IR) (Wei *et al.*, 2012). More recently, the importance of small RNAs in the DSB repair pathway was highlighted in animals. The loss of the small RNA biogenesis machinery, such as the Dicer endonuclease, impacts the DNA repair response in Drosophila (Castel *et al.*, 2014; Francia *et al.*, 2012). Taking these findings together, one could imagine that SMRC-1 might recruit the EKL-1[M] siRNA machinery to the vicinity of the stalled replication forks (Figure 1). The association between SMRC-1 and the EKL-1[M] complex might signal the requirement of siRNA production to assist degradation of aberrant transcripts (Figure 1). To test that whether EKL-1[M] is important for generating siRNAs, a RNA immunoprecipitation (RIP) experiment using antibody against EKL-1[M] could be done to identify small RNAs that are bound to EKL-1[M]. In addition, it would be interesting to test

that whether the ekl-1^m mutant is defective in DSB repair since the evidence from other species is that small RNA plays an important role in repairing DNA damage.

In Chapter II, we hypothesized that SMRC-1 might help limit DSBs by recruiting MET-2 to deposit H3K9me2 marks near the stalled replication forks. In the vicinity of repetitive sequences, the compact heterochromatin structure inhibits the formation of DSBs. Based on the findings in chapter IV, we postulate that SMRC-1 might add another layer of siRNA regulation to ensure transcription fidelity by silencing aberrant transcripts arising from damaged DNA. In summary, we propose dual roles of SMRC-1 to ensure genome integrity and transcription fidelity when replication stress occurs.
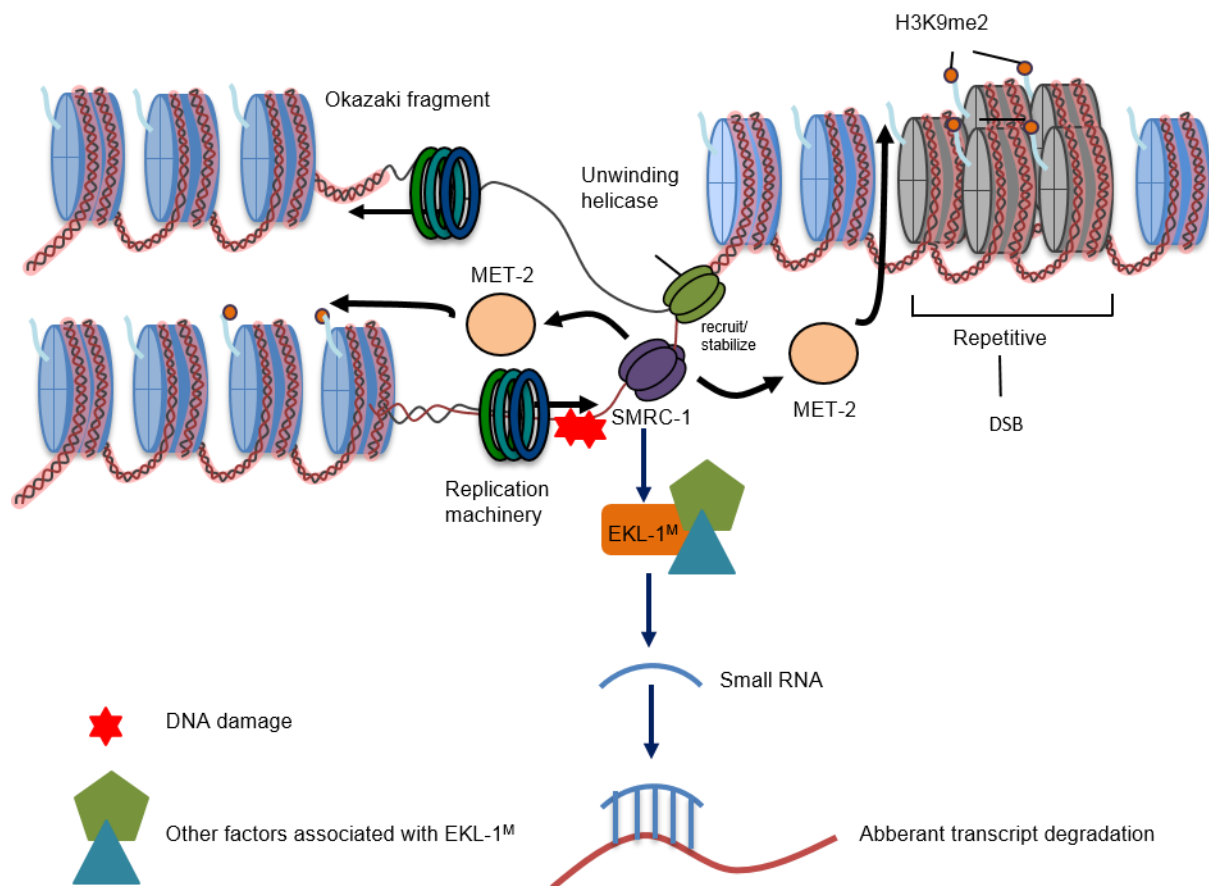
Figure 5.1 A model proposed to illustrate the orchestrated interactions among the three proteins studies in this thesis: MET-2, SMRC-1 and EKL-1[M.] We hypothesize that SMRC-1 plays an important role in maintaining the genomic integrity near replication forks by recruiting the H3K9me2 methyltransferase MET-2 and a hypothesized small RNA machinery member EKL-1[M]. The interaction between SMRC-1 and MET-2 might help to establish the heterochromatic status of nascent chromatin freshly replicated; whereas the interaction between SMRC-1 and EKL-1[M] facilitates the degradation of the aberrant transcript from the damaged sites.

Appendix

Introduction

In this chapter, I will discuss studies stemming from the molecular identification of *ego-3*. The *ego-3(om40)* mutation was identified as a genetic enhancer of *glp-1(bn18)*. The *glp-1(bn18);ego-3(om40)* double mutant exhibits severe reduction of germline proliferation compared to either single mutant at 20°C (Qiao *et al.*, 1995). *ego-3(om40)* single mutants display a variety of both somatic and germline defects. The mutant is generally slow growing compared to wild type (Qiao *et al.*, 1995). In addition, the *ego-3* mutants are severely uncoordinated (Unc) during larval stages ; intriguingly, the Unc phenotype disappears when the animals reach adulthood (Qiao *et al.*, 1995). An early germline defect of *ego-3* mutants is seen at L3 stage when the germline proliferation arrests. Later, germline development resumes at L4 stage. However, a significant portion of the *ego-3(om40)* adults have proximal proliferation, which leads to sterility of these animals. In addition, oocytes appear defective in *ego-3(om40)* mutants. We

recently determined that *ego-3* and *hsp-90* are the same gene (Lissemore *et al.*, in preparation).

I also studied the potential link between EKL-1 (described in Chapter IV) and two heat shock response proteins (HSPs), HSP-90 and HSP-1. HSP-90 is a conserved protein important for folding, stabilizing and trafficking of certain and is responsible for correct folding of its client proteins. *hsp-1* encodes another heat shock family protein HSP70A, which is expressed throughout the whole worm (wormbase.org). The association between HSP-1 and EKL-1 will be investigated in this chapter. Additionally, the implication of this interaction for the distribution of EKL-1 to P-granules will also be addressed here.

Results

hsp-90* RNAi phenocopies *ego-3(om40)

The molecular identification of *ego-3* was recently completed using a combination of genetic mapping and whole genome sequencing approaches (Lissemore, *et al.*, unpublished data). Only one mutation causing an amino acid change in the *hsp-90/daf-21* gene, was found in the genetic interval containing *ego-3*. In *C. elegans*, *hsp-90* has been shown to be important for chemosensation and dauer formation (Thomas *et al.*, 1993). Based on previous analysis, the proximal proliferation in *hsp-90(om40)* was hypothesized to be a gain-of-function phenotype, whereas other aspects of the *hsp-90(om40)* phenotypes were shown to be a loss-of-function. To elucidate whether the proximal tumor is a consequence of a loss-of-function or gain-of-function mutation in *hsp-90*, RNAi was utilized to knockdown the HSP-90 protein and see if this causes

proximal proliferation. *hsp*-90(RNAi) caused severe phenotypes, including sterility and developmental arrest. These are consistent with the known *hsp-90* null phenotype (Table 1, Figure 1 and Figure 2). Interestingly, around 5% of the treated males and hermaphrodites exhibited a proximal germline tumor (Table 1, Figure 1 and Figure 2). This result indicates that the *hsp-90(om40)* proximal tumor is caused by a loss of function. Therefore, *om40* appears to be a partial loss-of-function allele with no gain-of-function character.

hsp-90(om40) mutant is defective in exo-RNAi

HSP-90 was identified as a candidate interactor of EKL-1 interactors in the study described in chapter IV. After *ego-3* was identified as *hsp-90,* I tested whether HSP-90 might be necessary for RNAi. To address this question, we asked whether *hsp-90(om40)* worms are RNAi defective. We used *gfp* RNAi to attempt knockdown GFP-tagged proteins in wild type *hsp-90(om40)* backgrounds and then assayed for loss of GFP.

    To distinguish the difference between somatic and germline RNAi, we utilized *gfp*-tagged transgenes that are expressed in either somatic tissue or germline. *gld-1::gfp* was used to test the effect of *hsp-90(om40)* on germline RNAi. In the adult germline, GLD-1 is majorly detected in the cytoplasm and enriched on the P granules during meiosis (Jones *et al.*, 1996). In a wiltype background; GLD-1::GFP signal drops, indicating that *gld-1::gfp* transgenic animals are sensitive to *gfp* RNAi (Figure 3A). However, GLD-1::GFP levels remained high in the *hsp-90(om40); gld-1::gfp* worms,

indicating they had little or no sensitivity to *gfp* RNAi (Figure 3A). This result suggests that *hsp-90(om40)* worms are defective in RNAi.

In order to confirm the above observation, we crossed another *gfp*-tagged transgene, *his-2::gfp* driven by the germline-specific *pie-1* promoter, into the *om40* background. *his-2* encodes an H3 histone, which is part of the histone core (wormbase.org). The transgenic strain HIS-2::GFP expresses in germline nuclei. Interestingly, HIS-2::GFP in the *hsp-90(om40)* mutant remains primarily in the cytoplasm (Figure 3B). Alvarez *et al* reported that HSP90 and HSC70 are important for transporting histone H3/H4 from the cytoplasm to the nucleus in yeast and human cells (Alvarez *et al.*, 2011). This might explain the aberrant expression pattern of HIS-2::GFP in the *om40* mutant, and it also provides further evidence that *om40* is a loss-of-function allele of *hsp-90*. With *gfp* RNAi treatment, *his-2::gfp* expression was significantly reduced in *hsp-90(+)* animals(Figure 3B). In contrast, HIS-2::GFP expression in the *hsp-90(om40)* background remained high after *gfp* RNAi treatment. This result is consistent with the conclusion that *hsp-90(om40)* is defective in RNAi (Figure 3B).

To test somatic RNAi, I attempted to use *cdh-3::gfp*, *cdh-3* encodes a cadherin-related protein primarily expressed in neuronal cells in the adult tail (Pettitt *et al.*, 1996). *gfp* RNAi was performed with *cdh-3::gfp* and *cdh-3::gfp;hsp-90(om40)* larval. The former was used as a control to test RNAi efficiency. Unfortunately, *cdh-3::gfp* expression was not knocked down by *gfp* RNAi (Figure 4). It might be that low turnover rate of the CDH-3::GFP protein or high expression level of CDH-3::GFP efficient knockdown *cdh-3::gfp*. Therefore, I decided not use *cdh-3::gfp* for the RNAi defective test.

HSP-1 binds to EKL-1 and mediates the localization of EKL-1 to P granules

Previous observations suggest a connection between heat shock proteins and the RNAi pathway. Heat shock proteins have been reported to be required for RNAi, and HSP-90 has been shown to bind to the human Argonaute protein AGO2 (Liu *et al.*, 2004; Rivas *et al.*, 2005). A genome-wide screen for genes that play roles in RNAi revealed *hsc-70* as an important component of RNAi in *Drosophila* (Dorner *et al.*, 2006). Additionally, work in our lab identified the HSC-70 homolog in *C. elegans*, HSP-1, as a candidate EKL-1 interactor (X. Xu and E. Maine, unpublished data). To validate the HSP-1 association with EKL-1 and test whether it plays a role in RNAi, we generated a *3xflag*-tagged *hsp-1* transgene via the CRISPR method. Anti-FLAG antibody recognized a 75 kDa protein of the expected size of HSP-1::3XFLAG in the transgenic strain that is absent in the wild type worms (data not shown). Consistent with EKL-1 co-IP and mass spectrometry data, I found that HSP-1::3XFLAG co-precipitates with EKL-1 (Figure 5A).

To examine that whether HSP-1 is important for the proper distribution and localization of EKL-1 to P granules, we obtained the *hsp-1* RNAi clone from the Ahringer RNAi "feeding" library (Kamath *et al.*, 2003). Wild type animals fed with *hsp-1* dsRNA as gravid adults produced progeny that died as embryos or young larvae. To obtain adult animals with germlines of relatively normal morphology, I optimized the condition of RNAi feeding. Wild type animals of different larval stages were placed on *hsp-1* RNAi feeding plates. Adult animals were sterile with very small germline when they were put on the RNAi plates as L1/L2 larval. The EKL-1 expression pattern in the germline of these animals was severely disrupted (Figure 5B), which could result from a general

disorder of P granule structure due to loss of HSP-1 function. In contrast, L4 animals

treated with *hsp-1* RNAi for 24 hours at room temperature had relatively normal

germline morphology. This RNAi condition was selected to conduct the following

experiments.

In *hsp-1(RNAi)* animals, EKL-1 was no longer distributed to P granules, suggesting

that HSP-1 is important for either proper folding or/and distribution of EKL-1 in the

germline. To test where the P granule structure was affected by *hsp-1(RNAi)*, we

examined the localization of GLH-2, which is a core component of the P granule

scaffold. Interestingly, the GLH-2 distribution in the RNAi treated worms remained

comparable to wild type animals without treatment (Figure 5C). Taken together, these

data indicate that HSP-1 is important for proper distribution of EKL-1 to P granules. We

hypothesize that a direct association with EKL-1 by HSP-1 is necessary for its

distribution. We speculate that HSP-1 might regulate not only the folding but also

trafficking of EKL-1.

Methods

RNA interference

RNAi was carried out as described in Chapter III. Briefly, animals of various larval

stages were subjected to RNAi feeding at 22°C for *hsp-1* and *hsp-90.*

Immunohistochemistry

Indirect immunolabeling procedures were carried out as previously described (Guo *et

al.*, 2015; Maine *et al.*, 2005; She *et al.*, 2009). Adults (24 hour post-L4) were dissected

in PBS + 0.2mM levamisole in deep-well slides. Worms were fixed with 3% PFA for 5

mins followed by a 100% cold methanol for 1 min and incubated with 30% GS/PBST as

the blocking reagent for 1 hour at room temperature. Primary antibody diluted in 30%

GS/PBST (rabbit anti-EKL-1, this study, 1:200) was added and tissues were incubated

at 15°C overnight. Secondary antibody was Alexafluor 488-conjugated donkey anti-

rabbit (1:200).

DAPI staining

DAPI-staining was performed as described (Qiao *et al*. 1995). Briefly, intact animals

were fixed with cold methanol and stained with DAPI to visualize DNA.

Table 1. Phenotypes of *him-8* worms subjected to *hsp-90* RNAi.

Sex	Total # of germlines	Wildtype	Proximal tumor	Small germline and enlarged nuclei
hermaphrodite	16	3	1	12
male	36	8	2	26

Both *him-8* hermaphrodite and male L3 worms were placed on the *hsp-90* RNAi plate

and maintained for 36 hours at room temperature. Adult worms were then immediately

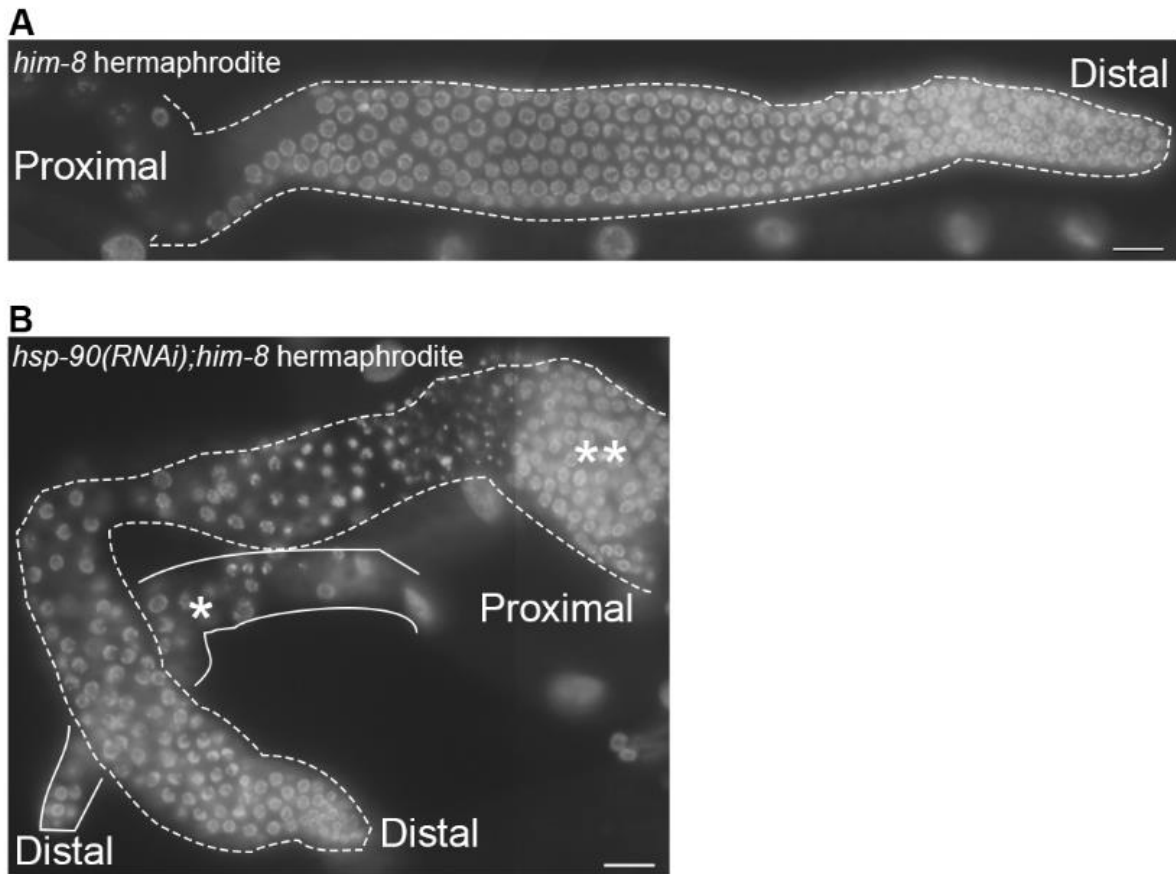dissected and fixed. DAPI staining reveals a variable germline phenotype.

Figure 1. *hsp-90* **RNAi phenocopies** *ego-3(om40)* **in hermaphrodites**

A.   *him-8* hermaphrodite as an experimental control stained with DAPI to visualize

germ cells.

B.   *him-8* L3 hermaphrodites were subjected to *hsp-90* RNAi for 36 hours at room

temperature. Adult animals were dissected and fixed before DAPI staining.

**indicates a proximal germline tumor
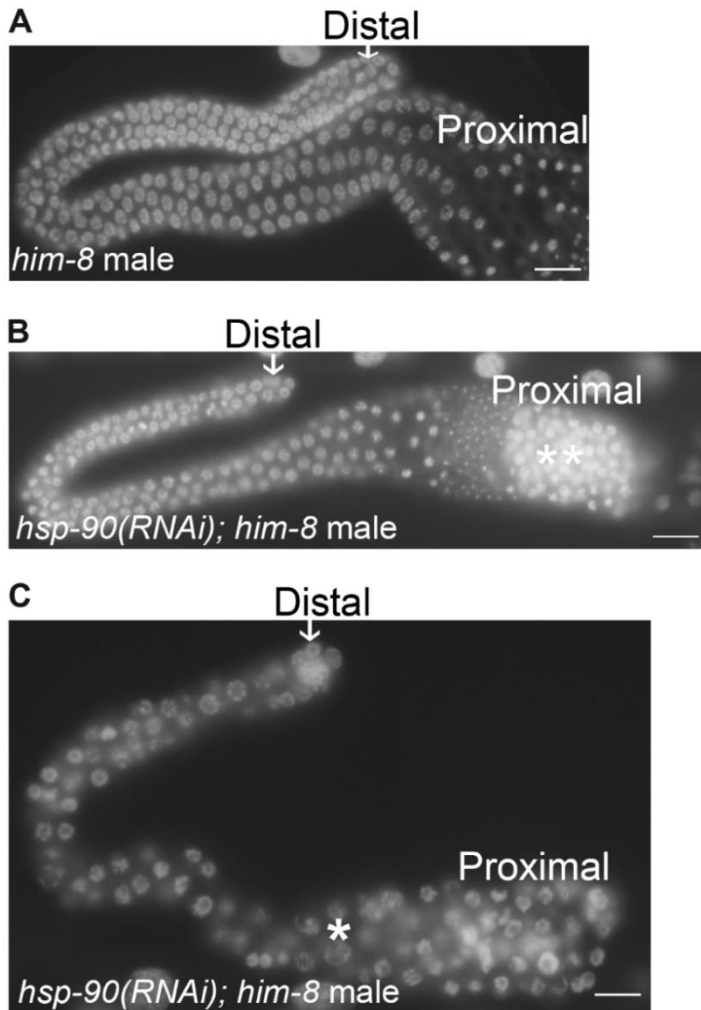
*indicates a small germline

Figure 2. *hsp-90* **RNAi phenocopies** *ego-3(om40)* **in males**

A.   *him-8* male as an experimental control stained with DAPI to visualize germ cells.

B.   *him-8* L3 males were subjected to *hsp-90* RNAi for 36 hours at room

temperature. Adult animals were dissected and fixed before DAPI staining.

Representative picture shows a proximal germline phenotype

**indicates a proximal germline tumor

C.   Representative picture of a small germline phenotype.
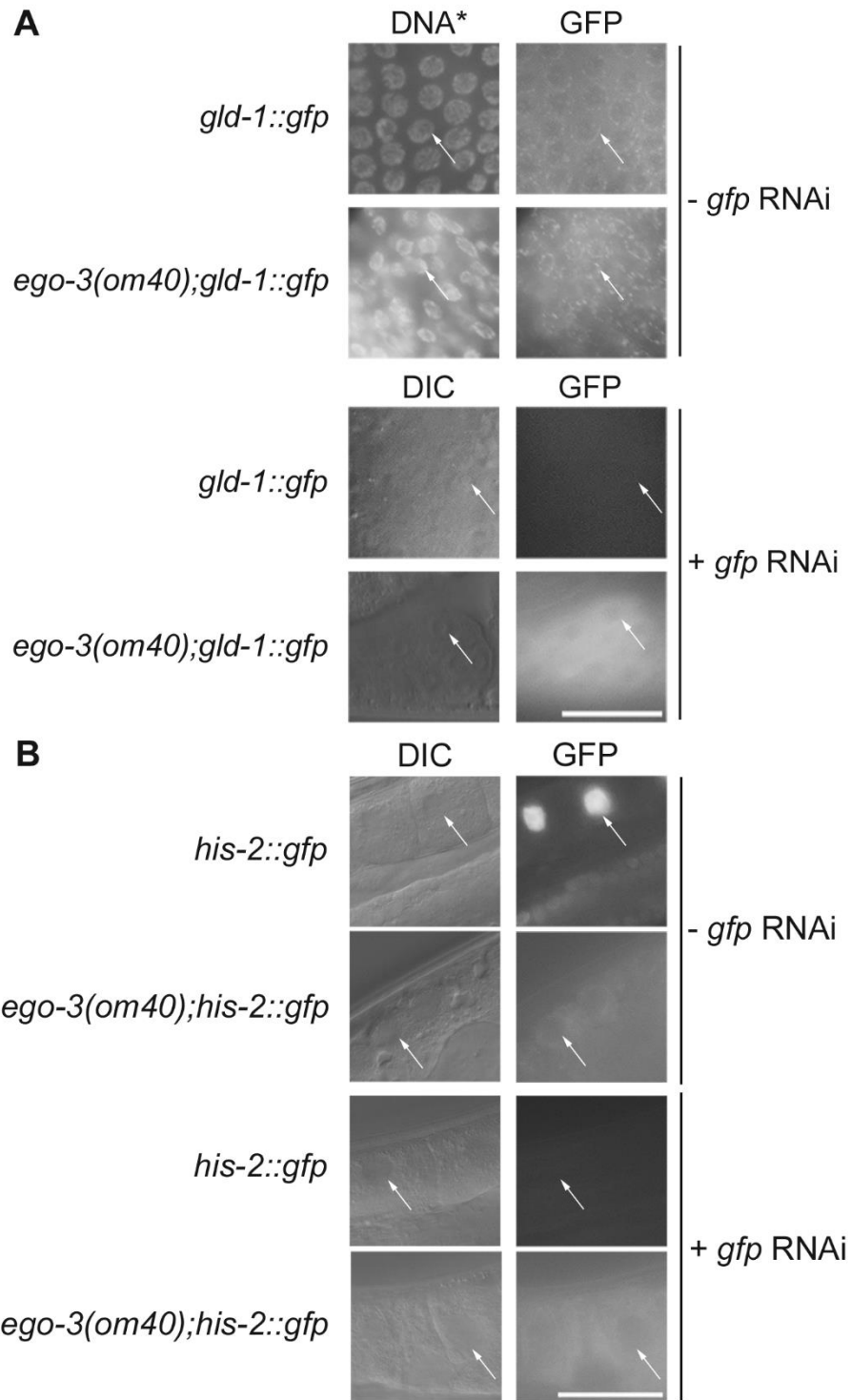
*indicates an enlarged nucleus

Figure 3. *om40* is germline exo-RNAi defective

A.   Top two panels: *gld-1::gfp* distribution in both wild type and *om40* background.
GLD-1 was localized to P granules in both genotypes.

Bottom two panels: *gfp* RNAi successfully suppressed the expression of the *gfp*
transgene in the wild type animals, and failed to silence *gfp* expression in the *om40*
worms.

B.   Top two panels: *his-2::gfp* distribution in both wild type and *om40* background.
H3 localized to the nucleus properly in the wild type background, however, the
distribution of H3 was diffused to the cytoplasm.

Bottom two panels: *gfp* RNAi successfully suppressed the expression of the *gfp*
transgene in the wild type animals, and failed to silence *gfp* expression in the *om40*
worms.

🢔 points to a representative nucleus in each genotype

Note: * DAPI was initially utilized to visualize DNA, but later I decided to use DIC, which
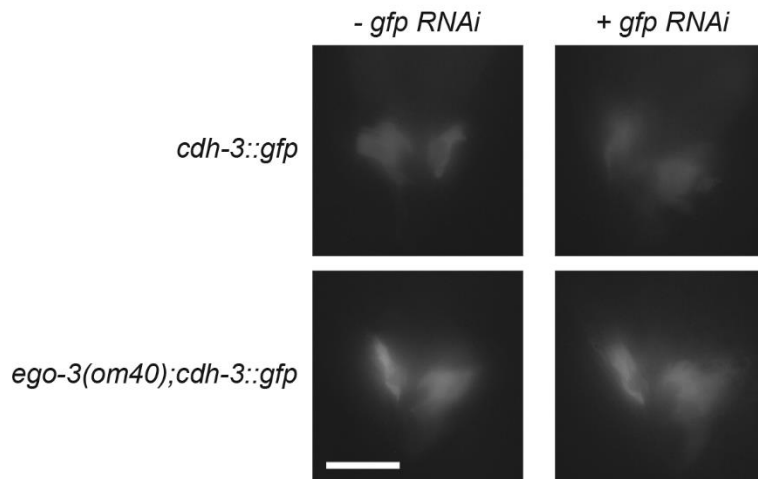is a sufficient and straightforward approach to visualize nuclei.

Figure 4. *gfp* **RNAi fails to suppress the expression of** *cdh-3::gfp* **in two neuronal cells in the tail.**
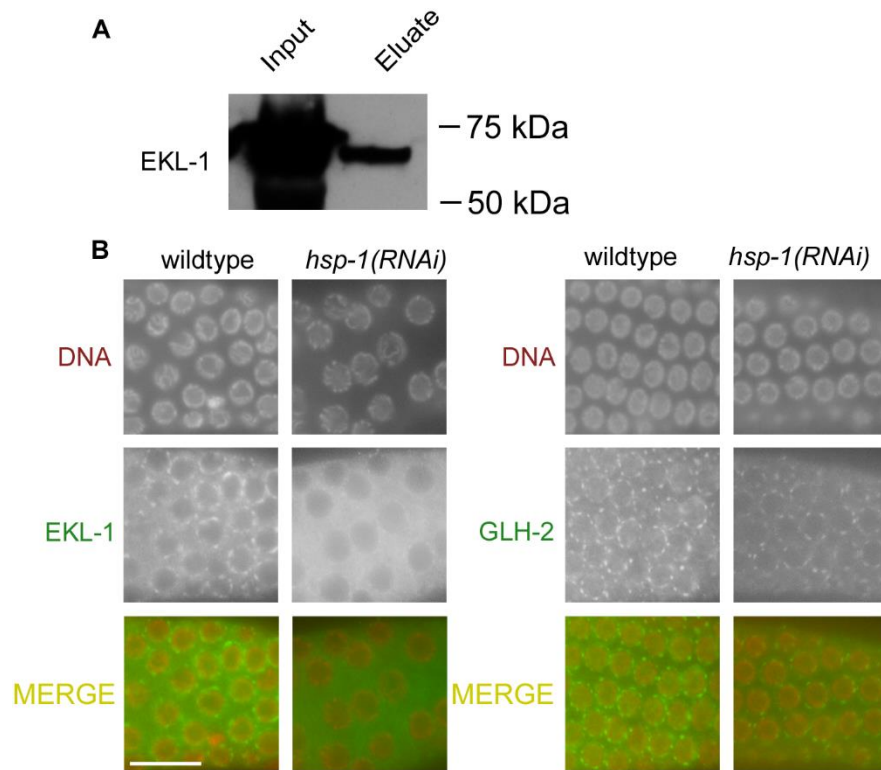
Figure 5. HSP-1 associates with EKL-1 and mediates the localization of EKL-1 to P granules

A.   Protein blot probed with anti-EKL-1 antibody. *hsp-1::3xflag* worms were harvested to perform immunoprecipitation using anti-FLAG antibody. Both input (left) and IP eluate (right) were subjected to protein blotting to probe for the presence of EKL-1.

B.   Wild type L4s were treated with *hsp-1* RNAi for 24 hours at room temperature. Adults were stained with either anti-EKL-1 (left two columns) or anti-GLH-2 (right two columns). EKL-1 was no longer distributed on the P granules, while the P granule structure remained intact as detected by GLH-2 labeling.

References

Agostinho, A., Meier, B., Sonneville, R., Jagut, M., Woglar, A., Blow, J., Jantsch, V., and Gartner, A. (2013). Combinatorial regulation of meiotic holliday junction resolution in C. elegans by HIM-6 (BLM) helicase, SLX-4, and the SLX-1, MUS-81 and XPF-1 nucleases. PLoS genetics *9*, e1003591.

Alabert, C., and Groth, A. (2012). Chromatin replication and epigenome maintenance. Nat Rev Mol Cell Biol *13*, 153-167.

Alpi, A., Pasierbek, P., Gartner, A., and Loidl, J. (2003). Genetic and cytological characterization of the recombination protein RAD-51 in Caenorhabditis elegans. Chromosoma *112*, 6-16.

Alvarez, F., Munoz, F., Schilcher, P., Imhof, A., Almouzni, G., and Loyola, A. (2011). Sequential establishment of marks on soluble histones H3 and H4. The Journal of biological chemistry *286*, 17714-17721.

Andersen, E.C., and Horvitz, H.R. (2007). <div xmlns="http://www.w3.org/1999/xhtml">Two C. elegans histone methyltransferases repress lin-3 EGF transcription to inhibit vulval development</div>. Development *134*, 2991-2999.

Arribere, J.A., Bell, R.T., Fu, B.X., Artiles, K.L., Hartman, P.S., and Fire, A.Z. (2014). Efficient Marker-Free Recovery of Custom Genetic Modifications with CRISPR/Cas9 in Caenorhabditis elegans. Genetics.

Arthanari, H., and Bolton, P.H. (2001). Functional and dysfunctional roles of quadruplex DNA in cells. Chemistry & biology *8*, 221-230.

Austin, J., and Kimble, J. (1989). Transcript analysis of glp-1 and lin-12, homologous genes required for cell interactions during development of C. elegans. Cell *58*, 565-571.

Baldi, S., and Becker, P. (2013). The variant histone H2A.V of Drosophila—three roles, two guises. Chromosoma *122*, 245-258.

Bansbach, C.E., Betous, R., Lovejoy, C.A., Glick, G.G., and Cortez, D. (2009). The annealing helicase SMARCAL1 maintains genome integrity at stalled replication forks. Genes & development *23*, 2405-2414.

Bean, C.J., Schaner, C.E., and Kelly, W.G. (2004). Meiotic pairing and imprinted X chromatin assembly in Caenorhabditis elegans. Nature genetics *36*, 100-105.

Bergerat, A., de Massy, B., Gadelle, D., Varoutas, P.-C., Nicolas, A., and Forterre, P. (1997). An atypical topoisomerase II from archaea with implications for meiotic recombination. Nature *386*, 414-417.

Bessler, J.B., Andersen, E.C., and Villeneuve, A.M. (2010). Differential Localization and Independent Acquisition of the H3K9me2 and H3K9me3 Chromatin Modifications in the *Caenorhabditis elegans* Adult Germ Line. PLoS genetics *6*, e1000830.

Betous, R., Glick, G.G., Zhao, R., and Cortez, D. (2013). Identification and characterization of SMARCAL1 protein complexes. PloS one *8*, e63149.

Betous, R., Mason, A.C., Rambo, R.P., Bansbach, C.E., Badu-Nkansah, A., Sirbu, B.M., Eichman, B.F., and Cortez, D. (2012). SMARCAL1 catalyzes fork regression and Holliday junction migration to maintain genome stability during DNA replication. Genes & development *26*, 151-162.

Bhalla, N., and Dernburg, A.F. (2005). A conserved checkpoint monitors meiotic chromosome synapsis in Caenorhabditis elegans. Science *310*, 1683-1686.

Bhat, K.P., Betous, R., and Cortez, D. (2015). High-affinity DNA-binding domains of replication protein A (RPA) direct SMARCAL1-dependent replication fork remodeling. The Journal of biological chemistry *290*, 4110-4117.

Billi, A.C., Fischer, S.E., and Kim, J.K. (2014). Endogenous RNAi pathways in C. elegans. WormBook, 1-49.

Boddy, M.N., Gaillard, P.-H.L., McDonald, W.H., Shanahan, P., Yates, J.R., and Russell, P. (2001). Mus81-Eme1 Are Essential Components of a Holliday Junction Resolvase. Cell *107*, 537-548.

Boerkoel, C.F., Takashima, H., John, J., Yan, J., Stankiewicz, P., Rosenbarker, L., Andre, J.L., Bogdanovic, R., Burguet, A., Cockfield, S.*, et al.* (2002). Mutant chromatin remodeling protein SMARCAL1 causes Schimke immuno-osseous dysplasia. Nature genetics *30*, 215-220.

Brenner, S. (1974). The Genetics of CAENORHABDITIS ELEGANS. Genetics *77*, 71-94.

Burma, S., Chen, B.P., Murphy, M., Kurimasa, A., and Chen, D.J. (2001). ATM phosphorylates histone H2AX in response to DNA double-strand breaks. The Journal of biological chemistry *276*, 42462-42467.

Castel, S.E., Ren, J., Bhattacharjee, S., Chang, A.Y., Sánchez, M., Valbuena, A., Antequera, F., and Martienssen, R.A. (2014). Dicer promotes transcription termination at sites of replication stress to maintain genome stability. Cell *159*, 572-583.

Cheung, I., Schertzer, M., Rose, A., and Lansdorp, P.M. (2002). Disruption of dog-1 in Caenorhabditis elegans triggers deletions upstream of guanine-rich DNA. Nature genetics *31*, 405-409.

Chowdhury, D., Keogh, M.-C., Ishii, H., Peterson, C.L., Buratowski, S., and Lieberman, J. (2005). γ-H2AX Dephosphorylation by Protein Phosphatase 2A Facilitates DNA Double-Strand Break Repair. Molecular cell *20*, 801-809.

Ciccia, A., Bredemeyer, A.L., Sowa, M.E., Terret, M.E., Jallepalli, P.V., Harper, J.W., and Elledge, S.J. (2009). The SIOD disorder protein SMARCAL1 is an RPA-interacting protein involved in replication fork restart. Genes & development *23*, 2415-2425.

Claycomb, J.M., Batista, P.J., Pang, K.M., Gu, W., Vasale, J.J., van Wolfswinkel, J.C., Chaves, D.A., Shirayama, M., Mitani, S., Ketting, R.F.*, et al.* (2009). The Argonaute CSR-1 and its 22G-RNA co-factors target germline genes and are required for holocentric chromosome segregation. Cell *139*, 123-134.

Colaiácovo, M.P., MacQueen, A.J., Martinez-Perez, E., McDonald, K., Adamo, A., La Volpe, A., and Villeneuve, A.M. (2003a). Synaptonemal Complex Assembly in C. elegans Is Dispensable for Loading Strand-Exchange Proteins but Critical for Proper Completion of Recombination. Developmental Cell *5*, 463-474.

Colaiácovo, M.P., MacQueen, A.J., Martinez-Perez, E., McDonald, K., Adamo, A., La Volpe, A., and Villeneuve, A.M. (2003b). Synaptonemal complex assembly in C. elegans is dispensable for loading strand-exchange proteins but critical for proper completion of recombination. Dev Cell *5*, 463-474.

Cox, K.E., Marechal, A., and Flynn, R.L. (2016). SMARCAL1 Resolves Replication Stress at ALT Telomeres. Cell reports *14*, 1032-1040.

Craig, A.L., Moser, S.C., Bailly, A.P., and Gartner, A. (2012). Methods for studying the DNA damage response in the Caenorhabdatis elegans germ line. Methods Cell Biol *107*, 321-352.

Creamer, K.M., and Partridge, J.F. (2011). RITS- connecting transcription, RNAi and heterochromatin assembly in Fission Yeast. Wiley interdisciplinary reviews RNA *2*, 632-646.

de Massy, B., Rocco, V., and Nicolas, A. (1995). The nucleotide mapping of DNA double-strand breaks at the CYS3 initiation site of meiotic recombination in Saccharomyces cerevisiae. The EMBO journal *14*, 4589-4598.

Dernburg, A.F., McDonald, K., Moulder, G., Barstead, R., Dresser, M., and Villeneuve, A.M. (1998). Meiotic Recombination in C. elegans Initiates by a Conserved Mechanism and Is Dispensable for Homologous Chromosome Synapsis. Cell *94*, 387-398.

Dodge, J.E., Kang, Y.K., Beppu, H., Lei, H., and Li, E. (2004). Histone H3-K9 methyltransferase ESET is essential for early development. Molecular and cellular biology *24*, 2478-2486.

Dorner, S., Lum, L., Kim, M., Paro, R., Beachy, P.A., and Green, R. (2006). A genomewide screen for components of the RNAi pathway in Drosophila cultured cells. Proceedings of the National Academy of Sciences *103*, 11880-11885.

Dorsett, M., and Schedl, T. (2009). A Role for Dynein in the Inhibition of Germ Cell Proliferative Fate. Molecular and cellular biology *29*, 6128-6139.

Duan, Q., Chen, H., Costa, M., and Dai, W. (2008). Phosphorylation of H3S10 blocks the access of H3K9 by specific antibodies and histone methyltransferase. Implication in regulating chromatin dynamics and epigenetic inheritance during mitosis. The Journal of biological chemistry *283*, 33585-33590.

Duchaine, T.F., Wohlschlegel, J.A., Kennedy, S., Bei, Y., Conte, D., Jr., Pang, K., Brownell, D.R., Harding, S., Mitani, S., Ruvkun, G.*, et al.* (2006). Functional proteomics

reveals the biochemical niche of C. elegans DCR-1 in multiple small-RNA-mediated pathways. Cell *124*, 343-354.

Eberl, D.F., Lorenz, L.J., Melnick, M.B., Sood, V., Lasko, P., and Perrimon, N. (1997). A new enhancer of position-effect variegation in Drosophila melanogaster encodes a putative RNA helicase that binds chromosomes and is regulated by the cell cycle. Genetics *146*, 951-963.

Elgin, S.C., and Reuter, G. (2013). Position-effect variegation, heterochromatin formation, and gene silencing in Drosophila. Cold Spring Harbor perspectives in biology *5*, a017780.

Elizondo, L.I., Cho, K.S., Zhang, W., Yan, J., Huang, C., Huang, Y., Choi, K., Sloan, E.A., Deguchi, K., Lou, S*., et al.* (2009). Schimke immuno-osseous dysplasia: SMARCAL1 loss-of-function and phenotypic correlation. Journal of medical genetics *46*, 49-59.

Fire, A., Xu, S., Montgomery, M.K., Kostas, S.A., Driver, S.E., and Mello, C.C. (1998). Potent and specific genetic interference by double-stranded RNA in Caenorhabditis elegans. Nature *391*, 806-811.

Fleckner, J., Zhang, M., Valcarcel, J., and Green, M.R. (1997). U2AF65 recruits a novel human DEAD box protein required for the U2 snRNP-branchpoint interaction. Genes & development *11*, 1864-1872.

Francia, S., Michelini, F., Saxena, A., Tang, D., de Hoon, M., Anelli, V., Mione, M., Carninci, P., and d'Adda di Fagagna, F. (2012). Site-specific DICER and DROSHA RNA products control the DNA-damage response. Nature *488*, 231-235.

Frokjaer-Jensen, C., Wayne Davis, M., Hopkins, C.E., Newman, B.J., Thummel, J.M., Olesen, S.-P., Grunnet, M., and Jorgensen, E.M. (2008). Single-copy insertion of transgenes in Caenorhabditis elegans. Nature genetics *40*, 1375-1383.

Gartner, A., Milstein, S., Ahmed, S., Hodgkin, J., and Hengartner, M.O. (2000). A conserved checkpoint pathway mediates DNA damage--induced apoptosis and cell cycle arrest in C. elegans. Molecular cell *5*, 435-443.

Gonzalez, M., and Li, F. (2012). DNA replication, RNAi and epigenetic inheritance. Epigenetics *7*, 14-19.

Greer, Eric L., Blanco, Mario A., Gu, L., Sendinc, E., Liu, J., Aristizábal-Corrales, D., Hsu, C.-H., Aravind, L., He, C., and Shi, Y. (2015). DNA Methylation on N6-Adenine in C. elegans. Cell *161*, 868-878.

Gu, S.G., Pak, J., Guang, S., Maniar, J.M., Kennedy, S., and Fire, A. (2012). Amplification of siRNA in Caenorhabditis elegans generates a transgenerational sequence-targeted histone H3 lysine 9 methylation footprint. Nature genetics *44*, 157-164.

Gu, W., Shirayama, M., Conte, D., Vasale, J., Batista, P.J., Claycomb, J.M., Moresco, J.J., Youngman, E., Keys, J., Stoltz, M.J.*, et al.* (2009). Distinct Argonaute-mediated 22G-RNA pathways direct genome surveillance in the C. elegans germline. Molecular cell *36*, 231-244.

Guang, S., Bochner, A.F., Burkhart, K.B., Burton, N., Pavelec, D.M., and Kennedy, S. (2010). Small regulatory RNAs inhibit RNA polymerase II during the elongation phase of transcription. Nature *465*, 1097-1101.

Guo, Y., Yang, B., Li, Y., Xu, X., and Maine, E.M. (2015). Enrichment of H3K9me2 on Unsynapsed Chromatin in Caenorhabditis elegans Does Not Target de Novo Sites. G3 *5*, 1865-1878.

Hall, I.M., Noma, K., and Grewal, S.I. (2003). RNA interference machinery regulates chromosome dynamics during mitosis and meiosis in fission yeast. Proceedings of the National Academy of Sciences of the United States of America *100*, 193-198.

Hammond, S.M., Boettcher, S., Caudy, A.A., Kobayashi, R., and Hannon, G.J. (2001). Argonaute2, a link between genetic and biochemical analyses of RNAi. Science *293*, 1146-1150.

Hansen, D., and Schedl, T. (2013). Chapter 4. Stem cell proliferation versus meiotic fate decision in C. elegans. Advances in experimental medicine and biology *757*, 71-99.

Harris, J., Lowden, M., Clejan, I., Tzoneva, M., Thomas, J.H., Hodgkin, J., and Ahmed, S. (2006a). Mutator Phenotype of Caenorhabditis elegans DNA Damage Checkpoint Mutants. Genetics *174*, 601-616.

Harris, J., Lowden, M., Clejan, I., Tzoneva, M., Thomas, J.H., Hodgkin, J., and Ahmed, S. (2006b). Mutator phenotype of Caenorhabditis elegans DNA damage checkpoint mutants. Genetics *174*, 601-616.

Henderson, S.T., Gao, D., Lambie, E.J., and Kimble, J. (1994). lag-2 may encode a signaling ligand for the GLP-1 and LIN-12 receptors of C. elegans. Development *120*, 2913-2924.

Hillers, K.J., Jantsch, V., Martinez-Perez, E., and Yanowitz, J.L. (2015). Meiosis. WormBook, 1-54.

Holdeman, R., Nehrt, S., and Strome, S. (1998). MES-2, a maternal protein essential for viability of the germline in Caenorhabditis elegans, is homologous to a Drosophila Polycomb group protein. Development *125*, 2457-2467.

Holsclaw, J.K., and Sekelsky, J. (2017). Annealing of Complementary DNA Sequences During Double-Strand Break Repair in Drosophila Is Mediated by the Ortholog of SMARCAL1. Genetics *206*, 467-480.

Jones, A.R., Francis, R., and Schedl, T. (1996). GLD-1, a Cytoplasmic Protein Essential for Oocyte Differentiation, Shows Stage- and Sex-Specific Expression duringCaenorhabditis elegansGermline Development. Developmental biology *180*, 165-183.

Kamath, R.S., Fraser, A.G., Dong, Y., Poulin, G., Durbin, R., Gotta, M., Kanapin, A., Le Bot, N., Moreno, S., Sohrmann, M.*, et al.* (2003). Systematic functional analysis of the Caenorhabditis elegans genome using RNAi. Nature *421*, 231-237.

Kassavetis, G.A., and Kadonaga, J.T. (2014). The annealing helicase and branch migration activities of Drosophila HARP. PloS one *9*, e98173.

Katz, D.J., Edwards, T.M., Reinke, V., and Kelly, W.G. (2009). A C. elegans LSD1 Demethylase Contributes to Germline Immortality by Reprogramming Epigenetic Memory. Cell *137*, 308-320.

Keeney, S., Giroux, C.N., and Kleckner, N. (1997). Meiosis-Specific DNA Double-Strand Breaks Are Catalyzed by Spo11, a Member of a Widely Conserved Protein Family. Cell *88*, 375-384.

Keeney, S., and Kleckner, N. (1995). Covalent protein-DNA complexes at the 5' strand termini of meiosis-specific double-strand breaks in yeast. Proceedings of the National Academy of Sciences of the United States of America *92*, 11274-11278.

Keka, I.S., Mohiuddin, Maede, Y., Rahman, M.M., Sakuma, T., Honma, M., Yamamoto, T., Takeda, S., and Sasanuma, H. (2015). Smarcal1 promotes double-strand-break repair by nonhomologous end-joining. Nucleic acids research *43*, 6359-6372.

Kelly, K.O., Dernburg, A.F., Stanfield, G.M., and Villeneuve, A.M. (2000a). Caenorhabditis elegans msh-5 is required for both normal and radiation-induced meiotic crossing over but not for completion of meiosis. Genetics *156*, 617-630.

Kelly, K.O., Dernburg, A.F., Stanfield, G.M., and Villeneuve, A.M. (2000b). Caenorhabditis elegans msh-5 is required for both normal and radiation-induced meiotic crossing over but not for completion of meiosis. Genetics *156*, 617-630.

Kelly, W.G., Schaner, C.E., Dernburg, A.F., Lee, M.H., Kim, S.K., Villeneuve, A.M., and Reinke, V. (2002). X-chromosome silencing in the germline of C. elegans. Development *129*, 479-492.

Keskin, H., Shen, Y., Huang, F., Patel, M., Yang, T., Ashley, K., Mazin, A.V., and Storici, F. (2014). Transcript-RNA-templated DNA recombination and repair. Nature *515*, 436-439.

Ketting, R.F., Haverkamp, T.H., van Luenen, H.G., and Plasterk, R.H. (1999). Mut-7 of C. elegans, required for transposon silencing and RNA interference, is a homolog of Werner syndrome helicase and RNaseD. Cell *99*, 133-141.

Khalil, A.M., Boyar, F.Z., and Driscoll, D.J. (2004). Dynamic histone modifications mark sex chromosome inactivation and reactivation during mammalian spermatogenesis.

Proceedings of the National Academy of Sciences of the United States of America *101*, 16583-16587.

Kim, Y., Rosenberg, S.C., Kugel, C.L., Kostow, N., Rog, O., Davydov, V., Su, T.Y., Dernburg, A.F., and Corbett, K.D. (2014). The chromosome axis controls meiotic events through a hierarchical assembly of HORMA domain proteins. Dev Cell *31*, 487-502.

Kimble, J., and Simpson, P. (1997). THE LIN-12/Notch SIGNALING PATHWAY AND ITS REGULATION. Annual Review of Cell and Developmental Biology *13*, 333-361.

Kobayashi, J. (2004). Molecular mechanism of the recruitment of NBS1/hMRE11/hRAD50 complex to DNA double-strand breaks: NBS1 binds to gamma-H2AX through FHA/BRCT domain. J Radiat Res *45*, 473-478.

Korf, I., Fan, Y., and Strome, S. (1998). The Polycomb group in Caenorhabditis elegans and maternal control of germline development. Development *125*, 2469-2478.

Kotwaliwale, C.V., Langley, S.A., Dose, A.C., Wang, C.W., and Dernburg, A.F. (2013). Chromatin and higher-order chromosome organization shape the recombination landscape in C. elegans. Epigenetics & Chromatin *6*, O17.

Lee, H.C., Aalto, A.P., Yang, Q., Chang, S.S., Huang, G., Fisher, D., Cha, J., Poranen, M.M., Bamford, D.H., and Liu, Y. (2010). The DNA/RNA-dependent RNA polymerase QDE-1 generates aberrant RNA and dsRNA for RNAi in a process requiring replication protein A and a DNA helicase. PLoS Biol *8*.

Lee, H.C., Chang, S.S., Choudhary, S., Aalto, A.P., Maiti, M., Bamford, D.H., and Liu, Y. (2009). qiRNA is a new type of small interfering RNA induced by DNA damage. Nature *459*, 274-277.

Li, Q., and Zhang, Z. (2012). Linking DNA replication to heterochromatin silencing and epigenetic inheritance. Acta Biochim Biophys Sin (Shanghai) *44*, 3-13.

Liu, J., Carmell, M.A., Rivas, F.V., Marsden, C.G., Thomson, J.M., Song, J.-J., Hammond, S.M., Joshua-Tor, L., and Hannon, G.J. (2004). Argonaute2 Is the Catalytic Engine of Mammalian RNAi. Science *305*, 1437-1441.

Liu, T., Rechtsteiner, A., Egelhofer, T.A., Vielle, A., Latorre, I., Cheung, M.-S., Ercan, S., Ikegami, K., Jensen, M., Kolasinska-Zwierz, P.*, et al.* (2011). Broad chromosomal domains of histone modification patterns in C. elegans. Genome research *21*, 227-236.

Liu, Y., and Maine, E.M. (2007). The Bro1-domain protein, EGO-2, promotes Notch signaling in Caenorhabditis elegans. Genetics *176*, 2265-2277.

Lugli, N., Sotiriou, S.K., and Halazonetis, T.D. (2017). The role of SMARCAL1 in replication fork stability and telomere maintenance. DNA repair *56*, 129-134.

MacMorris, M., Brocker, C., and Blumenthal, T. (2003). UAP56 levels affect viability and mRNA export in Caenorhabditis elegans. Rna *9*, 847-857.

MacQueen, A.J., Colaiácovo, M.P., McDonald, K., and Villeneuve, A.M. (2002). Synapsis-dependent and -independent mechanisms stabilize homolog pairing during meiotic prophase in C. elegans. Genes & development *16*, 2428-2442.

MacQueen, A.J., Phillips, C.M., Bhalla, N., Weiser, P., Villeneuve, A.M., and Dernburg, A.F. (2005). Chromosome sites play dual roles to establish homologous synapsis during meiosis in C. elegans. Cell *123*, 1037-1050.

Maine, E.M., Hauth, J., Ratliff, T., Vought, V.E., She, X., and Kelly, W.G. (2005). EGO-1, a putative RNA-dependent RNA polymerase, is required for heterochromatin assembly on unpaired dna during *C. elegans* meiosis. Curr Biol *15*, 1972-1978.

Margueron, R., and Reinberg, D. (2010). Chromatin structure and the inheritance of epigenetic information. Nat Rev Genet *11*, 285-296.

Marin, V.A., and Evans, T.C. (2003). Translational repression of a C. elegans Notch mRNA by the STAR/KH domain protein GLD-1. Development *130*, 2623-2632.

Matsui, T., Leung, D., Miyashita, H., Maksakova, I.A., Miyachi, H., Kimura, H., Tachibana, M., Lorincz, M.C., and Shinkai, Y. (2010). Proviral silencing in embryonic stem cells requires the histone methyltransferase ESET. Nature *464*, 927-931.

McMurchy, A.N., Stempor, P., Gaarenstroom, T., Wysolmerski, B., Dong, Y., Aussianikava, D., Appert, A., Huang, N., Kolasinska-Zwierz, P., Sapetschnig, A.*, et al.* (2017). A team of heterochromatin factors collaborates with small RNA pathways to combat repetitive elements and germline stress. eLife *6*, e21666.

Merritt, C., Rasoloson, D., Ko, D., and Seydoux, G. (2008). 3′ UTRs Are the Primary Regulators of Gene Expression in the C. elegans Germline. Current Biology *18*, 1476-1482.

Michalik, K.M., Böttcher, R., and Förstemann, K. (2012). A small RNA response at DNA ends in Drosophila. Nucleic acids research *40*, 9596-9603.

Mlynarczyk-Evans, S., Roelens, B., and Villeneuve, A.M. (2013). Evidence That Masking of Synapsis Imperfections Counterbalances Quality Control to Promote Efficient Meiosis. PLoS genetics *9*, e1003963.

Morthorst, T.H., and Olsen, A. (2013). Cell-nonautonomous inhibition of radiation-induced apoptosis by dynein light chain 1 in Caenorhabditis elegans. Cell Death Dis *4*, e799.

Neale, M.J., Pan, J., and Keeney, S. (2005). Endonucleolytic processing of covalent protein-linked DNA double-strand breaks. Nature *436*, 1053-1057.

O'Neil, N.J., Martin, J.S., Youds, J.L., Ward, J.D., Petalcorin, M.I., Rose, A.M., and Boulton, S.J. (2013). Joint molecule resolution requires the redundant activities of MUS-81 and XPF-1 during Caenorhabditis elegans meiosis. PLoS genetics *9*, e1003582.

Paix, A., Wang, Y., Smith, H., Lee, C.-Y.S., Calidas, D., Lu, T., Smith, J., Schmidt, H., Krause, M., and Seydoux, G. (2014a). Scalable and Versatile Genome Editing Using Linear DNAs with Micro-homology to Cas9 Sites in Caenorhabditis elegans. Genetics.

Paix, A., Wang, Y., Smith, H., Lee, C.-Y.S., Calidas, D., Lu, T., Smith, J., Schmidt, H., Krause, M., and Seydoux, G. (2014b). Scalable and Versatile Genome Editing Using Linear DNAs with Micro-homology to Cas9 Sites in Caenorhabditis elegans. Genetics.

Pasierbek, P., Jantsch, M., Melcher, M., Schleiffer, A., Schweizer, D., and Loidl, J. (2001). A Caenorhabditis elegans cohesion protein with functions in meiotic chromosome pairing and disjunction. Genes & development *15*, 1349-1360.

Paull, T.T., Rogakou, E.P., Yamazaki, V., Kirchgessner, C.U., Gellert, M., and Bonner, W.M. (2000). A critical role for histone H2AX in recruitment of repair factors to nuclear foci after DNA damage. Current Biology *10*, 886-895.

Petalcorin, M.I.R., Galkin, V.E., Yu, X., Egelman, E.H., and Boulton, S.J. (2007). Stabilization of RAD-51–DNA filaments via an interaction domain in Caenorhabditis elegans BRCA2. Proceedings of the National Academy of Sciences *104*, 8299-8304.

Pettitt, J., Wood, W.B., and Plasterk, R.H. (1996). cdh-3, a gene encoding a member of the cadherin superfamily, functions in epithelial cell morphogenesis in Caenorhabditis elegans. Development *122*, 4149.

Petty, E.L., Collette, K.S., Cohen, A.J., Snyder, M.J., and Csankovszki, G. (2009). Restricting dosage compensation complex binding to the X chromosomes by H2A.Z/HTZ-1. PLoS genetics *5*, e1000699.

Phillips, C.M., and Dernburg, A.F. (2006). A family of zinc-finger proteins is required for chromosome-specific pairing and synapsis during meiosis in C. elegans. Dev Cell *11*, 817-829.

Poole, L.A., and Cortez, D. (2016). SMARCAL1 and telomeres: Replicating the troublesome ends. Nucleus *7*, 270-274.

Postow, L., Woo, E.M., Chait, B.T., and Funabiki, H. (2009). Identification of SMARCAL1 as a component of the DNA damage response. The Journal of biological chemistry *284*, 35951-35961.

Qiao, L., Lissemore, J.L., Shu, P., Smardon, A., Gelber, M.B., and Maine, E.M. (1995). Enhancers of glp-1, a gene required for cell-signaling in Caenorhabditis elegans, define a set of genes required for germline development. Genetics *141*, 551-569.

Reddy, K.C., and Villeneuve, A.M. (2004). C. elegans HIM-17 Links Chromatin Modification and Competence for Initiation of Meiotic Recombination. Cell *118*, 439-452.

Riddle, D.L., Blumenthal, T., Meyer, B.J., and Priess, J.R. (1997). Introduction to C. elegans. In C elegans II, D.L. Riddle, T. Blumenthal, B.J. Meyer, and J.R. Priess, eds. (Cold Spring Harbor (NY)).

Rinaldo, C., Bazzicalupo, P., Ederle, S., Hilliard, M., and La Volpe, A. (2002). Roles for Caenorhabditis elegans rad-51 in meiosis and in resistance to ionizing radiation during development. Genetics *160*, 471-479.

Rivas, F.V., Tolia, N.H., Song, J.-J., Aragon, J.P., Liu, J., Hannon, G.J., and Joshua-Tor, L. (2005). Purified Argonaute2 and an siRNA form recombinant human RISC. Nature structural & molecular biology *12*, 340-349.

Rogakou, E.P., Pilch, D.R., Orr, A.H., Ivanova, V.S., and Bonner, W.M. (1998). DNA Double-stranded Breaks Induce Histone H2AX Phosphorylation on Serine 139. Journal of Biological Chemistry *273*, 5858-5868.

Rosu, S., Zawadzki, K.A., Stamper, E.L., Libuda, D.E., Reese, A.L., Dernburg, A.F., and Villeneuve, A.M. (2013). The C. elegans DSB-2 Protein Reveals a Regulatory Network that Controls Competence for Meiotic DSB Formation and Promotes Crossover Assurance. PLoS genetics *9*, e1003674.

Saito, T.T., Youds, J.L., Boulton, S.J., and Colaiacovo, M.P. (2009). Caenorhabditis elegans HIM-18/SLX-4 interacts with SLX-1 and XPF-1 and maintains genomic integrity in the germline by processing recombination intermediates. PLoS genetics *5*, e1000735.

Sarraf, S.A., and Stancheva, I. (2004). Methyl-CpG binding protein MBD1 couples histone H3 methylation at lysine 9 by SETDB1 to DNA replication and chromatin assembly. Molecular cell *15*, 595-605.

Sasagawa, Y., Yamanaka, K., Nishikori, S., and Ogura, T. (2007). Caenorhabditis elegans p97/CDC-48 is crucial for progression of meiosis I. Biochemical and biophysical research communications *358*, 920-924.

Sasagawa, Y., Yamanaka, K., Saito-Sasagawa, Y., and Ogura, T. (2010). Caenorhabditis elegans UBX cofactors for CDC-48/p97 control spermatogenesis. Genes to cells : devoted to molecular & cellular mechanisms *15*, 1201-1215.

Sato, A., Isaac, B., Phillips, C.M., Rillo, R., Carlton, P.M., Wynne, D.J., Kasad, R.A., and Dernburg, A.F. (2009). Cytoskeletal forces span the nuclear envelope to coordinate meiotic chromosome pairing and synapsis. Cell *139*, 907-919.

Schroeter, E.H., Kisslinger, J.A., and Kopan, R. (1998). Notch-1 signalling requires ligand-induced proteolytic release of intracellular domain. Nature *393*, 382-386.

Schultz, D.C., Ayyanathan, K., Negorev, D., Maul, G.G., and Rauscher, F.J. (2002). SETDB1: a novel KAP-1-associated histone H3, lysine 9-specific methyltransferase that contributes to HP1-mediated silencing of euchromatic genes by KRAB zinc-finger proteins. Genes Dev *16*, 919-932.

Schumacher, B., Hofmann, K., Boulton, S., and Gartner, A. (2001). The C. elegans homolog of the p53 tumor suppressor is required for DNA damage-induced apoptosis. Current biology : CB *11*, 1722-1727.

Severson, A.F., Ling, L., van Zuylen, V., and Meyer, B.J. (2009). The axial element protein HTP-3 promotes cohesin loading and meiotic axis assembly in C. elegans to implement the meiotic program of chromosome segregation. Genes & development *23*, 1763-1778.

Severson, A.F., and Meyer, B.J. (2014). Divergent kleisin subunits of cohesin specify mechanisms to tether and release meiotic chromosomes. eLife *3*, e03467.

She, X., Xu, X., Fedotov, A., Kelly, W.G., and Maine, E.M. (2009). Regulation of heterochromatin assembly on unpaired chromosomes during *Caenorhabditis elegans* meiosis by components of a small RNA-mediated pathway. PLoS Genet *5*, e1000624.

Sijen, T., Fleenor, J., Simmer, F., Thijssen, K.L., Parrish, S., Timmons, L., Plasterk, R.H., and Fire, A. (2001). On the role of RNA amplification in dsRNA-triggered gene silencing. Cell *107*, 465-476.

Smardon, A., Spoerke, J.M., Stacey, S.C., Klein, M.E., Mackin, N., and Maine, E.M. (2000). EGO-1 is related to RNA-directed RNA polymerase and functions in germ-line development and RNA interference in C. elegans. Curr Biol *10*, 169-178.

Smith, G.R., Boddy, M.N., Shanahan, P., and Russell, P. (2003). Fission Yeast Mus81·Eme1 Holliday Junction Resolvase Is Required for Meiotic Crossing Over but Not for Gene Conversion. Genetics *165*, 2289.

Smolikov, S., Schild-Prüfert, K., and Colaiácovo, M.P. (2009). A yeast two-hybrid screen for SYP-3 interactors identifies SYP-4, a component required for synaptonemal complex assembly and chiasma formation in Caenorhabditis elegans meiosis. PLoS genetics *5*, e1000669.

Stamper, E.L., Rodenbusch, S.E., Rosu, S., Ahringer, J., Villeneuve, A.M., and Dernburg, A.F. (2013). Identification of DSB-1, a Protein Required for Initiation of Meiotic Recombination in Caenorhabditis elegans, Illuminates a Crossover Assurance Checkpoint. PLoS genetics *9*, e1003679.

Storici, F., Bebenek, K., Kunkel, T.A., Gordenin, D.A., and Resnick, M.A. (2007). RNA-templated DNA repair. Nature *447*, 338-341.

Struhl, G., and Adachi, A. (1998). Nuclear access and action of notch in vivo. Cell *93*, 649-660.

Struhl, G., and Adachi, A. (2000). Requirements for presenilin-dependent cleavage of notch and other transmembrane proteins. Molecular cell *6*, 625-636.

Sulston, J.E., Schierenberg, E., White, J.G., and Thomson, J.N. (1983). The embryonic cell lineage of the nematode Caenorhabditis elegans. Developmental biology *100*, 64-119.

Tabara, H., Sarkissian, M., Kelly, W.G., Fleenor, J., Grishok, A., Timmons, L., Fire, A., and Mello, C.C. (1999). The rde-1 gene, RNA interference, and transposon silencing in C. elegans. Cell *99*, 123-132.

Tabara, H., Yigit, E., Siomi, H., and Mello, C.C. (2002). The dsRNA binding protein RDE-4 interacts with RDE-1, DCR-1, and a DExH-box helicase to direct RNAi in C. elegans. Cell *109*, 861-871.

Thomas, J.H., Birnby, D.A., and Vowels, J.J. (1993). Evidence for parallel processing of sensory information controlling dauer formation in Caenorhabditis elegans. Genetics *134*, 1105-1117.

Thompson, P.J., Dulberg, V., Moon, K.M., Foster, L.J., Chen, C., Karimi, M.M., and Lorincz, M.C. (2015). hnRNP K coordinates transcriptional silencing by SETDB1 in embryonic stem cells. PLoS genetics *11*, e1004933.

Towbin, Benjamin D., González-Aguilera, C., Sack, R., Gaidatzis, D., Kalck, V., Meister, P., Askjaer, P., and Gasser, Susan M. (2012). Step-Wise Methylation of Histone H3K9 Positions Heterochromatin at the Nuclear Periphery. Cell *150*, 934-947.

Turner, J.M.A. (2007). Meiotic sex chromosome inactivation. Development *134*, 1823.

Turner, J.M.A., Mahadevaiah, S.K., Fernandez-Capetillo, O., Nussenzweig, A., Xu, X., Deng, C.-X., and Burgoyne, P.S. (2005). Silencing of unsynapsed meiotic chromosomes in the mouse. Nature genetics *37*, 41-47.

Updike, D., and Strome, S. (2010). P Granule Assembly and Function in Caenorhabditis elegans Germ Cells. Journal of andrology *31*, 53-60.

Van Wynsberghe, P.M., and Maine, E.M. (2013). Epigenetic control of germline development. Advances in experimental medicine and biology *757*, 373-403.

Wei, W., Ba, Z., Gao, M., Wu, Y., Ma, Y., Amiard, S., White, C.I., Rendtlew Danielsen, J.M., Yang, Y.G., and Qi, Y. (2012). A role for small RNAs in DNA double-strand break repair. Cell *149*, 101-112.

Whittle, C.M., McClinic, K.N., Ercan, S., Zhang, X., Green, R.D., Kelly, W.G., and Lieb, J.D. (2008). The genomic distribution and function of histone variant HTZ-1 during C. elegans embryogenesis. PLoS genetics *4*, e1000187.

Winand, N.J., Panzer, J.A., and Kolodner, R.D. (1998). Cloning and characterization of the human and Caenorhabditis elegans homologs of the Saccharomyces cerevisiae MSH5 gene. Genomics *53*, 69-80.

Wood, W.B. (1988). 1 Introduction to C. elegans Biology.

Xu, L., Paulsen, J., Yoo, Y., Goodwin, E.B., and Strome, S. (2001). Caenorhabditis elegans MES-3 is a target of GLD-1 and functions epigenetically in germline development. Genetics *159*, 1007-1017.

Yang, L., Mei, Q., Zielinska-Kwiatkowska, A., Matsui, Y., Blackburn, M.L., Benedetti, D., Krumm, A.A., Taborsky, G.J., and Chansky, H.A. (2003). An ERG (ets-related gene)-

associated histone methyltransferase interacts with histone deacetylases 1/2 and transcription co-repressors mSin3A/B. The Biochemical journal *369*, 651-657.

Yang, L., Xia, L., Wu, D.Y., Wang, H., Chansky, H.A., Schubach, W.H., Hickstein, D.D., and Zhang, Y. (2002). Molecular cloning of ESET, a novel histone H3-specific methyltransferase that interacts with ERG transcription factor. Oncogene *21*, 148-152.

Yanowitz, J.L. (2008). Genome integrity is regulated by the Caenorhabditis elegans Rad51D homolog rfs-1. Genetics *179*, 249-262.

Yigit, E., Batista, P.J., Bei, Y., Pang, K.M., Chen, C.C., Tolia, N.H., Joshua-Tor, L., Mitani, S., Simard, M.J., and Mello, C.C. (2006). Analysis of the C. elegans Argonaute family reveals that distinct Argonautes act sequentially during RNAi. Cell *127*, 747-757.

Yin, Y., and Smolikove, S. (2013). Impaired Resection of Meiotic Double-Strand Breaks Channels Repair to Nonhomologous End Joining in Caenorhabditis elegans. Molecular and cellular biology *33*, 2732-2747.

Yochem, J., and Greenwald, I. (1989). glp-1 and lin-12, genes implicated in distinct cell-cell interactions in C. elegans, encode similar transmembrane proteins. Cell *58*, 553-563.

Yokoo, R., Zawadzki, K.A., Nabeshima, K., Drake, M., Arur, S., and Villeneuve, A.M. (2012). COSA-1 reveals robust homeostasis and separable licensing and reinforcement steps governing meiotic crossovers. Cell *149*, 75-87.

Youds, J.L., Barber, L.J., Ward, J.D., Collis, S.J., O'Neil, N.J., Boulton, S.J., and Rose, A.M. (2008). DOG-1 is the Caenorhabditis elegans BRIP1/FANCJ homologue and functions in interstrand cross-link repair. Molecular and cellular biology *28*, 1470-1479.

Youds, J.L., O'Neil, N.J., and Rose, A.M. (2006). Homologous recombination is required for genome stability in the absence of DOG-1 in Caenorhabditis elegans. Genetics *173*, 697-708.

Yu, Z., Kim, Y., and Dernburg, A.F. (2016). Meiotic recombination and the crossover assurance checkpoint in Caenorhabditis elegans. Semin Cell Dev Biol *54*, 106-116.

Yusufzai, T., and Kadonaga, J.T. (2008). HARP is an ATP-driven annealing helicase. Science *322*, 748-750.

Zeller, P., Padeken, J., van Schendel, R., Kalck, V., Tijsterman, M., and Gasser, S.M. (2016). Histone H3K9 methylation is dispensable for Caenorhabditis elegans development but suppresses RNA:DNA hybrid-associated repeat instability. Nature genetics *48*, 1385-1395.

Zhou, Z., Hartwieg, E., and Horvitz, H.R. (2001). CED-1 is a transmembrane receptor that mediates cell corpse engulfment in C. elegans. Cell *104*, 43-56.

<center>**Curriculum vitae**</center>

Bing Yang
Department of Biology
Syracuse University
Syracuse, NY 13244
Email: biyang@syr.edu

Education

2011	B.S. Wuhan University, Hubei, China
2011-present	Graduate student, Department of Biology, Syracuse University

Research Experience

07/2012-Present   Ph. D. Student with Dr. Eleanor Maine, Dept. of Biology, SU
Project: Identifying genes that interact with MET-2 (histone H3K9me2 methyltransferase) in *C. elegans*

01/2012-06/2012   Rotation Student with Drs. Sandra Hewett and James Hewett, Dept. of Biology, SU
Project: Studying the regulation of system xc- by microRNA-26b in glioma cell lines

09/2011-12/2011   Rotation Student with Dr. Eleanor Maine, Dept. of Biology, SU
Project: The genetic mapping of *ego-7(om57)*, which shows abnormal H3K9me2 pattern in *C. elegans* germ line

Publications

Lissemore, J. L., E. Connors, Y. Liu, L. Qiao, **B. Yang**, M. L. Edgley, S. Flibotte, J. Taylor, V. Au, D. G. Moerman, and E. M. Maine. (2018) The molecular chaperone HSP90 promotes Notch signaling in the germline of *Caenorhabditis elegans. G3*, in press.

Guo, Y., **B. Yang**, Y. Li, X. Xu and E. M. Maine (2015) Enrichment of H3K9me2 on unsynapsed chromatin in *Caenorhabditis elegans* does not target *de novo* sites. *G3* **5**(9): 1865-1878.

In preparation

B. Yang, X. Xu, L. Russell, M. Sullenberger, J. Yanowitz and E. M. Maine. *C. elegans* SMRC-1 links DNA repair and chromatin regulation.

Mutlu, B., H-M Chen, J.J. Moresco, B.D. Orelo, **B. Yang**, J. Gaspar, S. Keppler-Ross, J.R. Yates III, D.H. Hall, E.M. Maine, and S.E. Mango. Gradual accumulation of MET-2/SETDB1 into nuclear hubs dictates the timing of heterochromatin formation in *C. elegans* embryos.

Research Conference Presentations

Bing Yang, X. Xu, L. Russell, M. Sullenberger, J. Yanowitz and E. M. Maine, "*C. elegans* SMRC-1 links DNA repair and chromatin regulation," 21st international *C. elegans* meeting, 2017, UCLA. (Talk)

Bing Yang, X. Xu, L. Russell, M. Sullenberger, J. Yanowitz and E. M. Maine, "*C. elegans* SMRC-1 links DNA repair and chromatin regulation," CNY *C. elegans* meeting, 2017, Upstate medical school. (Talk)

Bing Yang, Xia Xu, Eleanor Maine, "SMRC-1, a putative annealing helicase, links chromatin regulation and DAN repair in the *C. elegans* germ line," The allied genetic conference (TAGC), 2016. (Poster)

Bing Yang, Xia Xu, Eleanor Maine, "Identifying genes involved in H3K9me2 regulation in C. *elegans*," 20th international *C. elegans* meeting, 2015, UCLA. (Poster)

Bing Yang, Xia Xu, Eleanor Maine, "Expression of MET-2, a histone methyltransferase, in the *C. elegans* germline," 19th International *C. elegans* Meeting, 2013. (Poster)

Yiqing Guo, Xia Xu, Bing Yang, Matthew Snyder, B. Chen, Jason Lieb, **Eleanor M. Maine**, "Chromatin regulation in the meiotic germline of *C. elegans*," Epigenetics Gordon Research Conference, 2013. (Poster)

Bold indicates presenter.